

MEASUREMENT OF ABSOLUTE TRANSITION PROBABILITIES  
FOR LINES OF Fe II

Thesis by  
Peter Lloyd Smith

In Partial Fulfillment of the Requirements  
For the Degree of  
Doctor of Philosophy

California Institute of Technology  
Pasadena, California  
1972

(Submitted May 10, 1972)

To LOIS

## ACKNOWLEDGMENTS

The author is happy to acknowledge the support and assistance of the entire staff of the Kellogg Radiation Laboratory. The friendly and stimulating research environment of this Laboratory was most encouraging.

Particular thanks is given to Professor Ward Whaling who suggested the project and provided guidance throughout. His patient advice and criticism were most helpful.

Dr. Donald L. Mickey, Dr. Mario Martinez-Garcia, Dr. R. B. King, Dr. George M. Lawrence and Mr. William Lennard provided invaluable advice and assistance during illuminating discussions and in the construction and operation of the apparatus. Wm. Hocker, T. Thuan, J. Sherfinski, Wm. Westbrook, R. Harmon and R. Sills helped with various aspects of the measurements and data analysis. R. G. Marcley assisted in the calibration of the standard lamp power supply. Dr. J. E. Ross of U.C.L.A. kindly used his program to calculate a solar abundance from our data.

This research was supported in part by the National Science Foundation [GP-28027] and the Office of Naval Research [N00014-67-A-0094-0022]. The author gratefully acknowledge the support of the California Institute of Technology in the form of Graduate Research Assistantships, Graduate Teaching Assistantships and Tuition Scholarships during his studies.

## ABSTRACT

Absolute transition probabilities have been measured for 38 lines from 5 levels in Fe II. The branching ratios for the transitions which depopulate each level were determined by observations of the relative line intensities in a hollow cathode discharge. The relative transition probabilities, which are proportional to the branching ratios, were normalized by measurement of the lifetime of the upper level using a beam-foil, time-of-flight technique. The lifetime is the reciprocal of the sum of the transition probabilities. Our transition probabilities are compared to values from five other measurements, the most comprehensive of which are those of Warner. The work of Warner is shown to contain a significant error which comes from his use of the, now discredited, transition probabilities of Corliss and co-workers for Fe I in the determination of the temperature of his source. A method for correcting the values published by Warner is given. Our transition probabilities for Fe II were used to calculate a value of the solar iron abundance of  $7.35 \pm 0.18$ , which supports other recent determinations based on Fe I lines.

## TABLE OF CONTENTS

	<u>Page</u>
ACKNOWLEDGMENTS	iii
ABSTRACT	iv
1. BRIEF OUTLINE	1
2. INTRODUCTION	3
2.1 Historical Survey and Motivation for this Work	3
2.2 Line Intensities and Transition Probabilities	6
3. MEASUREMENT OF THE LIFETIMES	10
3.1 The Beam-Foil Method	10
3.2 Cascading	12
3.3 The Apparatus	13
3.4 Investigation of the Spectrum	16
3.5 Lifetime Measurements	19
3.6 Corrections to the Data	20
3.7 Results	25
4. MEASUREMENT OF THE BRANCHING RATIOS	27
4.1 Introduction	27
4.2 Apparatus and Equipment	27
4.3 Branching Ratio Measurement	28
4.4 Lines with $\lambda < 2250 \text{ \AA}$ and $\lambda > 3500 \text{ \AA}$	32
4.5 Analysis of the Data	34
4.6 Self-Absorption	39

	<u>Page</u>
5. RESULTS AND DISCUSSION	43
5.1 Transition Probabilities	43
5.2 Comparison with Other Work	44
5.3 Discussion of the Measurements of Warner	47
5.4 The Solar Iron Abundance	56
5.5 Possible Errors in this Work	61
APPENDIX A – EQUILIBRIUM CHARGE DISTRIBUTIONS OF C, N, Ar AND Fe IN CARBON (reprint)	64
APPENDIX B – LIFETIMES AND TRANSITION PROBA- BILITIES FOR SOME Fe II LEVELS BY THE BEAM-FOIL METHOD (reprint)	69
APPENDIX C – OPTICAL EQUIPMENT AND COMPONENTS	73
C.1 Lenses	73
C.2 Filters	73
C.3 The Standard Lamp	75
C.4 McPherson Spectrometer System	78
C.5 Rowland Spectrometer System	79
C.6 Optical Alignment of the Rowland Spectrometer	80
C.7 Hollow Cathode Source	81
APPENDIX D – SPECTROMETER CALIBRATION	84
D.1 Introduction	84
D.2 Previous Work	85

	<u>Page</u>
D. 3 Efficiency Calibration for $\lambda \geq 2500 \text{ \AA}$	85
D. 4 Efficiency Calibration for $\lambda \leq 2500 \text{ \AA}$	90
D. 5 Efficiency Calibration Check	93
REFERENCES	95
TABLES	100
FIGURES	117

## 1. BRIEF OUTLINE

This thesis discusses the measurement of some absolute transition probabilities for lines from the decay of five levels in Fe II. The transition probability is required for astrophysical calculations, especially calculations of elemental abundances.

In Part 2, an historical survey of some determinations of the solar iron abundance is given. The discrepancy between various measurements suggested that the transition probabilities used in the calculations should be remeasured. This was the motivation for undertaking this work. Also in Part 2, there is a brief discussion of the relations between transition probability, oscillator strength, level lifetime, and line intensity.

Part 3 discusses the measurement of the level lifetimes by the beam-foil technique. Details of the apparatus and method are given along with an outline of the method of data analysis.

In Part 4, the relative intensity or branching-ratio measurements are discussed, including a description of the techniques and the data analysis. A test to ensure that self-absorption had not affected the results is described.

In Part 5, the transition probabilities are calculated from the branching ratios and the level lifetimes; and comparison with other measurements is made. Finally, the solar iron abundance is calculated from the transition probability values determined in this experiment.

Following the main part of the thesis are four Appendices. Appendix A is a copy of a paper dealing with equilibrium charge distributions which are of interest for the beam-foil lifetime measurements. Appendix B is a copy of a paper dealing with the lifetime measurements. Appendix C describes the optical equipment and components used in the experiment and includes a discussion of the hollow cathode discharge tube used for the branching ratio measurements. The last part of the thesis, Appendix D, explains the procedure for the measurement of the relative detection efficiency of the spectrometers as a function of wavelength.

## 2. INTRODUCTION

### 2.1 HISTORICAL SURVEY AND MOTIVATION FOR THIS WORK

Until 1969 there was a puzzling discrepancy between values for the solar iron abundance obtained from different studies of the sun.

For the photosphere, a value of  $\log_{10}N(\text{Fe}) = 6.6^*$  had been obtained by Goldberg et al. (1960) and many others (Jeffries, 1966). This value was based on measurements of the intensity of Fe I (neutral iron) absorption lines. Warner (1968) calculated an abundance of 6.5 from Fe II ( $\text{Fe}^+$ ) absorption lines. In contrast, Withbroe (1969) and Grevesse and Swings (1969) determined photospheric iron abundances of 7.5 and 7.63 from very weak [Fe II]<sup>†</sup> absorption lines.

Pottasch (1967) determined an abundance of 7.5 from his study of [Fe VIII] through [Fe XVI] emission lines in the solar corona. Pecker and Pottasch (1969) found an abundance of 7.8 from

---

\* Astrophysical element abundances are usually expressed in logarithmic form relative to  $10^{12}$  atoms of hydrogen:

$$\log_{10} N(\text{Fe}) = \log_{10} \frac{N_{\text{Fe}}}{N_{\text{H}}} + 12.$$

† A transition which is forbidden by the usual electric dipole selection rules is indicated by [ ].

their study of Fe I and Fe II emission lines in the chromosphere, the thin transition region between the corona and the photosphere.

Furthermore, Urey (1967) found that Type I carbonaceous chondrites, which in general have element abundances similar to those of the sun, had an iron abundance of 7.55.

It was the feeling of many workers in this field that the transition probabilities used in the abundance calculations were of dubious accuracy. \* All abundance calculations were based on the same transition probabilities contained in the continuing critical compilations of Corliss and co-workers at the U. S. National Bureau of Standards (N. B. S.). Corliss and Tech (1968) are the authors of the most recent of these compilations for Fe I. Warner (1967) gives the most complete listing of transition probabilities for allowed transitions in Fe II.

Many experimental programs were undertaken in an effort to resolve the confusion by remeasuring the transition probabilities. Much of the work on Fe I is essentially complete (Garz and Kock,

---

\* L. H. Aller, in the concluding remarks at the I. A. U. Symposium No. 26, 'Abundance Determinations in Stellar Spectra', said, 'All participants agreed that much more work, both experimental and theoretical, should be done on f-values . . . . for the atoms and ions of the iron group.', (see Abundance Determinations in Stellar Spectra, ed. H. Hubenet, Academic Press (1966)). The relationship between the oscillator strength and the f-value is discussed in Sect. 2.2.

1969; Bridges and Wiese, 1970; Martinez-Garcia et al., 1971; and Martinez-Garcia, 1971<sup>\*</sup>). There was agreement among these various workers that the N. B. S. compilations were in error by a significant factor which increased with the energy of the upper level of the transition to a value of 25 for levels at 6 eV. Consequently, all of the Fe I abundance values based on the N. B. S. transition probabilities are too low. A revised solar iron abundance of about 7.5 has been calculated by Garz et al. (1969) and by Martinez-Garcia and Whaling (1971) from the new Fe I transition probabilities. This higher value removes the discrepancy mentioned earlier. There is, however, still some disagreement. Ross (1970) favors an abundance of about 7.2.

Additional experimental programs were begun to study Fe II transition probabilities. One of these programs is the subject of this thesis. In the past, somewhat less attention has been paid to Fe II than to Fe I, in part because the spectrum is more difficult to produce and study. However, Fe II composes some 95% of the solar photosphere and comparison of the abundance values based on Fe I and Fe II would provide a test of current solar models.

As is so often the case with thesis research on problems of current interest, there have been several developments since the work was started. Grasdalen et al. (1969), Baschek et al. (1970) and

---

\* This work will hereafter be referred to as 'Martinez'.

Wolnik et al. (1971) measured Fe II oscillator strengths. Their values, and those of Roder (1962), will be discussed in Sect. 5.2. The values from these four experiments show reasonable agreement. There is, on the other hand, disagreement with Warner (1967). Baschek et al. (1970) derived an iron abundance of  $7.63 \pm .20$ .

This thesis describes a third method for measurement of Fe II absolute transition probabilities. The method is similar to that used by Martinez for Fe I. Comparison will be made with other values and the problem of the solar iron abundance will be discussed.

## 2.2 LINE INTENSITIES AND TRANSITION PROBABILITIES

The solar spectrum is a line absorption spectrum superimposed on a continuum. The absorption intensity,  $I_{ik}$ , is a function of  $N$ , the solar element abundance, and the Einstein absorption coefficient  $B_{ik}$ , where  $i$  refers to the initial, or lower, level and  $k$  refers to the final, or upper, level. As  $B_{ik}$  and  $A_{ki}$ , the transition probability for spontaneous emission\*, are related in a simple manner (Foster, 1964), we have

$$I_{ik} = f(N, A_{ki}). \quad (2-1)$$

The relationship between  $N$  and  $A_{ki}$  is such that

$$I_{ik} = f(NA_{ik}). \quad (2-1')$$

---

\* Usually referred to as 'the transition probability'.

The functional form is complex, but knowledge of  $I_{ik}$ ,  $A_{ki}$  and an assumed solar model permits calculation of  $N$  (see Aller, 1963).

For allowed transitions between upper level  $k$  and lower level  $i$ , Condon and Shortley (1967) give the transition probability as

$$A_{ki} = \frac{64\pi^4}{3hg_k \lambda_{ki}^3} \sum_{n, m} |\langle K_n | \bar{P} | I_m \rangle|^2. \quad (2-2)$$

$P$  is the electric dipole operator,  $\lambda_{ki} = \frac{c}{\nu_{ki}} = \frac{ch}{E_k - E_i}$  and  $g_k$  is the statistical weight of state  $k$ . The sums are over the  $2J + 1$  substates of both levels.

The transition probability is related to the absorption oscillator strength\*,  $f_{ik}$ , by

$$f_{ik} = \frac{g_k}{g_i} \frac{m_e c \lambda^2 A_{ki}}{8\pi^2 e^2} \quad (2-3)$$

$$= (1.449 \times 10^{-16}) \lambda^2 (\text{\AA}) \frac{g_k}{g_i} A_{ki}. \quad (2-3')$$

In order to calculate the matrix elements, the various wave functions,  $K_n$  and  $I_m$ , must be known accurately. This is not possible for elements such as iron which are best described by intermediate coupling. As approximate methods do not yield useful results, atomic transition probabilities for complex atoms must be measured experimentally.

---

\* Usually referred to as 'the oscillator strength'.

In the study of a foil-excited beam (see Part 3), collisional de-excitation of the upper levels may be neglected (see Sect. 3.5). In this case, the emission intensity of a spectral line corresponding to a transition from initial state  $k$  to final state  $i$  is related to the transition probability and to the population of the initial state in a manner first discussed by Einstein. A discussion is given by Wiese (1968). Specifically, if there are  $n_k$  particles in the excited state,  $k$ , then the number of spontaneous emission processes,  $k \rightarrow i$ , per unit time is

$$I_{ki} = \frac{dn_k}{dt} = -n_k A_{ki}. \quad (2-4)$$

$I_{ki}$  is the total photon intensity.

Typically, a given upper state may decay into several lower states. So

$$\sum_i I_{ki} = \frac{dn_k}{dt} = -n_k \sum_i A_{ki} \quad (2-5)$$

and

$$n_k(t) = n_k(t=0) \exp \left[ - \left( \sum_i A_{ki} \right) t \right]. \quad (2-6)$$

The mean lifetime of the upper state is given by

$$\tau = \frac{\int_0^{\infty} n_k(t) t dt}{\int_0^{\infty} n_k(t) dt} = \frac{1}{\sum_i A_{ki}}. \quad (2-7)$$

From Eq. 2-4, 5, 7,

$$\frac{I_{kj}}{\sum_i I_{ki}} = \frac{-n_k A_{kj}}{-n_k \sum_i A_{ki}} = \frac{A_{kj}}{\sum_i A_{ki}} = \tau A_{kj} \quad (2-8)$$

so that

$$A_{kj} = \frac{1}{\tau} \left( \frac{I_{kj}}{\sum_i I_{ki}} \right). \quad (2-9)$$

The ratio  $\frac{I_{kj}}{\sum_i I_{ki}}$  gives the fraction of the decays of a state  $k$  which end up in state  $j$ . This ratio is known as the branching ratio.

Direct measurement of absolute transition probabilities is, in general, difficult, as, from Eq. 2-4, it can be seen that  $A_{ki}$  is related to  $n_k$ , the number of particles in the upper level. For a given upper level, the relative transition probabilities for the decays which depopulate the level can be measured by measuring the relative intensity of the decays (see Eq. 2-8). The relative transition probabilities differ from the absolute transition probabilities by a numerical constant. In this work, the relative values are normalized by measurement of the lifetime and reference to Eq. 2-8.

Other techniques for the measurement of lifetimes and relative transition probabilities are discussed by Foster (1964) and Wiese (1968).

### 3. MEASUREMENT OF THE LIFETIMES \*

#### 3.1 THE BEAM-FOIL METHOD

The atomic lifetimes were measured by the beam-foil method which has been discussed in several review articles (Bashkin, 1968a, 1968b, 1968c; Whaling, 1968; Bickel, 1968; Heroux, 1968). It is essentially a time-of-flight technique. Ions of the element to be studied are accelerated to a known velocity and then made to traverse a thin foil, usually of some low Z material in order to reduce scattering. During passage through the foil, the ions undergo a large number of collisions and reach an equilibrium ionization distribution (see Appendix A). The collisions also leave the ions in excited electronic states and these decay as the ions move away from the foil.

Consider a group of ions which passed through the foil in a short time  $\Delta t$  at  $t = 0$ . Assume that  $n_0$  of these ions were in the upper level to be studied at that time. Then, as there is no repopulation by collision with the residual gas (see Sect. 3.5), the population of the decaying level in this group of ions obeys the usual

---

\* This work was previously described at the 'Second International Conference on Beam-Foil Spectroscopy'. The conference proceedings were published in *Nuc. Instr. and Methods*, 90 (1970). Our paper is reproduced as Appendix B of this thesis.

exponential law

$$n(t) = n_0 \exp(-t/\tau). \quad (3-1)$$

As the velocity is constant, this equation can be written

$$n(x) = n_0 \exp(-x/v\tau) \quad (3-1')$$

where  $v$  is the beam velocity and  $x = vt$  is the distance from the foil. The number of decays in an interval  $dx$  at a distance  $x$  from the foil is

$$|dn(x)| = n(x) \frac{dx}{v\tau} = n_0 \exp(-x/v\tau) \frac{dx}{v\tau}. \quad (3-2)$$

If the rate of production of ions excited to the upper level of interest is constant, then  $dn(x)$  is also constant, as a function of time.

A measurement of  $dn(x)$  as a function of  $x$  is equivalent to a measurement of  $n(x)$  as a function of  $x$  (see Eq. 3-2). A plot of  $\log_{10} dn(x)$  versus  $x$  gives the light decay curve which was used to determine  $\tau$ . The decay constant  $\tau$  is known as the mean life or lifetime and is related to the transition probabilities in the manner discussed in Sect. 2.2.

None of the light decay curves were of the simple exponential form described by Eq. 3-1, but appeared to be the sum of several exponential decays. This was attributed to repopulation of the level of interest by cascading from higher levels.

### 3.2 CASCADING

Consider a group of atoms with three levels  $i$ ,  $j$ , and  $k$  such that  $E_i < E_j < E_k$ , and a decay channel  $k \rightarrow j \rightarrow i$ . We will discuss the behavior of this group of atoms as a function of time, but from Sect. 3.1 it can be seen that this is equivalent to behavior as a function of distance from the foil for atoms in the beam. If the two upper levels have, respectively, lifetimes of  $\tau_k$  and  $\tau_j$  ( $\tau_k \neq \tau_j$ ) and populations of  $N_k$  and  $N_j$  at a time defined as  $t = 0$ , then

$$\frac{dn_k}{dt} = -\frac{n_k}{\tau_k} \quad (3-3)$$

$$\frac{dn_j}{dt} = -\frac{n_j}{\tau_j} + \frac{n_k}{\tau_k}. \quad (3-4)$$

Using the additional conditions that  $n_k(t = \infty) = n_j(t = \infty) = 0$ , then Eq. 3-3 gives

$$n_k(t) = N_k \exp(-t/\tau_k) \quad (3-5)$$

and Eq. 3-4 gives

$$n_j(t) = C_j \exp(-t/\tau_j) + C_k \exp(-t/\tau_k). \quad (3-6)$$

$C_j$  and  $C_k$  are constants given by

$$C_k = \frac{\tau_j N_k}{\tau_k - \tau_j} \quad (3-7)$$

and

$$C_j = N_j - \frac{\tau_j N_k}{\tau_k - \tau_j} = N_j - C_k. \quad (3-8)$$

Of course, level j can be repopulated by decays from more than one higher level, but the analysis is similar. As  $N_j$ ,  $N_k$ ,  $\tau_j$ , and  $\tau_k$  are all positive, there are only four possible combinations of  $\tau_j$ ,  $\tau_k$ ,  $C_j$  and  $C_k$ ;

- a)  $\tau_j > \tau_k$ ;  $C_k < 0$ ,  $C_j > |C_k| > 0$
- b)  $\tau_j < \tau_k$ ;  $C_k > 0$ 
  - i)  $C_j > C_k > 0$  (3-9)
  - ii)  $C_k > C_j > 0$
  - iii)  $C_k > |C_j| > 0$ ,  $C_j < 0$

Hypothetical light decay curves for these four cases are shown in Fig. 1. All light decay curves observed were of the form

$$\begin{aligned} \tau_j &< \tau_k \\ C_j &> C_k > 0. \end{aligned}$$

### 3.3 THE APPARATUS

A schematic diagram of the apparatus is shown in Fig. 1 of Appendix B.  $Fe^+$  ions were produced in a source similar to that described by Magnuson et al. (1965) and accelerated by a Van de Graaff accelerator to energies of 200 to 400 keV. The magnetic analyzer, which had a resolution,  $\frac{\Delta P}{P}$ , sufficient to separate mass

56 from mass 58, ensured that ions from residual contaminants in the source were removed from the beam to be studied. The resolution of the electrostatic analyzer was such that the velocity of the beam was constant to  $\pm 1\%$ . The analyzer was calibrated to an accuracy of better than  $1\%$  with the  $^{19}\text{F}(p, \alpha\gamma)^{16}\text{O}$  reaction which has a resonance at 340.45 keV.

The  $\text{Fe}^+$  ions were passed through a carbon foil of  $5 \pm 3$  or  $10 \pm 4 \mu\text{g}/\text{cm}^2$  nominal thickness. The tolerances on the thickness are those given by the manufacturer\*. The foils were mounted on a tungsten mesh of 0.025 mm thickness, 8 lines/mm and 70% transmission†. The mesh served to prolong the useful life of the foil and did not appear to affect the lifetime measurements. Lifetimes measured with foils supported at the edges only were the same as those measured with mesh supported foils to within the experimental uncertainty.

The charge distribution of the ions which had passed through the foil had been measured by Smith and Whaling (1969). This paper is included as Appendix A. Minor corrections to this paper are indicated by the work of Hvelplund et al. (1970), who used a more accurate method of determining the energy loss in the foil than did Smith and Whaling (1969).

---

\* Yissum Research Development Co., Hebrew University, Jerusalem, Israel.

† Buckbee Mears Co., St. Paul, Minnesota 55101.

The charge distribution data in Appendix A indicate that the maximum fraction of  $\text{Fe}^+$  is produced in the beam at an energy of around 150 keV. However, for our particular accelerator, the beam current available in the range 150 to 1000 keV is an increasing function of energy. Consequently, the optimum energy range for the production of the strongest Fe II spectrum was about 200 to 400 keV. Lifetime measurements were made at several energies within this range.

A monochromator (see Sect. 4, Appendix C) was mounted on a lathe bed so that it could be moved parallel to the moving beam of ions, as shown in Fig. 1 of Appendix B. A segment of the beam, which was viewed at  $90^\circ$  to its direction of motion, was imaged on the entrance slit using two achromatic lenses (see Sect. 1, Appendix C) to form a compound lens of about 9 cm focal length. The magnification was 0.6. Because the beam had an angular spread due to scattering collisions in the foil (see Sect. 3.6), demagnification was desirable as it permitted observation of a larger vertical extent.

Single photons passing through the monochromator were detected by a refrigerated photomultiplier tube. The output pulses from the photomultiplier tube were amplified using a Tennelec preamplifier and a Hamner amplifier-discriminator and then counted using RIDL scalers. This equipment is listed in Table 1.

The ion beam was nominally about  $0.1 \mu\text{A}$ , but was not constant. Consequently it was necessary to monitor the beam intensity. This was accomplished by using a fixed monitor phototube

which detected all light emitted by the beam between  $3500\text{\AA}$  and  $4100\text{\AA}$  within a given solid angle. It was assumed that this light intensity would be proportional to the beam current and thus proportional to the rate of production of ions in the upper level of interest. The phototube, an RCA 8575 used in a current measuring mode, was placed near to, but slightly downstream from, the foil (see Fig. 1, Appendix B). A Corning 7-51 filter limited the range of wavelengths detected and made the monitor less sensitive to room light. The phototube current was integrated using the Elcor current integrator. Photons detected by the monochromator were counted for a time period required to collect a given charge from the monitor photomultiplier tube. This time corresponded to the production of a fixed number of ions excited to the level of interest.

This technique for monitoring the beam intensity was compared to that used by Martinez. He used a Faraday cup to measure the beam current directly. This latter method is not as satisfactory because, as the foil ages, slight punctures will allow some ions to pass through the foil without being excited. These will not contribute to the light intensity observed yet will be included as part of the monitor current.

### 3.4 INVESTIGATION OF THE SPECTRUM

One difficulty with making observations at  $90^\circ$  to the beam motion, as shown in Fig. 1 of Appendix B, is the Doppler broadening introduced by the finite acceptance angle of the lens. The Doppler

shift is given by

$$\Delta\lambda = \lambda \frac{v}{c} \cos \theta \quad (3-10)$$

where  $\theta$  is the angle between the beam direction and the direction of observation and  $v$  is the beam velocity. The Doppler broadening is given by

$$\lambda_{\max} - \lambda_{\min} = \lambda \frac{v}{c} \left[ (\cos \theta)_{\max} - (\cos \theta)_{\min} \right] \quad (3-11)$$

$$= 2\lambda \frac{v}{c} \sin \theta \sin \left( \frac{\Delta\theta}{2} \right). \quad (3-11')$$

Note that observation at  $90^\circ$  to the beam gives zero Doppler shift but maximum Doppler broadening for a given acceptance angle  $\Delta\theta$ .

Observation along the line of motion,  $\theta \approx 0$ , on the other hand, gives maximum Doppler shift but minimum Doppler broadening.

The full acceptance angle of the lens was about  $.17$  or  $10^\circ$ . For  $\lambda = 3000 \text{ \AA}$  and  $v = 1.27 \times 10^8 \text{ cm/sec}$  ( $E(\text{Fe}^+) = 400 \text{ keV}$ ), we have,

- i) at  $90^\circ$ , Doppler shift =  $0 \text{ \AA}$   
Doppler broadening =  $2.2 \text{ \AA}$
- ii) at  $0^\circ$ , Doppler shift =  $13 \text{ \AA}$   
Doppler broadening =  $.05 \text{ \AA}$ .

These values may be compared to the expected instrumental width of  $0.5\text{Å}$  measured with exit and entrance slit set at 40 microns and a reciprocal dispersion of  $13\text{ Å/mm}$ . With this slit width, the counting rate near the foil for a strong line would be about 50 Hz compared to about 1 Hz for background counts from all sources.

The initial scan of the spectrum, to determine which lines could be studied, required the best possible resolution. Consequently observation along the line of motion of the beam was required.\* The apparatus shown in the inset of Fig. 1 of Appendix B was used for this purpose. The mirror was damaged by the beam but had a useful life of some tens of hours before replacement was necessary. The spectrum was scanned from  $2300\text{ Å}$  to  $2800\text{ Å}$  at  $0.5\text{ Å}$  intervals. Most strong Fe II lines are in this region. The most useful portion, which contains five of the seven lines studied, is given in Fig. 2 of Appendix B. The full width at half maximum for the peaks is about  $0.5\text{ Å}$ . The identifications were made using the table of oscillator strengths published by Warner (1967) and with the aid of Moore (1950). The strong lines observed were those with large oscillator strengths. The lines chosen for lifetime measurements were those which were positively identified (usually by observing other members of the multiplet) and well separated from nearby lines. They are listed in Table 1 of Appendix B.

---

\* Stoner and Leavitt (1971) have recently suggested a method for reducing the Doppler broadening while observing the beam at  $90^\circ$  to its direction of motion.

### 3.5 LIFETIME MEASUREMENTS

The light decay curve was obtained by moving the monochromator along the lathe bed and measuring the light intensity of the beam, relative to the monitor current, as a function of the distance from the foil. This distance was measured with a machinists' dial-indicator to an accuracy of .005 in or 0.1 mm. Greater accuracy would have been possible if the foil mounting mesh had not tended to buckle slightly. As a consequence of this buckling, as a given spot on the foil aged and a new portion had to be used, the position of the foil relative to the monochromator may have changed slightly. The decay curve was measured for about 5 to 10 cm, or about 50 to 100 nsec, depending upon the velocity. As can be seen from Fig. 3 of Appendix B, this distance is sufficient to permit accurate determination of the lifetime of the long-lived cascade.

Various studies were made to determine the effect of the beam on the foils. The electrostatic analyzer used for the charge distribution measurements (Appendix A) was used to measure the energy of the particles which had passed through the foil. The energy loss in the foil was observed to increase after long bombardment. The optical density also increased. Thus it appeared that the foils got thicker with bombardment, possibly as a result of deposit of hydrocarbons in the residual gas by the beam. An effort was made to switch to a new foil often enough that the foils were never punctured by the beam. In addition, a decay curve, such as that shown in Fig. 3 of Appendix B, is a composite of, typically,

four measurements made sequentially during a single accelerator run. Foil changes were made after about 4 or 5 points were measured (~5 minutes).

For several levels, foils of both 5 and 10  $\mu\text{g}/\text{cm}^2$  thickness were used. When corrected for the change in energy loss, no difference in the measured lifetimes was observed (see Table 2).

The  $\text{Fe}^+$  beam was at most about 0.5  $\mu\text{A}$  or  $3 \times 10^{12}$  particles/sec, with a cross section of 1 mm by 2 mm. At a velocity of  $10^8$  cm/sec (1 mm/nsec), corresponding to an energy of 300 keV, the beam density was about  $1.5 \times 10^6$  particles/ $\text{cm}^3$ . The residual gas pressure was better than  $5 \times 10^{-6}$  torr or  $2 \times 10^{11}$  particles/ $\text{cm}^3$ . The mean free path at this pressure, assuming a cross section of  $10^{-15}$   $\text{cm}^2$ , is 50 m. Because of the low particle density and the low radiation density, stimulated emission, both collision induced and radiation induced, was completely negligible; and the light radiated from the beam was entirely due to spontaneous transitions from the levels which were excited by passage through the foil (Bickel, 1967).

### 3.6 CORRECTIONS TO THE DATA

Several steps were required in order to extract the lifetime from the raw decay curve. The procedure will be outlined briefly and then discussed in more detail. Corrections for dark counts, continuum background and angular spreading of the beam led to a corrected light decay curve. This was fitted as a decay as a function of distance. Then, by considering the energy loss in the foil, a

corrected velocity was determined which permitted calculation of the lifetime.

The gross number of counts,  $n_g$ , measured for the decay curve contained several background components. The first was a beam independent background,  $n_{bi}$ , which consisted primarily of photomultiplier dark noise. The dark counting rate was essentially constant and  $n_{bi}$  could be calculated from the rate and the counting time and then subtracted from the gross counts. There was also a beam dependent background,  $n_{bd}$ . This appears as the continuum between the spectrum lines. A light decay curve for this background was measured several Ångstroms away from the peak of interest, as shown in the inset in Fig. 3 of Appendix B. The gross data points,  $n_{bdg}$ , for this curve, which is shown in Fig. 3 of Appendix B, were also corrected for a beam independent component,  $n_{bdi}$ . So, we have

$$n_{bd} = n_{bdg} - n_{bdi} \quad (3-12)$$

and

$$n = n_g - n_{bi} - n_{bd} \quad (3-13)$$

$$= n_g - n_{bi} - n_{bdg} + n_{bdi} \quad (3-13')$$

The statistical uncertainty in a number of counts that is measured directly, such as  $n_g$ , is  $\pm\sqrt{n_g}$ . The beam independent background components were measured for a time  $T_{bi}$  with a result such as  $n_{bis} \pm \sqrt{n_{bis}}$ . Because of the fluctuating beam current,

the time  $t_g$  for the measurement of  $n_g$  was not constant. The background correction was then

$$n_{bi} \pm \sigma_{bi} = \frac{t_g}{T_{bi}} (n_{bis} \pm \sqrt{n_{bis}}) \quad (3-14)$$

so that

$$n \pm \sigma = (n_g \pm \sqrt{n_g}) - (n_{bdg} \pm \sqrt{n_{bdg}}) - (n_{bi} \pm \sigma_{bi}) + (n_{bdi} \pm \sigma_{bdi}) \quad (3-15)$$

$$\begin{aligned} &= n_g - n_{bdg} - n_{bi} + n_{bdi} \\ &\pm \sqrt{n_g + n_{bdg} + \left(\frac{t_g}{T_{bi}}\right)^2 n_{bis} + \left(\frac{t_{bdg}}{T_{bdi}}\right)^2 n_{bdis}} \quad (3-15') \end{aligned}$$

$$\begin{aligned} &= n_g - n_{bdg} - n_{bi} + n_{bdi} \\ &\pm \sqrt{n_g + n_{bdg} + \frac{(n_{bi})^2}{n_{bis}} + \frac{(n_{bdi})^2}{n_{bdis}}} \quad (3-15'') \end{aligned}$$

The last step is made using Eq. 3-14 for purposes of calculation with the computer.

The final correction was to account for ions that were scattered from their original trajectory as a result of collisions in the foil. The optical system produced an image of the beam on the entrance slit of the monochromator and a simple slit system was built to scan this image to determine its size (see Fig. 2). In order to increase the beam intensity to an easily detectable level, the

spectrometer was set at zeroth order so that all light from the beam was observed. The results are shown in Fig. 4 of Appendix B. At large distances from the foil, some particles which had been scattered were outside the field of view of the monochromator optical system when they radiated. In the worst case, a 200 keV beam through a  $10 \mu\text{g}/\text{cm}^2$  foil, observations 50 mm from the foil had to be increased by 20% to account for ions not seen. This correction changed the computed value of the cascade lifetime but had a negligible effect upon the value of the lifetime of interest.

A non-linear, weighted, least-squares computer program was used to fit the data to the functional form given by Eq. 3-6. The weight was equal to  $1/\sigma^2$ , where  $\sigma$  is given by Eq. 3-15. All light decay curves were similar to that of Fig. 3 of Appendix B, or, in the notation of Sect. 3.2,  $\tau_j < \tau_k$  and  $C_j > C_k > 0$ . The computer program used an iterative procedure to find the best fit of the data to the functional form by varying all four parameters. The technique was to minimize

$$\chi^2 = \sum_{\text{all data points}} \left[ \frac{dn(x_i)_{\text{experimental}} - dn(x_i)_{\text{calculated}}}{\sigma(x_i)} \right]^2. \quad (3-16)$$

One would expect that  $\chi^2 \cong N$  for a good fit, where  $N$  is the number of data points. Generally,  $0.6 \leq \frac{\chi^2}{N} \leq 1.0$ , indicating a decent fit.

The parameters calculated by the computer program give the mean decay length rather than the lifetime. In order to make the

conversion, the velocity of the beam must be known. The velocity is not simply  $(2mE)^{1/2}$ ; a correction must be made for the energy loss in the foil. Only the electronic term in the theoretical analysis of Lindhard et al. (1963) was used because the particles observed had not undergone any large angle nuclear scatterings. The energy loss correction was increased by 30% in view of the experimental measurements for other ions in carbon foils by Fastrup et al. (1966). A somewhat more accurate correction could be made but it was not necessary in view of other larger uncertainties, especially in the foil thickness\*. Differentiating the logarithm of  $E = 1/2mv^2$ , we get

$$\frac{dv}{v} = \frac{dE}{2E}. \quad (3-18)$$

---

\* Lennard (1972) has pointed out that, although the energy loss corrections used in this work were essentially correct in magnitude, it was only by chance. Neglect of the nuclear stopping is valid for scattering angles less than  $1^\circ$  only (Hvelplund and Fastrup, 1968), and the arbitrary increase of 30% based on the results for other elements in carbon is not justified. According to Lennard (1972) a more valid correction would be

$$\frac{dE}{dx} = \left. \frac{dE}{dx} \right|_{\text{electronic}} + \left. \frac{dE}{dx} \right|_{\text{nuclear}} \quad (3-17)$$

$$= [ .00526 E(\text{MeV})^{0.59} + .00225 E(\text{MeV})^{-0.49} ] \cdot t \quad (3-17')$$

where  $t$  is the foil thickness in  $\mu\text{g}/\text{cm}^2$  and the energy loss is measured in MeV.

$dE/E$  has a maximum value, within our range of experimental parameters, when one has a 200 keV beam incident on a  $10 \mu\text{g}/\text{cm}^2$  foil. In this case

$$\frac{dv}{v} = \frac{1}{2} \left( \frac{dE}{E} \right) = \frac{1}{2} (.11 \pm .04) \approx .06 \pm .02. \quad (3-19)$$

The large uncertainty is a consequence of the foil manufacturer's stated tolerance on the foil thickness. The velocity correction is so small that any modifications to it would be second order and thus could be neglected.

### 3.7 RESULTS

The results are given in Table 2. The uncertainties given in the body of the table are the probable errors assigned by the computer program in the process of making the fit. The mean values of the lifetimes were calculated from

$$\langle \tau \rangle = \frac{\sum_i \frac{\tau_i}{\sigma_i^2}}{\sum_i \frac{1}{(\sigma_i)^2}} \quad \left( \begin{array}{l} \text{sum over all} \\ \text{measurements of} \\ \text{a given lifetime} \end{array} \right) \quad (3-20)$$

where the  $\sigma_i$  are the computer generated probable errors. The uncertainty given for the mean in Table 2 is the weighted root mean square deviation of the values from the mean. The values of Anderson (1970) are included for comparison. There is good agreement.

The lifetime values for  $\lambda\lambda$  2550 Å and 2767 Å are the results of rather crude measurements but have been included because of the good agreement with Anderson (1970). A more complete study of these lifetimes would not have been profitable. For 2550 Å there are two lines in the same multiplet which could not be resolved. For 2767.50 Å there are decays from the same upper level in the vacuum ultraviolet, making branching-ratio measurements (see Part 4) impossible with our equipment. Although there is some scatter in the results of various measurements, there is no consistent dependence upon beam energy or foil thickness.

Although the uncertainties given for the lifetimes in Table 2 are considerably less than 10%, this value was used in the transition probability calculations (see Sect. 5.1) to allow for any errors in the correction procedures discussed in Sect. 3.6.

## 4. BRANCHING RATIOS

### 4.1 INTRODUCTION

In order to determine the absolute transition probabilities for the transitions from a certain upper level, both the lifetime and the branching ratio for all the decays must be known (see Sect. 2.2).

The branching ratio

$$\frac{I_{ki}}{\sum_j I_{kj}}$$

can be determined by observing the intensity  $I_{kj}$  of all the decays from the upper level with a calibrated detector, i. e. a detector for which the detection efficiency as a function of wavelength is known.

The possible decay modes for the levels whose lifetimes had been measured were obtained from the tables of Moore (1945, 1950) and are listed in Table 2 of Appendix B. The consequences of any omitted decay modes will be discussed in Sect. 5.5.

### 4.2 APPARATUS AND EQUIPMENT

A schematic diagram of the apparatus is shown in Fig. 3. A discussion of the hollow cathode source, including the operating parameters, is given in Sect. 7 of Appendix C. The Rowland spectrometer used in these measurements is described in Sect. 5 of Appendix C and the calibration of the detection efficiency of this instrument is discussed in Appendix D. The electronics are listed

in Table 1.

#### 4.3 BRANCHING RATIO MEASUREMENT

Before measuring relative intensities, the spectrum had to be studied to find the lines of interest. The logarithmic scale on the count-rate meter proved very useful for this purpose. Scans of the spectrum were made for about  $10\text{\AA}$  on either side of the principal lines at the rate of  $0.8\text{\AA}/\text{min}$  or  $0.8\text{\AA}/\text{in}$  on the chart. The prominent lines were identified using Moore (1945, 1950). In all cases, the line of interest was either positively identified by its location relative to the other lines or, in the case of slight discrepancies between the measured and literature wavelength values, by the absence of any known line at the measured wavelength. Harrison (1969) and Striganov and Sventitskii (1968) were used to check the identifications. In no case was the difference between measured and literature wavelength values greater than  $0.02\text{\AA}$ . This small discrepancy was attributed to slight non-linearity in the scanning mechanism of the Rowland spectrometer.

Martinez found that even when the carrier gas pressure and the discharge current were held constant, the intensity of the lines in the hollow cathode discharge varied as a function of time. Consequently, he used a thin, quartz prism at  $45^\circ$  to the optical path as a beam splitter. A second spectrometer (the McPherson instrument) was used to monitor the intensity of a certain transition while the other transitions from the same upper level were being

measured. Because the index of refraction of quartz is a function of wavelength, use of the prism caused some difficulty in alignment. Consequently, an A-B-A-C-A... form of comparison was considered for this work, using only one monochromator. It was found that most changes in hollow cathode line intensity were relatively small and slow (less than 10% per hour) so that an A-B-C-A-D-E-A... comparison could be used. The monitored line intensity was checked after every two measurements or every  $20 \pm 5$  minutes. The results were normalized to give a constant value for the intensity of line 'A'.

A spectral line has a finite width which is a result of several effects; natural width from the finite lifetime of the upper level, Doppler width due to the random kinetic motion of the atoms in the source and collisional broadening due to the perturbing effects of the source atoms on each other. However, the dominant contribution to the observed width of a spectral line is usually the non-zero slit width of the spectrometer. The observed width is, roughly,

$$\Delta\lambda = \frac{d\lambda}{d\ell} (\Delta\ell) \quad (4-1)$$

where  $\frac{d\lambda}{d\ell}$  is the reciprocal dispersion (see Sect. 5, Appendix C) and  $\Delta\ell$  is the maximum of the entrance or exit slit widths. It was observed that the width of the spectral lines studied with the Rowland spectrometer was related to the slit width as given by Eq. 4-1. This indicated that the instrumental width was greater than the inherent width of the lines. In this case, the line intensity is given

by the observed intensity at the peak.

In order to avoid difficulties in trying to find the location of the spectral line maximum, the discriminator output was fed into a count-rate meter, the output of which was continuously monitored with a strip-chart recorder. The count-rate meter (see Table 1) was set to give a 3% standard error, relative to full scale, on all ranges. This was done by internal choice of appropriate time constant for each range. The scanning rate was made slow enough so that any large changes in count rate took place over a time period considerably longer than the time constant. For example, the minimum peak intensity typically observed with the Rowland spectrograph was about 500 Hz and this would be observed on the 1 KHz full scale range. For a 3% standard error on this range, the time constant was of the order of one second as the standard error is given by

$$\frac{\sqrt{N}}{N} = \frac{1}{\sqrt{N}} = \frac{1}{\sqrt{1000}} \cong 0.03. \quad (4-2)$$

The scan rate was 0.08 Å/min, or, as the full width at half maximum was about 0.06 Å, about 45 seconds were required to scan the peak region. As this is many times the time constant, it was felt that the chart recorder output accurately recorded the counting rate as a function of time. When the McPherson spectrometer was used for scanning peaks, the parameters were adjusted similarly to ensure accurate scanning.

In order to check for possible errors in this procedure for determining line intensities, the spectrometer slits were opened and flat-topped line profiles were observed without scanning. The intensity value given by the rate meter-chart recorder system was compared to the actual rate as determined with a timer and scaler. Over a count rate range,  $500 \text{ Hz} \leq R \leq 50 \text{ KHz}$ , it was found that

$$\frac{R_{\text{chart}} - R_{\text{scaler}}}{R_{\text{scaler}}} = +0.03 \pm 0.01. \quad (4-3)$$

The uncertainty is the approximate deviation of the various measurements from the mean. As only relative intensity values were required, this essentially constant discrepancy was ignored. This result also confirmed our ability to read intensity values from the chart recording in a consistent manner.

All lines between  $2250 \text{ \AA}$  and  $3500 \text{ \AA}$  were studied with the Rowland system in second order. Measurement of lines outside this range will be discussed in the next section (4.4). Before the relative intensity measurements were begun, preliminary studies of the lines were made with and without glass cut-off filters to ensure that first order lines did not blend with the lines of interest. If there were blends, filters were used. This required that the filter transmission be known as a function of wavelength (see Sect. 2, Appendix C). To avoid the introduction of additional uncertainty in the result, filters were used only when a blend of first and second order lines was actually a problem. The use of filters is indicated in Table 4.

The relative intensity of each line was compared at least 4 times to that of other lines from the same upper level. Two measurements were made with argon as a carrier gas and two were made with neon. Use of two gases avoided the problem of possible unidentified blends of the lines being studied with untabulated lines from the carrier gas. In several cases, the relative intensity of a particular line was significantly higher when measured with one carrier gas as compared to the other (e. g., 2579 Å was 50% stronger when measured with neon carrier; 2879 Å was 25% stronger when measured with argon carrier). In such cases, the weaker intensity was considered correct. These lines are noted in Table 4.

The hollow cathode carrier gas pressure and the discharge current were maintained at constant values throughout the measurements made on a given day. No attempt was made to do more than approximately reproduce these conditions for succeeding measurements. The Rowland spectrometer entrance slit was varied in the range 25 to 35 microns, being held constant for a given set of measurements, of course.

#### 4.4 LINES WITH $\lambda < 2250 \text{ \AA}$ OR $\lambda > 3500 \text{ \AA}$

As can be seen from Fig. 20, the sensitivity of the Rowland system decreases very rapidly for  $\lambda < 2250 \text{ \AA}$ . In fact, the three lines given in Table 2 of Appendix B with  $\lambda \leq 2100 \text{ \AA}$  could not be seen at all. Consequently a double comparison was used. The McPherson system was used to compare the lines below 2100 Å with a few strong

and well resolved lines with wavelengths greater than 2500 Å and from the same upper levels. The latter were then compared with other lines from their respective upper levels using the Rowland system. These lines, and the resulting relative intensities are given in Table 3. A discussion of the analysis of the data and an explanation of the uncertainty limits follows in the next section (4.5). The transmission of the quartz end window of the hollow cathode (see Table 3) was needed for the relative intensity calculation because the quartz was not part of the 'McPherson system' (see Sect. 4, Appendix C).

The two lines at longest wavelengths (4954 Å and 5019 Å) could not be studied in second order because of the physical limitations of the Rowland spectrograph. Consequently, these lines were compared in first order to lines below 3200 Å; 4954 Å being compared to 3162 Å and 5019 Å being compared to 3187 Å. The shorter wavelength lines were then compared in second order to other lines from their respective upper levels (see Eqs. 4-21 and 4-22).

Another difficulty with these lines at 5000 Å was that they were very weak. It was necessary to increase the source discharge current to 600 MA when making the first order comparison. In view of these difficulties, it should be noted that these longer wavelength lines were the only ones that were suitable for a calculation of the solar iron abundance (see Sect. 5.4).

#### 4.5 ANALYSIS OF THE DATA

Sketches of some portions of the hollow cathode Fe II spectrum are shown in Fig. 4. As explained in Sect. 4.3, the identifications were confirmed by comparing the position of the line of interest with several nearby lines, which, for the most part, are not shown in Fig. 4. For some cases (see 2753.29 Å line in Fig. 4) the line to be studied was well resolved and the background level could be determined with some certainty. Consequently, there was confidence that the intensity could be measured to  $\pm 5\%$ . However, for other lines (see 2554.95, 2934.49 and 3360.10 Å in Fig. 4) the background level was not at all well defined. In these cases, an uncertainty of 10 to 100% had to be assigned to the measured intensity. This uncertainty is called the reading error.

After the intensity data had been obtained from the chart recordings, the relative intensities were calculated in the following manner. All the data for the lines from a given upper level were arranged in the form of a matrix

$$\begin{pmatrix} D_{11} & D_{12} & D_{13} & \cdot & \cdot & \cdot & \cdot & \cdot \\ D_{21} & D_{22} & D_{23} & \cdot & \cdot & \cdot & \cdot & \cdot \\ \cdot & \cdot & \cdot & & & & & \\ \cdot & \cdot & \cdot & & & & D_{ki} & \end{pmatrix} \quad (4-4)$$

where the first subscript (row) referred to measurements made on a given day and the second subscript (column) referred to a particular

wavelength. The zeroth order method of finding the branching ratios would be to calculate

$$BR(\lambda_i) = \frac{\sum_k D_{ki}}{\sum_k \sum_i D_{ki}}. \quad (4-5)$$

However, because the operating conditions varied somewhat from day to day, this method is somewhat inaccurate because it tends to weight too heavily the data taken on the day when the intensity was greatest. Consequently, the rows of the matrix were normalized

$$\begin{pmatrix} b_1 D_{11} & b_1 D_{12} & b_1 D_{13} & \cdot & \cdot & \cdot & \cdot \\ b_2 D_{21} & b_2 D_{22} & b_2 D_{23} & \cdot & \cdot & \cdot & \cdot \\ \cdot & \cdot & \cdot & \cdot & \cdot & \cdot & \cdot \\ \cdot & \cdot & \cdot & \cdot & \cdot & \cdot & \cdot \end{pmatrix} \quad (4-6)$$

so that

$$\sum_i b_k D_{ki} = \text{constant for all rows}. \quad (4-7)$$

Then the columns were normalized also

$$\begin{pmatrix} b_1 d_1 D_{11} & b_1 d_2 D_{12} & b_1 d_3 D_{13} & \cdot & \cdot & \cdot & \cdot \\ b_2 d_1 D_{21} & b_2 d_2 D_{22} & b_3 d_3 D_{23} & \cdot & \cdot & \cdot & \cdot \\ \cdot & \cdot & \cdot & \cdot & \cdot & \cdot & \cdot \\ \cdot & \cdot & \cdot & \cdot & \cdot & \cdot & \cdot \end{pmatrix} \quad (4-8)$$

so that

$$\sum_k b_k d_i D_{ki} = \text{constant for all columns.} \quad (4-9)$$

As the rows and columns were obviously interrelated, an iterative procedure was necessary to obtain the desired conditions; given by Eq. 4-9 and

$$\sum_k b_k d_i D_{ki} = \text{constant for all rows.} \quad (4-10)$$

The relative intensities are now given by  $1/d_i$ .

If the data were perfect, every element in the matrix would now have been the same. The deviation from the mean gives some idea of the scatter in the data. If the mean is  $D_0$  then the probable fractional uncertainty in  $d_i$  is

$$\delta_i = \left[ \frac{\sum_k (D_0 - b_k d_i D_{ki})^2}{k_{\max} D_0^2} \right]^{1/2}. \quad (4-11)$$

$\delta_i$  is called the consistency error. It was generally less than 10%, that is, less than the reading error, except in the cases where the background level was not only difficult to determine, but difficult to determine consistently.

The measured relative intensities (proportional to  $1/d_i$ ) were converted to actual relative intensities by using the measured efficiency of the spectrometer system,  $\epsilon(\lambda_i)$  (see Appendix D);

$$I_i \equiv I(\lambda_i) = \frac{1}{d_i \epsilon(\lambda_i) f(\lambda_i)} \quad (4-12)$$

$f(\lambda_i)$  is the transmission of the filter used, if any. Two more possible uncertainties have thus been introduced; the calibration error,  $\Delta\epsilon(\lambda_i)$ , and the filter transmission error,  $\Delta f(\lambda_i)$ . Note that these "errors" represent fractional, not absolute, uncertainties. As the reading error and consistency error for a given line were not completely independent, the largest of them was arbitrarily called  $\Delta_i$  and the fractional uncertainty in  $I_i$  was computed

$$\frac{\delta I_i}{I_i} = \sqrt{(\Delta_i)^2 + (\Delta\epsilon(\lambda_i))^2 + (\Delta f(\lambda_i))^2} \quad (4-13)$$

The branching ratio is then given by

$$BR(\lambda_{ki}) = \frac{I_{ki}}{\sum_j I_{kj}} \equiv \frac{a_i}{\sum_j a_j} \equiv f_i \quad (4-14)$$

The additional suffix  $k$  has been introduced to indicate that this discussion applies only to lines from one upper level. The fractional uncertainty in the branching ratio is calculated in the following way;

$$\delta f_i \equiv \delta [BR(\lambda_{ki})] = \sum_m \frac{\partial f_i}{\partial a_m} \delta a_m \quad (4-15)$$

$$(\delta f_i)^2 = \sum_m \left( \frac{\partial f_i}{\partial a_m} \right)^2 \delta a_m^2$$

as the errors in the various terms are independent.

$$\frac{\partial f_i}{\partial a_m} = \frac{-a_i}{\left(\sum_j a_j\right)^2} \quad \text{for } m \neq i \quad (4-17)$$

$$\frac{\partial f_i}{\partial a_i} = \frac{\partial f_m}{\partial a_m} = \frac{\sum_j a_j - a_i}{\left(\sum_j a_j\right)^2} \quad \text{for } m = i \quad (4-18)$$

$$(\delta f_i)^2 = \left(\frac{1}{\sum_j a_j}\right)^2 \left[ \sum_{m \neq i} (a_i)^2 (\delta a_m)^2 + \left(\sum_j a_j - a_i\right)^2 (\delta a_i)^2 \right] \quad (4-19)$$

$$\begin{aligned} \left(\frac{\delta[\text{BR}(\lambda_{ki})]}{\text{BR}(\lambda_{ki})}\right)^2 &= \left(\frac{\delta f_i}{f_i}\right)^2 \\ &= \left(\frac{1}{\sum_j a_j}\right)^2 \left[ \sum_{m \neq i} (\delta a_m)^2 + \left(\sum_j a_j - a_i\right)^2 \left(\frac{\delta a_i}{a_i}\right)^2 \right] \\ &= \left(\frac{1}{\sum_j a_j}\right)^2 \left[ \sum_{m \neq i} (a_m)^2 \left(\frac{\delta a_m}{a_m}\right)^2 + \left(\sum_j a_j - a_i\right)^2 \left(\frac{\delta a_i}{a_i}\right)^2 \right] \end{aligned} \quad (4-20)$$

In Sect. 4.4 it was shown that a double comparison was required to determine the relative intensity of the two lines at 5000 Å. In these cases,

$$I_{ki}^{(2)} = \frac{I_{ki}^{(1)}}{I_{kj}^{(1)}} I_{kj}^{(2)} \quad (4-21)$$

where the superscripts refer to the spectrograph order. As there were only two lines involved in each comparison,

$$\frac{I_{ki}^{(1)}}{I_{kj}^{(1)}} = \frac{\langle D_i/D_j \rangle}{\epsilon^{(1)}(\lambda_i)/\epsilon^{(1)}(\lambda_j)} \quad (4-22)$$

$D_i$  and  $D_j$  are the measured relative intensities of the two lines and  $\langle \rangle$  means the average over all measurements of the intensity ratio.

Table 4 gives the relative intensity (see Eq. 4-12), the reading error, the consistency error, the calibration error, the uncertainty in the relative intensity as well as the branching ratio and the uncertainty in the branching ratio for all lines studied. The filter transmission error was not included because it was significantly less than the other uncertainties involved (see Sect. 2, Appendix C).

#### 4.6 SELF-ABSORPTION

The hollow cathode discharge used in these measurements is an extended light source of finite depth. Light emitted at some point in the interior may be absorbed by an atom as the light passes through the source. This process, known as self-absorption, will decrease the observed intensity of strong lines more than that of weak lines. If the iron atom density is sufficiently low, self-absorption will not be a problem. The experimental tests to be discussed in this section confirmed that this was the case.

A study of self-absorption has been made by Cowan and Dieke (1948). In general, the extent to which self-absorption will be present for a given transition depends upon the number of atoms along the line of sight which are capable of absorbing the particular photon and upon the Einstein absorption coefficient,

$$B_{ik} = \frac{\lambda_{ki}^3}{8 \pi h} A_{ki}. \quad (4-23)$$

If  $I_{ki}$  is the intensity of the spectral line, then the decrease in intensity is

$$\begin{aligned} dI_{ki} &\propto I_{ki} N_i B_{ik} \\ &\propto I_{ki} N_i A_{ki} \lambda_{ki}^3 \end{aligned} \quad (4-24)$$

where  $N_i$  is the population of the lower level. In this work, the range of transition probabilities spans three orders of magnitude while the range of wavelengths is only a factor of two. Consequently, for lines with the same lower level at least, the fractional change in intensity caused by self-absorption will be greatest for the strong lines. If  $I'_{ki}$  is defined as the observed intensity outside the source, then

$$I'_{ki} \equiv I_{ki} - dI_{ki} = I_{ki} (1 - \alpha N_i A_{ki} \lambda_{ki}^3) \quad (4-25)$$

where  $\alpha$  is a constant which gives some measure of the self-absorption. If two lines from the same upper level are compared

under two sets of conditions such that the lower level populations are different, then

$$\left( \frac{I'_{ki}}{I'_{kl}} \right)_1 = \left( \frac{I_{ki}}{I_{kl}} \right) \left[ \frac{1 - \alpha(N_i)_1 A_{ki} \lambda_{ki}^3}{1 - \alpha(N_l)_1 A_{kl} \lambda_{kl}^3} \right] \quad (4-26)$$

and

$$\left( \frac{I'_{ki}}{I'_{kl}} \right)_2 = \left( \frac{I_{ki}}{I_{kl}} \right) \left[ \frac{1 - \alpha(N_i)_2 A_{ki} \lambda_{ki}^3}{1 - \alpha(N_l)_2 A_{kl} \lambda_{kl}^3} \right]. \quad (4-26')$$

(Recall from Sect. 2.2 that the ratio  $I_{ki}/I_{kl}$  will be independent of changes in the level populations.) If

$$\left( \frac{I'_{ki}}{I'_{kl}} \right)_1 = \left( \frac{I'_{ki}}{I'_{kl}} \right)_2 \quad (4-27)$$

for both weak and strong lines, then self-absorption has not affected the results. Note that this test is conclusive even if  $\left( \frac{N_i}{N_l} \right)_1 = \left( \frac{N_i}{N_l} \right)_2$  as long as  $(N_i)_1 \neq (N_i)_2$ , etc.

In the hollow cathode source, the relative intensities of Fe II lines from different upper levels may be varied by changing the carrier gas pressure or the discharge current. This was attributed to a change in the population distribution of the various levels.

Twenty of the better resolved lines were studied with source parameters somewhat different from those used for the branching ratio measurements, in order to take advantage of the change in level

populations. The discharge current was 375 mA and the argon pressure was 2 torr compared to 460 mA and 2.5 to 3 torr for the earlier measurements. These new operating conditions resulted in a reduction of the line intensities of roughly a factor of two indicating that the level populations had indeed changed. The decrease in intensity resulted in an increase in the uncertainty of the measured intensities.

The ratio

$$\frac{(\text{measured relative intensity})_{\text{low pressure, low current}}}{(\text{measured relative intensity})_{\text{normal operating conditions}}} \quad (4-28)$$

is plotted in Fig. 5 against the transition probability. The error limits shown are only the uncertainty from the reading error (see Sect. 4.5) for the new, low intensity measurements. The intensities were measured relative to the strongest line from each upper level. The weighted mean of the ratio is  $.986 \pm .118$ . The uncertainty is the weighted deviation of the values from the mean. This value, coupled with the fact that no dependence upon transition probability is evident in Fig. 5 leads to the conclusion that self-absorption has not affected the results.

## 5. RESULTS AND DISCUSSION

### 5.1 TRANSITION PROBABILITIES

The transition probability is related to the lifetime and to the branching ratio by

$$A(\lambda_{kj}) \equiv A_{kj} = \frac{1}{\tau_k} \left( \frac{I_{kj}}{\sum_i I_{ki}} \right) \quad (5-1)$$

as shown in Sect. 2.2. The transition probability and the value of  $gf$ , where  $f$  is the oscillator strength defined by Eq. 2-3 and  $g$  is the statistical weight of the lower level, are given in Table 5 for each of the lines studied.  $\text{Log}_{10} gf$ , which is frequently given by other authors and is used in abundance calculations, is also given in Table 5. The uncertainty listed is given by

$$\Delta A_{kj} = A \left\{ \left[ \frac{\delta(BR_{kj})}{BR_{kj}} \right]^2 + \left[ \frac{\delta\tau_k}{\tau_k} \right]^2 \right\}^{\frac{1}{2}} \quad (5-2)$$

where  $\frac{\delta(BR_{kj})}{BR_{kj}}$  is defined in Eq. 4-20 and  $\frac{\delta\tau_k}{\tau_k} = 0.1$  as discussed in Sect. 3.7.

## 5.2 COMPARISON WITH OTHER WORK

The most extensive study of Fe II transition probabilities has been made by Warner (1967)\* who measured, in a laboratory spark, 650 lines of Fe II and 1700 lines from other once-ionized elements of the iron group. His transition probabilities have been widely used in astronomical studies of these elements. Comparison between our results and those of Warner is given in Table 6.

In addition to our work and that of Warner, there are four other laboratory measurements of Fe II transition probabilities by Roder (1962), Grasdalen et al. (1969), Baschek et al. (1970), and Wolnik et al. (1971). The six experiments are compared in Table 7. It is not possible to make a direct comparison between our work and the other experiments, except for that of Warner, as we have not measured any lines in common. However, an indirect comparison can be made by comparing all results to those of Warner. This is done in Fig. 6 where  $\log_{10} \frac{A_W}{A_X}$  is plotted as a function of  $E_2$ , the upper level energy or excitation potential.  $A_X$  refers to the transition probabilities of Roder (1962), Grasdalen et al. (1969), Baschek et al. (1970), Wolnik et al. (1971) and this work. It is clear from Fig. 6 that Warner's results are larger than those of other experimenters

---

\* Hereafter referred to as Warner or, as a subscript, W. Warner lists values of  $\log_{10} gf$  for Fe II. These were converted to transition probabilities ( $A_W$ ) for the sake of comparison. We will discuss Warner's results in terms of transition probabilities rather than oscillator strengths.

by a factor ranging from  $10^{0.2} = 1.6$  to  $10^{1.0} = 10$ . The results of Roder (1962), Baschek et al. (1970), Wolnik et al. (1971) and this work span rather limited ranges of excitation potential but the work of Grasdalen et al. (1969) provides confirmation of the conclusion that Warner's results are too large over a considerable range of excitation potential. The results of Roder (1962) and Wolnik et al. (1971) are apparently larger than those of Baschek et al. (1970) and Grasdalen et al. (1969) by roughly a factor of  $10^{0.3} = 2$ .

In addition to the laboratory measurements, several determinations of Fe II transition probabilities have been made from observations of line intensities in stellar spectra. Groth (1961), who published the most comprehensive list of transition probabilities determined in this way, estimated his values from a model atmosphere analysis of  $\alpha$  Cygni. Again, the comparison of the values of Groth (1961) with our values and those of other recent measurements must be made by comparing all the values to those given by Warner. Figure 7 of Warner (1967) shows a plot of  $\log \frac{A_W}{A_{\text{Groth}}}$  as a function of  $E_2$ , directly comparable to Fig. 6 of this work. The relative agreement is good; both figures show deviations from Warner's results by a factor which is approximately constant but which decreases slightly as  $E_2$  is increased. As for the absolute normalization of the results of Groth (1961), it appears, from Fig. 7 of Warner and Fig. 6 of this work, that

$$\left\langle \log \frac{A_W}{A_{\text{Groth}}} \right\rangle - \left\langle \log \frac{A_W}{A_x} \right\rangle \approx \left\langle \log \frac{A_x}{A_{\text{Groth}}} \right\rangle \approx 0.2$$

( $\langle \rangle$  = average).

This apparent error in magnitude in the work of Groth (1961) is probably a result of errors in the parameters chosen for his stellar model.

Kuzmickyte and Uspalis (1970) have made theoretical calculations of transition probabilities for  $3d^64p \rightarrow 3d^7$  transitions in Fe II. Unfortunately, the only lower terms considered,  $a^4F$ ,  $a^4P$  and  $a^2G$ ,\* are of low excitation potential with the result that most of the multiplets are in the vacuum ultraviolet. There are, however, seven lines of this sort measured by Warner in multiplets 6 and 8 (multiplet 8 is the same as multiplet 78u). It was found that

$$\left\langle \log \frac{A_W}{A_{K+U}} \right\rangle = 1.0 \pm 0.1$$

where the uncertainty is the r. m. s. deviation from the mean. This indicates good relative agreement with Warner, but, when this value is compared with the information shown in Fig. 6, it could be concluded that the values of Kuzmickyte and Uspalis (1970) are

---

\* See Moore (1945, 1950) for term designations and multiplet numbers.

smaller than the values  $A_x$  by roughly a factor of  $10^{0.4} = 2.5$ .

Further evidence of this is provided by the three lines from multiplet 93u measured in this experiment which are included in the study of Kuzmickyte and Uspalis (1970). For these lines,

$$\left\langle \log \frac{A_{\text{this work}}}{A_{K+U}} \right\rangle = 0.30 \pm 0.06.$$

The good relative agreement (indicated by the small values of the r. m. s. deviation from the mean) shown by the results of these theoretical calculations for a restricted group of terms gives promise of successful calculation of Fe II transition probabilities in the future.

### 5.3 DISCUSSION OF THE MEASUREMENTS OF WARNER

The work of Warner is far more extensive than that of any of the other workers who have measured Fe II transition probabilities in the laboratory (see Sect. 5.2). Consequently, it would be worthwhile to study Warner's analysis to see if his results can be corrected. This study will be divided into five parts:

- a) Warner's determination of the temperature of his source,  $T_W$ ,
- b) the correct temperature of Warner's source,  $T_{W, \text{correct}}$ ,
- c) Warner's determination of the wavelength sensitivity of his plates,  $\epsilon(\lambda)$ ,

- d) Warner's relative and absolute values and discussion of Warner's excitation potential dependent correction function,  $C(E_2)$ ,
- e) a correction to Warner's results.

Before proceeding, however, mention should be made of the measurements of Fe I transition probabilities by Corliss and co-workers. Because Warner's analysis was dependent upon these values, a summary outline of this work is given as follows:

- i) Meggers et al. (1961): 39,000 relative spectral line intensities for 70 elements.
- ii) Corliss and Bozeman (1962):\* from data of Meggers et al.; 25,000 absolute transition probabilities for neutral and singly ionized elements; excitation potential dependent correction factor,  $C_{C+W}(E_2)$ , used for lines from levels with  $E_2 \geq 50$  kK in order to have agreement between theoretical and measured f-values.
- iii) Corliss and Warner (1964, 1966):\* revised and expanded C + B for Fe I only.
- iv) Corliss and Tech (1968):\* essentially the same as C + W but with correction function,  $C_{C+W}(E_2)$ , removed.

---

\* The work of Corliss and co-workers will be referred to as C+B, C+W, and C+T.

a) Warner's determination of the temperature of his source

Warner measured photographically the emission spectra of 8 iron group elements in a high-voltage spark discharge. From his plates, he determined the temperature of his source. The Einstein-Boltzmann equation relates the line intensity,  $I$ , to the temperature and other parameters

$$I = \frac{C_1 gA}{\lambda} \exp\left(\frac{-E_2}{kT}\right) \quad (5-3)$$

where  $C_1 = \frac{Nhc}{u}$ , a constant for a given source.  $N$  is the particle density and  $u$  is the partition function. Warner studied Fe I lines on his plates over a limited range of wavelengths such that  $\epsilon(\lambda)$  would be constant. For these lines he used the transition probabilities of C+W,  $A_{C+W}$ , to calculate

$$\begin{aligned} \log_{10}\left(\frac{(I_{\text{observed}})^\lambda}{gA_{C+W}}\right) &= \log_{10}\left(\frac{I \epsilon(\lambda) \lambda}{gA_{C+W}}\right) \\ &= \log_{10}\left[C_1 \epsilon(\lambda) \exp\left(\frac{-E_2}{kT_W}\right)\right] \\ &= C_2 - 0.625 \frac{E_2}{T_W} \end{aligned} \quad (5-4)$$

where  $C_2$  is a constant for the limited range of wavelengths considered.  $E_2$  is expressed in  $\text{cm}^{-1}$  or Kayzers ( $1 \text{ cm}^{-1} = 1 \text{ K}$ ) and  $T_W$  is the temperature in  $^\circ\text{K}$  to be determined by Warner for his source. He plotted  $\log_{10} \frac{I_{\text{obs}} \lambda}{gA_{C+W}}$  as a function of  $E_2$  and determined the

temperature from the slope of the curve,  $\frac{-0.625}{T_W}$ . Because of some uneasiness about the correction function,  $C_{C+W}(E)$ , applied by C+W to transition probabilities for lines from levels with  $E_2 \geq 50$  kK, Warner did not use such lines for this procedure.

b) The correct temperature of Warner's source,  $T_{W, \text{correct}}$

If the C+W transition probabilities used by Warner contained an error dependent upon  $E_2$ , then the value determined for  $T_W$  would be wrong. If the correct transition probabilities were given by A, then

$$\begin{aligned} \log\left(\frac{I_{\text{obs}}\lambda}{gA}\right) &= \log\left(\frac{I_{\text{obs}}\lambda}{gA_{C+W}}\right) + \log\left(\frac{A_{C+W}}{A}(E_2)\right) \\ &= \log C_2 - 0.625 \frac{E_2}{T_{W, \text{correct}}} \quad (5-5) \\ &= \log C_2 - 0.625 \frac{E_2}{T_W} + \log\left(\frac{A_{C+W}}{A}(E_2)\right). \end{aligned}$$

Therefore

$$0.625 \frac{E_2}{T_{W, \text{correct}}} = 0.625 \frac{E_2}{T_W} - \log\left(\frac{A_{C+W}}{A}(E_2)\right). \quad (5-5')$$

Bridges and Wiese (1970) showed that the results of C+T, which are essentially the same as those of C+W for  $E_2 \leq 50$  kK, were indeed in error by a factor which depended upon  $E_2$ . From Fig. 1 of Bridges and Wiese (1970) we determined that

$$\log\left(\frac{A_{C+W}}{A}\right) = \log\left(\frac{A_{C+T}}{A}\right) = 3.8 \times 10^{-5} E_2 - .95. \quad (5-6)$$

So

$$\frac{E_2}{T_{W, \text{correct}}} = \frac{E_2}{T_W} - \frac{1}{0.625} [3.8 \times 10^{-5} E_2 - .95]. \quad (5-7)$$

We are concerned only with the slope of a linear function of  $E_2$ , so we have

$$\frac{1}{T_{W, \text{correct}}} = \frac{1}{T_W} - \frac{3.8 \times 10^{-5}}{.625}. \quad (5-8)$$

Warner's value for  $T_W$  was  $6130^\circ\text{K}$ . This gives  $T_{W, \text{correct}} = 9,700^\circ\text{K}$ .

c) Warner's determination of the wavelength sensitivity of his plates,  $\epsilon(\lambda)$

Warner used his incorrect value for the temperature,  $T_W$ , in his determination of the plate sensitivity,  $\epsilon_W(\lambda)$ . The plate sensitivity determined using the correct temperature will be denoted  $\epsilon(\lambda)$ .

Using C+W transition probabilities for Fe I lines seen on his plates, Warner calculated an expected intensity for each line from Eq. 5-3,

$$I_{\text{calc}} = \frac{C_1 g A_{C+W}}{\lambda} \exp\left(\frac{-E_2}{kT_W}\right). \quad (5-9)$$

Then

$$\epsilon_{W(\lambda)} = \frac{I_{\text{obs}}}{I_{\text{calc}}} = \frac{I_{\text{obs}}}{\frac{C_1 g A_{C+W}}{\lambda} \exp\left(\frac{-E_2}{kT_W}\right)}. \quad (5-10)$$

As only a relative value of  $\epsilon_{W(\lambda)}$  was desired, it was not necessary to know the value of  $C_1$ . Despite his error in determining his source temperature, Warner obtained consistent values for  $\epsilon_{W(\lambda)}$  regardless of the value of  $E_2$  being considered. This was a consequence of the relation between the errors in  $A_{C+W}$  and the error in  $T_W$ . For if

$$\epsilon(\lambda) = \frac{I_{\text{obs}}}{I} = \frac{I_{\text{obs}}}{\frac{C_1 g A}{\lambda} \exp\left(\frac{-E_2}{kT_{W, \text{correct}}}\right)}, \quad (5-11)$$

then

$$\frac{\epsilon_{W(\lambda)}}{\epsilon(\lambda)} = \frac{I}{I_{\text{calc}}} = \frac{A}{A_{C+W}} \exp\left(-\left(\frac{E_2}{kT_{W, \text{correct}}} - \frac{E_2}{kT_W}\right)\right) \quad (5-12)$$

and

$$\begin{aligned} \log \frac{\epsilon_{W(\lambda)}}{\epsilon(\lambda)} &= -\log\left(\frac{A_{C+W}}{A}\right) - 0.625 E_2 \left(\frac{1}{T_{W, \text{correct}}} - \frac{1}{T_W}\right) \\ &= 0 \end{aligned} \quad (5-13)$$

using Eq. 5-5'.

- d) Warner's relative and absolute transition probabilities and a discussion of the excitation potential dependent correction function,  $C(E_2)$

Warner then calculated relative transition probabilities from Eq. 5-3,

$$A_{W, \text{relative}} = \frac{I_{\text{obs}}}{\left(\frac{C_1 g}{\lambda}\right) \epsilon(\lambda) \exp\left(\frac{-E_2}{kT}\right)}. \quad (5-14)$$

He placed his relative values on an absolute scale by appealing to a number of theoretical transition probabilities, computed by means of the coulomb approximation. For this procedure, he made use only of multiplets selected for closeness to LS-coupling. Warner claimed that his absolute scale was established with a standard error of  $\pm 12\%$  in this way. The values obtained in this manner will be denoted as  $A'_W$ . For lines with  $E_2 \leq 50$  kK, Warner found that

$$A'_W = C_3 A_{W, \text{relative}} \quad (5-15)$$

where  $C_3$  is a constant. However, the difference between the measured and calculated values was not constant for  $E_2 \geq 50$  kK. Consequently, Warner found it necessary to introduce a correction function,  $C(E_2)$ , similar to that used by C+W. This function is shown in the inset of Fig. 7. Warner's published values,  $A_W$ , contain this function;

$$A_W = C(E_2) A'_W. \quad (5-16)$$

Warner justified the need for the correction function by concluding that there was a departure from local thermodynamic equilibrium (LTE) in his discharge for high excitation levels.

We now know that Warner's estimate of the temperature of his source was incorrect. We will show that, if the correct temperature had been used in his analysis, Warner would not have needed the correction factor. Using  $T_{W, \text{correct}}$  in Eq. 5-14,

$$A_{\text{relative}} = \frac{I_{\text{obs}}}{\frac{C_1 g}{\lambda} \epsilon(\lambda) \exp\left(\frac{-E_2}{kT_{W, \text{correct}}}\right)}. \quad (5-17)$$

If we assume Warner's normalization,  $C_3$ , to be correct, then

$$A \equiv C_3 A_{\text{relative}} \quad (5-18)$$

and

$$\begin{aligned} \frac{A'_W}{A} &= \exp\left[\frac{-E_2}{k} \left(\frac{1}{T_{W, \text{correct}}} - \frac{1}{T_W}\right)\right] \\ \log \frac{A'_W}{A} &= -0.625 E_2 \left(\frac{1}{T_{W, \text{correct}}} - \frac{1}{T_W}\right) \\ &= 3.8 \times 10^{-5} E_2(\text{K}) \end{aligned} \quad (5-19)$$

from Eq. 5-8. This relationship is shown by the dotted line in Fig. 7. The data are better fitted by the solid line in Fig. 7, a line

with the same slope but a different intercept.

$$\log \frac{A'_W}{A} = -0.81 + 3.8 \times 10^{-5} E_2(K). \quad (5-19')$$

The discrepancy in the intercept indicates an error in Warner's absolute normalization whereas the fit to the solid line confirms the error made by Warner in establishing the temperature of his source.

e) A correction to Warner's results

It is significant that the only error found in Warner's relative transition probabilities was the temperature error caused by his use of the now discredited C+W values. Thus, it is possible that Warner's results may be corrected by using Eq. 5-16 and Eq. 5-19'. If the corrected values of the absolute transition probabilities obtained from Warner's data are denoted  $A_W^*$ , then

$$\begin{aligned} \log A_W^* &= \log \left( \frac{A}{A'_W} \right) + \log \left( \frac{A'_W}{A_W} \right) + \log A_W \\ &= [0.81 - 3.8 \times 10^{-5} E_2(K)] - \log C(E_2) + \log A_W. \end{aligned} \quad (5-20)$$

Recalling that  $\log(gf) = \log A + \text{constant}$ , we then have

$$\begin{aligned} \log(gf)_{W, \text{correct}} &= [0.81 - 3.8 \times 10^{-5} E_2(K)] \\ &\quad - \log C(E_2) + \log(gf)_W \end{aligned} \quad (5-21)$$

where  $\log(gf)_W$  is tabulated by Warner. In Sect. 5-4, an attempt will be made to determine the solar iron abundance using these

corrected values for Fe II oscillator strengths.

$\text{Log } \frac{A_W^*}{A_X}$  is plotted in Fig. 8 and Fig. 9 as a function of wavelength and  $A_X$ , respectively. The corrected values show considerable scatter when compared to the recent measurements,  $A_X$ . However, there is no evidence for any dependence upon wavelength or upon the strength of the line.

#### 5.4 THE SOLAR IRON ABUNDANCE

As the main impetus for this work was the controversy about the solar iron abundance, it would be inappropriate to conclude without discussing the matter. Unfortunately, the lines for which we were able to measure transition probabilities are not well suited to abundance calculations. Their ultimate application to the solar abundance problem will be indirect; they will be used as calibration points for normalization of relative transition probabilities. However, some limited conclusions will be drawn from our transition probability values in this section.

The main reason that our values are not applicable to the abundance problem is that most of the lines studied have wavelengths less than 2900 Å. For this region accurate measurements of solar equivalent widths\* have not been made.

---

\* The equivalent width is related to the line intensity. The definitions of this and other astrophysical parameters are given by Aller (1963).

Several comprehensive photoelectric measurements of the solar spectrum for  $\lambda \geq 2900 \text{ \AA}$  have been analyzed by Moore et al. (1966), who list six of the lines studied in our experiment. They are given in Table 8 along with the parameters of interest in a discussion of the solar iron abundance.  $3132 \text{ \AA}$  is blended with Ni I and  $3360 \text{ \AA}$  is blended with a molecular band. Some information about the solar iron abundance could be obtained from the other four lines, but, before presenting the results, a brief discussion of the methods of analysis is in order.

One method of stellar abundance determination is known as curve of growth analysis (see Aller, 1963). For a given line in a star, the curve of growth is a plot of  $\log W$ , where  $W$  is the equivalent width, against  $\log Nf$ , where  $N$  is the number of absorbing atoms and  $f$  is the oscillator strength (constant for a given line). Small values of  $Nf$  give Gaussian absorption profiles for which  $W \propto Nf$ . For large values of  $Nf$ , large 'wings' dominate the line shape and  $W \propto (Nf)^{1/2}$ .

For astrophysical analysis, a curve of growth is a plot of  $\log \left( \frac{W}{\lambda} \right)$  against  $\log (gf\Gamma)$  for many lines of a particular star (see Warner, 1968).  $\Gamma$  is a function of the ionization potential of the element, the energy of the upper level, the wavelength of the line and the solar model. Cayrel and Jugaku (1963) have tabulated  $\Gamma$  values for Fe II using a particular model that is currently accepted. For weak lines

$$\log(W/\lambda) = \log(gf\Gamma) + \log\left(\frac{N_{\text{Fe}}}{N_{\text{H}}}\right).^* \quad (5-22)$$

On the plot of the curve of growth, this represents a line of unit slope ( $45^\circ$ ) with  $\log(N_{\text{Fe}}/N_{\text{H}}) = \log(W/\lambda)$  for  $\log(gf\Gamma) = 0$ . For stronger lines

$$\log(W/\lambda) \leq \log(gf\Gamma) + \log\left(\frac{N_{\text{Fe}}}{N_{\text{H}}}\right). \quad (5-23)$$

If a theoretical curve of growth is available, it is sometimes possible to make an abundance determination from individual lines not on the weak line portion of the curve of growth. This procedure is dependent upon a knowledge of various solar model parameters and, consequently, is rather inaccurate (see Aller, 1963). For weak lines, however, the relationship given by Eq. 5-22 can be used to estimate the element abundance. It will be seen from Eq. 5-23 that the result is always a value less than or equal to the correct abundance, depending upon the strength of the line. The data for the four lines are plotted in Fig. 10. It is clear that  $3162 \text{ \AA}$  and  $3187 \text{ \AA}$  are not on the weak line portion of the curve. Assuming the other

---

\* To avoid confusion, note that  $N_{\text{Fe}}/N_{\text{H}}$  refers to the actual abundance ratio. Values of  $\log(N_{\text{Fe}}/N_{\text{H}})$  from curve of growth analysis must be modified by the addition of 12 to give abundances in the standard form used in Sect. 2.1,

$$\log N(\text{Fe}) \equiv \log \frac{N_{\text{Fe}}}{N_{\text{H}}} + 12.$$

lines are on or below the weak portion of the curve, a solar iron abundance of  $\geq 7.28 \pm 0.18$  is derived from  $4954\text{\AA}$  and a value of  $\geq 7.44 \pm 0.19$  is derived from  $5019\text{\AA}$ . The uncertainty is due to the uncertainty in the measured transition probabilities or gf-values. Some additional uncertainty should be included because of the uncertainty in the equivalent width.

A second method of solar abundance determination is a fine-analysis model atmosphere calculation. This method will be independent of parameters such as the microturbulence velocity and the damping constant, if it is applied only to weak lines;  $W \leq 20\text{ m\AA}$ . The data for  $4954\text{\AA}$  and  $5019\text{\AA}$  were analyzed by Ross (1972) of UCLA to determine an iron abundance by this method. The technique used was a direct-integration, curve of growth program which chooses an abundance and, from it, computes, by direct integration, an equivalent width. This procedure is repeated until the equivalent width is equal to that observed. The abundance determined from  $4954\text{\AA}$  was  $7.27 \pm .18$  and the abundance determined from  $5019\text{\AA}$  was  $7.41 \pm .18$ . These values are in excellent agreement with the results from our crude curve of growth analysis. The mean value of all determinations discussed is  $7.35 \pm 0.18$ .

Ross (1972) questions the equivalent widths given by Moore et al.. Using his measurements of the equivalent width for our two lines, Ross (1972) determined an average abundance value of 7.14 from observations of the center of the solar disc and 7.38 from observations at  $\mu = \cos \theta = 0.5$ . The average of these values is

7.26 or a factor of  $10^{0.09} = 23\%$  lower than the value resulting from use of the equivalent widths of Moore et al. (1966).

Warner (1968) calculated a solar iron abundance based on Fe II. His laboratory oscillator strengths (Warner, 1967), which did not extend to weak lines, were supplemented with astrophysical values obtained from model atmosphere studies of two stars and normalized to agree with Warner's laboratory data. These oscillator strengths were corrected using Eq. 5-21 and a curve of growth was plotted in Fig. 11. The values of  $\log \frac{W}{\lambda}$  and  $\log \Gamma = \log C - \log(gf)_W$  given by Warner (1968) were used.

It is apparent from Fig. 11 that the lines of high excitation potential,  $E_2 \geq 56$  kK, are in error as they lie significantly below the curve of growth. This indicates a systematic error in the determination of oscillator strengths for high excitation lines by astrophysical analysis.

The data from lines with  $E_2 \leq 56$  kK indicate a solar iron abundance of  $7.28 \pm 0.13$ , where the uncertainty represents the approximate scatter in the data. This value is in good agreement with the results of our experiment, showing that some use can be made of the values given by Warner (1967) when they are corrected as shown in Eq. 5-20 and Eq. 5-21.

The solar iron abundance value of  $7.35 \pm 0.18$  determined in this section clearly disagrees with the old result of 6.5 obtained by Goldberg et al. (1960) and others for Fe I and Warner (1968) for Fe II. On the other hand, it is lower than the recent values determined from

other studies of Fe II and Fe I (see Sect. 2.1). These studies indicated an abundance of from 7.45 to 7.65. However, considering the large uncertainty in our value, it must be concluded that our result supports an abundance in this range.

#### 5.4 POSSIBLE ERRORS IN THIS WORK

There are several criticisms that can be made of this work. It would be interesting to discuss them briefly, especially to consider any possible effects upon the results.

- (a) The measured lifetimes may be in error, despite the close agreement with the results of Anderson (1970). As shown in Sect. 3.2, when there is one cascading level above the level of interest, the desired lifetime is usually the shortest observed in any cascading decay. It is possible that the lifetime measured is that of a cascade from a higher level and that the true lifetime is somewhat shorter. This is not likely for all levels measured; at least some lifetimes are probably correct. If the measured lifetime was longer than the correct value, it can be seen from Eq. 5-1,

$$A = \frac{1}{\tau} (\text{Branching Ratio}),$$

that the correct transition probabilities would be larger than those given.

- (b) If some of the strong lines had been self-absorbed (see Sect. 4.6) in the hollow cathode discharge, the branching ratios for the strong lines would be too small and those for the weak lines would be too large. From Eq. 5.1, this would lead to transition probabilities that were too small for the strong lines and transition probabilities that were too large for the weak lines. No evidence for such an effect is seen in Fig. 9.
- (c) It is possible that the tables of Moore (1945, 1950) do not list all possible decay channels for the upper levels studied. This could be because the lines omitted were very weak or because they were outside the wavelength range covered in the tables ( $200 \text{ \AA} \leq \lambda \leq 13000 \text{ \AA}$ ). In either case, our branching ratios would be too large and, consequently, the measured transition probabilities would also be too large. Use of the correct A values would increase the discrepancy between our work and that of Warner (1967) but would give a larger value for the solar iron abundance calculated from our values, more in agreement with other recent determinations (see Sect. 5.4). It is difficult to make a quantitative estimate of this effect upon the results, although it is expected to be small.
- (d) The only portion of the spectrometer efficiency calibrations which was not measured or at least checked during this work was the calibration of the McPherson instrument for  $\lambda \leq 2500 \text{ \AA}$  (see Appendix D). This measurement had been made by Martinez but could not be repeated because there was no other

high quality monochromator that could be used with the Xenon lamp to form a monochromatic source. The Czerny-Turner optics of the McPherson instrument involve three reflecting surfaces (see Fig. 17). The reflectance of these surfaces for short wavelengths may decrease with time because of an accumulation of dust, oil, etc. on the surfaces. If this were the case, the branching ratio for the lines below 2250 Å would have been larger than that measured. Consequently, the branching ratios for the other lines from the same upper levels would have been smaller, giving, as a result, smaller transition probabilities for the lines from upper levels  $y^2G_{9/7}^0$  and  $y^2G_{7/2}^0$ . If the transition probabilities were smaller, the discrepancy between our work and that of Warner would increase and a larger value for the solar iron abundance would result from our work.

## APPENDIX A

Reprinted from:

PHYSICAL REVIEW

VOLUME 188, NUMBER 1

5 DECEMBER 1969

Equilibrium Charge Distributions of C, N, Ar, and Fe in Carbon<sup>†</sup>

Peter L. Smith and Ward Whaling

California Institute of Technology, Pasadena, California 91109

(Received 1 July 1969)

The equilibrium charge distributions have been measured for carbon and argon in the energy range from 370 to 1450 keV, for iron in the energy range from 190 to 1450 keV, and for nitrogen from 180 to 1450 keV. Equilibrium was established by passing accelerated ions through  $10 \mu\text{g}/\text{cm}^2$  carbon foils. The ions of different charge were separated electrostatically and detected with a CsI(Tl) scintillator. Additional measurements were made to ensure that equilibrium had been achieved and that the effect of the residual gas was small. The values of the charge fractions are thought to be correct to within  $\pm 5\%$  and agree well with the limited available data.

## INTRODUCTION

Knowledge of the equilibrium charge distribution resulting from the passage of high-velocity ions through matter is useful in the planning and analysis of experiments in several fields. For example, in tandem accelerators, ions are stripped at the high-voltage terminal. Also, in energy-loss calculations, it is necessary to know the mean-squared charge on the stopped ion. Our particular interest is for beam-foil spectroscopy, in which the ion velocity is chosen to optimize production of the ionic state of interest. Also, the identification of the radiating ion is aided by the knowledge of the relative charge fractions and their variation with energy. There is no theory which allows one to calculate the charge distributions, although empirical formulas have been developed for use in fitting data.<sup>1,2</sup> Consequently, such equilibrium charge distributions must be measured experimentally.

## EXPERIMENTAL METHOD

The apparatus is shown in Fig. 1. The ions were produced in a thermal source<sup>3</sup> in the high-voltage terminal of an electrostatic accelerator. The desired mass was selected by magnetic deflection, which bent the beam through  $6^\circ$ , followed by electrostatic deflection through  $80^\circ$  to measure and control the ion energy. The electrostatic analyzer was calibrated against the  $^{19}\text{F}(\rho, \alpha\gamma)^{16}\text{O}$  resonance at 340.45 keV before and after the measurements. The uncertainty in the incident beam energy was  $\pm 1\%$ .

The beam passed through collimator A ( $0.05 \times 0.84$  mm) and then through a self-supporting carbon foil where the charge-state equilibrium was established. The supplier<sup>4</sup> quoted a foil thickness  $10 \pm 4 \mu\text{g}/\text{cm}^2$  whereas our own measurements of the energy of the ions emerging from the foil,

again by electrostatic deflection, are consistent with the energy loss in a foil of thickness  $10 \pm 2 \mu\text{g}/\text{cm}^2$ . To decrease straggling for iron beams of 200, 300, and 400 keV,  $5 \pm 3 \mu\text{g}/\text{cm}^2$  foils were used. Collimator B (0.025 mm diam) defined a narrow beam which was then separated into the various charge components in an electric field. The particles were detected by two thin CsI(Tl) scintillators viewed by a Dumont 6291 phototube outside the vacuum. The distance from the foil to the scintillators was 29 cm. The pressure in the target chamber was less than  $10^{-5}$  mm Hg at all times.

In order to avoid problems resulting from the fluctuations in the intensity of the ion beam, a series of alternating measurements of the number of particles in a given charge state and then of the number in the total beam were made, each for the same time interval. The sequence timer controlled this operation; gating the scalars, switching the voltage on the deflector plates, and blocking the neutral beam when a certain charge state was being measured. The cycle of measurements lasted 5 sec and was repeated three times for each value of the voltage on the deflector plates. As the deflector voltage was varied, each charge state was swept across the upper scintillator. A typical plot of the results is shown in Fig. 2. The neutral component was measured by selecting a deflector voltage at which no charge state hit the upper scintillator (e.g., at a value of 700 in Fig. 2) and by deactivating the chopper to allow the neutral component to strike the lower scintillator.

Preliminary attempts at such measurements employed surface-barrier detectors, including position-sensitive detectors. These proved to be unsatisfactory, at least for heavy ions such as iron and argon, because of energy loss and straggling in the gold window and because of the pulse-height defect for heavy ions. In addition, because

## EQUILIBRIUM CHARGE DISTRIBUTION

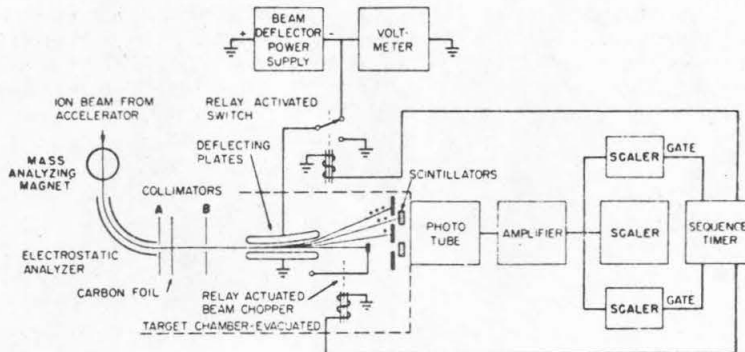


FIG. 1. Schematic diagram of charge-distribution measurement apparatus.

the beam collimators defined a very small area, the dose (or particles per unit area) quickly damaged the detector.

## DISCUSSION OF RESULTS

The slit in front of the upper scintillator was considerably wider than the physical spread of the beam, which was determined by the collimators and by the variations in energy resulting from straggling in the foil. Consequently, the peaks in Fig. 2 have flat tops which give the values of the charge fractions. Note that the background was about 0.4%. It was generally less than 1% but significantly greater than the beam-independent background. When corrected for the small background, the sum of the charge fractions was seldom exactly unity, usually averaging about 0.98. Various explanations for the background and for the loss of beam were considered: charge-changing collisions with the residual-gas mole-

cules, the decay of autoionizing levels, scattering from the residual gas or the deflector plates, extreme energy loss and straggling in the foil, and scattering from the edges of collimator B (a 0.025-mm hole punched in 0.0064-mm aluminum foil). Only the last explanation is consistent with the observation of a flat pressure-independent background.

The intensity of the beam from the accelerator was adjusted to give at least 1000 total beam counts per second in the undeflected beam or at least 6000 per point. As the average of all the points in the flat portion of the curve was used to compute the charge fraction, the statistical uncertainty was generally less than 1%. However, fluctuations in the accelerator beam current led to a much larger root-mean-square deviation from the average for the points in the flat portion of the curve. The relation  $(\Delta P/P) \leq \pm 5\%$ , where  $P$  is the charge fraction and  $\Delta P$  is the rms deviation of the values which were averaged to give  $P$ ,

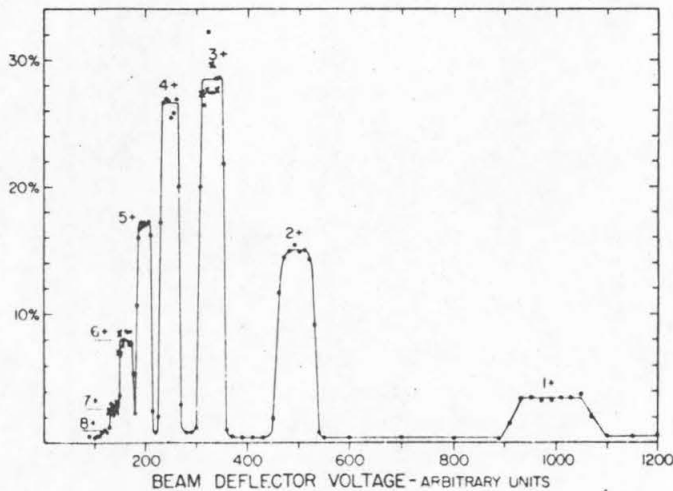


FIG. 2. Ratio of counts in upper scintillator to counts in lower scintillator as a function of the voltage on the deflector plates for argon at 1450-keV beam energy. The circles and crosses refer to separate sets of measurements. The curve is drawn to aid the eye.

## EQUILIBRIUM CHARGE DISTRIBUTION

holds for two-thirds of the values for which  $P \geq 10\%$ . Thus, we think that the measured values of the charge fractions are accurate to  $\pm 5\%$  of their values (i. e.,  $P \pm 0.05 P$ ).

Corrections were made for the energy loss in the foil following a theoretical treatment by Lindhard, Scharff, and Schiott.<sup>5</sup> Only the electronic stopping term was considered because the particles which passed through the collimators were not those which had undergone large-angle nuclear scatterings. The results are tabulated in Table I.

Various studies were made to determine the effect of the beam on the foils. The energy loss in the foil was observed to increase by about 50% after 2 h of bombardment. Normally, the foils were used for about 5 min.

For iron with beam energies of 700 and 1500 keV and for nitrogen with a beam energy of 1400 keV, foils of both 10 and 20  $\mu\text{g}/\text{cm}^2$  thickness were used. When corrected for energy loss, the data

were consistent for the two foils, indicating that equilibrium had been established in the thinner foil.

## COMPARISON WITH OTHER MEASUREMENTS

There are few data available in the literature for these ions in this energy range. Seeger and Kavanagh<sup>6</sup> have published data for carbon in VN from 1.65 to 3.5 MeV. Our data extrapolate smoothly to fit theirs. There are no data for iron.

There are data for celluloid targets at 680 and 1220 keV with a nitrogen beam and at 1400 keV with an argon beam.<sup>7</sup> Comparison with our results is shown in Table II and, for nitrogen only, in Fig. 3. The agreement is within the uncertainty of the values which are taken from the graphs in Ref. 7. The dependence on foil material is not expected to be significant.<sup>1</sup>

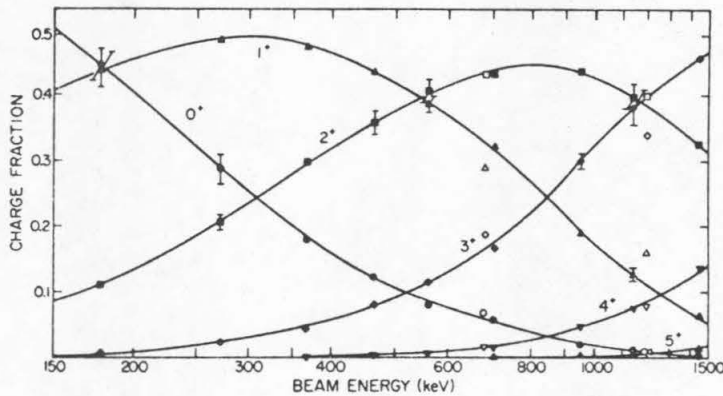


FIG. 3. Equilibrium charge distribution for nitrogen in carbon foils. The open symbols refer to data from Ref. 7. Root-mean-square deviations less than  $\pm 0.02$  are not shown. The curves are drawn to aid the eye.

TABLE II. Comparison of present measurements in carbon foils with those of Nikolaev *et al.* (Ref. 7) in celluloid. California Institute of Technology (Caltech) values are taken from smooth curves through experimental points listed in Table I.

Charge	Argon 1400 keV		Nitrogen			
	Caltech	Ref. 7	680 keV		1220 keV	
			Caltech	Ref. 7	Caltech	Ref. 7
0	0.0	0	6.0	7	1.0	1
1	3.3	3	32.5	29	11.2	16
2	15.3	15	43.2	43	38.4	40
3	28.8	29	16.6	19	39.9	34
4	26.1	27	1.7	2	8.7	8
5	16.3	15			0.8	1
6	7.4	8				
7	2.3	3				
8	0.5					

TABLE I. Equilibrium charge fractions (%) as a function of emergent beam energy.

Energy (keV)	Iron									
	190	289	388	468	566	664	761	957	1154	1450
Ion charge										
0	30.9±1.7	20.7±0.6	14.7±0.5	10.9±0.7	8.2±0.7	5.1±0.2	4.2±0.3	1.9±0.1	1.8±0.2	0.3±0.1
1	55.9±3.0	53.4±2.0	47.1±0.7	41.6±0.8	33.3±1.2	25.9±0.4	21.2±0.8	12.7±0.7	7.4±0.8	3.5±0.1
2	11.5±1.0	19.7±1.0	25.4±1.2	28.1±0.2	29.7±0.9	29.5±0.3	27.6±0.7	21.9±0.7	14.8±1.5	8.9±0.4
3	1.5±0.1	4.9±0.5	9.1±0.6	12.6±0.7	17.5±0.6	21.1±0.2	22.6±0.4	24.3±1.0	23.1±1.0	16.7±0.2
4	0.2±0.1	1.1±0.1	3.1±0.1	5.3±0.2	8.2±0.3	12.3±0.5	15.6±0.4	20.8±1.0	23.6±1.4	26.0±0.5
5		0.2±0.1	0.6±0.1	1.5±0.1	2.8±0.2	4.9±0.2	6.9±0.4	12.4±0.4	17.2±0.8	24.3±0.7
6					0.4±0.1	1.2±0.1	1.7±0.1	4.8±0.4	8.7±0.8	13.8±0.7
7							0.2±0.1	1.2±0.1	2.6±0.2	5.2±0.2
8									0.6±0.1	1.1±0.1
9									0.2±0.1	0.2±0.1

Energy (keV)	Nitrogen									
	180	275	373	465	567	713	960	1155	1450	
Ion Charge										
0		44.5±2.5	31.0±2.2	18.2±0.9	12.4±0.4	8.2±0.3	6.0±0.2	2.2±0.1	1.3±0.1	0.3±0.1
1		43.6±2.7	46.8±0.8	47.4±0.6	43.4±0.4	38.6±1.2	32.2±0.8	19.0±0.4	12.8±1.0	6.3±0.1
2		11.1±0.9	20.0±1.2	28.8±0.5	35.8±1.7	40.7±1.7	43.2±0.5	43.7±0.6	39.8±1.9	32.6±0.4
3		0.7±0.1	2.2±0.1	4.5±0.2	8.1±0.3	11.7±0.4	16.9±0.5	30.0±1.2	38.1±2.8	45.8±0.5
4				0.1±0.1	0.4±0.1	0.8±0.1	1.5±0.1	4.8±0.3	7.5±0.6	13.8±0.1
5							1.1±0.1	0.3±0.1	0.5±0.1	1.2±0.1

Energy (keV)	Argon							
	372	469	566	762	958	1155	1450	
Ion charge								
0			7.5±0.5	4.8±0.4	3.4±0.3	1.5±0.1	0±0.1	0±0.1
1			35.0±1.9	26.7±0.8	22.9±1.2	14.4±0.4	8.7±0.2	5.9±0.3
2			31.9±1.5	33.8±1.0	33.2±1.8	30.2±1.0	25.5±0.7	20.3±0.6
3			18.4±0.9	23.0±0.7	25.5±1.7	29.8±0.7	32.7±0.9	31.3±0.5
4			5.9±0.3	8.8±0.2	10.8±1.2	15.7±1.0	20.3±0.4	23.8±0.5
5			1.3±0.1	2.3±0.4	3.4±0.2	6.2±0.2	8.8±0.3	12.4±0.4
6			0.1±0.1	0.5±0.1	0.8±0.1	1.7±0.2	3.1±0.1	5.0±0.3
7						0.4±0.1	0.8±0.1	1.2±0.1
8								0.1±0.1

Energy (keV)	Carbon							
	369	470	567	762	960	1156	1450	
Ion charge								
0		18.7±0.6	12.7±0.3	10.0±0.3	4.5±0.4	2.5±0.6	1.0±0.1	0.4±0.2
1		51.0±0.3	48.1±2.3	43.1±2.0	33.8±1.9	23.8±2.0	16.1±0.7	8.3±0.5
2		27.3±0.9	34.4±2.1	39.6±1.3	47.7±2.0	50.6±4.1	49.7±2.4	43.1±2.8
3		2.9±0.2	4.6±0.2	6.7±0.8	13.0±0.5	20.8±1.6	29.2±1.9	40.6±1.4
4		0.1±0.1	0.1±0.1	0.6±0.1	1.0±0.2	2.1±0.2	4.0±0.2	7.5±0.3

P. L. SMITH AND W. WHALING

<sup>†</sup>Supported in part by the National Science Foundation (GP-9114) and the Office of Naval Research [Nonr-220 (47); Nonr-220(49)].

<sup>1</sup>C. S. Zaidins, California Institute of Technology, 1962 (unpublished) [a somewhat condensed version of this report may be found in J. B. Marion and F. C. Young, *Nuclear Reaction Analysis* (North-Holland Publishing Co., Amsterdam, 1968)]; Ph.D. thesis, California Institute of Technology, 1967 (unpublished), Appendix I.

<sup>2</sup>I. S. Dmitriev and V. S. Nikolaev, *Zh. Eksperim. i Teor. Fiz.* 47, 615 (1964) [English transl.: *Soviet Phys. - JETP* 20, 409 (1965)].

<sup>3</sup>G. D. Magnuson, C. E. Carlston, P. Mahadevan, and A. R. Comeaux, *Rev. Sci. Instr.* 36, 136 (1965).

<sup>4</sup>Yissum Research Development Company, Hebrew University, Jerusalem, Israel.

<sup>5</sup>J. Lindhard, M. Scharff, and H. E. Schiott, *Kgl. Danske Videnskab. Selskab, Mat.-Fys. Medd.* 33, No. 14 (1963).

<sup>6</sup>P. A. Seeger and R. W. Kavanagh, *Nucl. Phys.* 46, 577 (1963).

<sup>7</sup>V. S. Nikolaev, I. S. Dmitriev, L. N. Fateeva, and Ya. A. Teplova, *Zh. Eksperim. i Teor. Fiz.* 39, 627 (1961) [English transl.: *Soviet Phys. - JETP* 12, 627 (1961)].

---

## APPENDIX B

NUCLEAR INSTRUMENTS AND METHODS 90 (1970) 47-50; © NORTH-HOLLAND PUBLISHING CO.

LIFETIMES AND TRANSITION PROBABILITIES FOR SOME Fe II LEVELS  
BY THE BEAM-FOIL METHOD†

P. L. SMITH\*, W. WHALING and D. L. MICKEY

California Institute of Technology, Pasadena, California, U.S.A.

The lifetimes of five levels in Fe II have been determined by the beam-foil method. Measurements were made at several energies between 200 and 400 keV using both 5 and 10  $\mu\text{g}/\text{cm}^2$  carbon foils. The various results for a given level agree to within  $\pm 8\%$  and show no significant variation with energy. There is good agreement with the results of Andersen. The experimental total transition probability, or reciprocal of the lifetime, was compared

## 1. Introduction

The amount of iron in the sun is an important astrophysical quantity that has been measured by many observers in several different ways. Unfortunately, the results of different measurements have been consistently contradictory. Determinations based on the strength of allowed transitions in Fe I and Fe II in the photosphere agreed in yielding an iron abundance ten times lower than results of measurements based on forbidden emission lines observed in the corona. Recent new values for the transition probabilities in Fe I<sup>1)</sup> and Fe II<sup>2)</sup> have brought the photospheric and coronal values into agreement. To check the  $gf$  values, which are a possible source of error in the old abundance determinations, we are using the beam-foil method to remeasure the transition probabilities for several lines in Fe II. These absolute normalization points should fix the scale of Fe II transition probabilities with a reliability equal to that of Fe I.

## 2. Lifetime measurement

The lifetimes were measured by the beam-foil technique. Our equipment is shown schematically in fig. 1. Iron ions were produced in a thermal source and accelerated with a Van de Graaff accelerator to energies of 200 to 400 keV. Mass and energy analysis insured that we had only iron ions with a velocity which was constant to within  $\pm 1\%$ . The Fe<sup>+</sup> ions were directed through a carbon foil 5 to 10  $\mu\text{g}/\text{cm}^2$  thick. The carbon was mounted on a tungsten mesh of 0.025 mm thickness, 8 lines/mm and 70% transmission. The mesh served to prolong the life of the carbon foil and yet did not appear to affect the lifetime measurements.

At the energies used, about 50% of the ions emerging

to the transition probability calculated from the oscillator strengths of Warner, corrected by using the normalization function of Warner and Cowly. There is disagreement by roughly a factor of three which would be significant in solar iron abundance calculations based on Fe II. It will be necessary to determine accurate branching ratios for all the transitions which depopulate the upper-levels studied in order to resolve this discrepancy.

from the foil were singly ionized<sup>3)</sup>. Lifetimes of those ions in excited electronic states were measured by time-of-flight techniques. A 0.3 m monochromator was mounted on a lathe bed so that it could be moved parallel to the moving beam of ions. The counting period was normalized by observing with the stationary monitor phototube. A Corning 7-51 filter in front of this phototube limited the light seen to the range 3300 to 4000 Å.

The wavelength range from 2300 to 2800 Å was scanned using a front-surface mirror at 45° to the ion beam to permit observation along the line of motion (see inset in fig. 1). This resulted in the maximum intensity with the minimum of Doppler broadening possible for our optical system. A portion of the resulting spectrum is shown in fig. 2. The identifications were easily made using the table of  $f$ -values published by Warner<sup>4)</sup>.

One of the light decay curves at 2592.78 Å is shown in fig. 3. The upper graph shows the data plotted on a

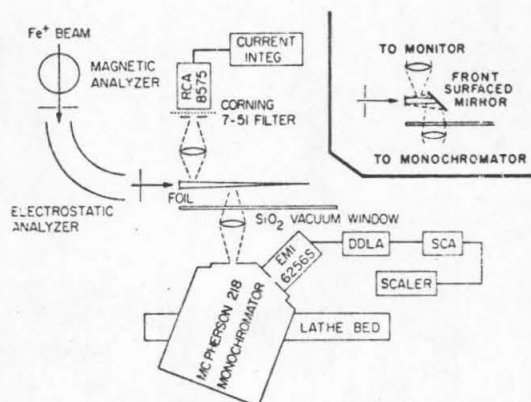


Fig. 1. Schematic diagram of lifetime measurement apparatus. The inset shows the apparatus used to determine the spectrum.

\* Presented the paper.

† Supported in part by the National Science Foundation (GP-9114, GP-19887) and the Office of Naval Research [Nonr-220(47)] and (N00014-67-A-0094-0015).

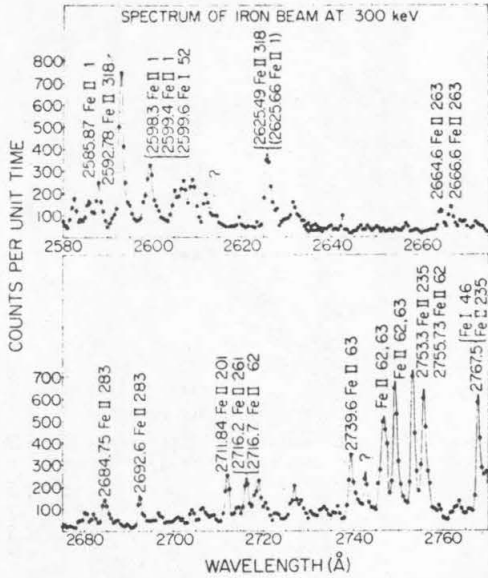


Fig. 2. The spectrum from 2580 Å → 2780 Å of the foil excited iron beam at 300 keV.

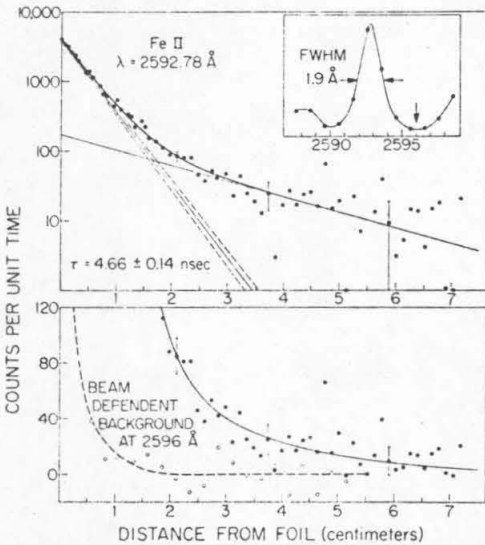


Fig. 3. The light decay curve at 2592.78 Å for an iron beam of 250 keV incident on a 5 μg/cm<sup>2</sup> foil. Typical statistical errors are shown. The solid curves show the computer generated, two exponential fit. The line profile is shown in the inset.

logarithmic scale while the lower one shows the tail of the curve and the beam dependent, continuum background which was measured at 2596 Å.

3. Results

In order to determine the lifetime from the decay curve, several corrections were necessary. Some of the ions were scattered outside the field of view of the optical system. Measurements of the beam profile were made by scanning across the image of the beam on the entrance slit of the monochromator. The shape was approximately Gaussian. The results, some of which are shown in fig. 4, showed that the spreading was

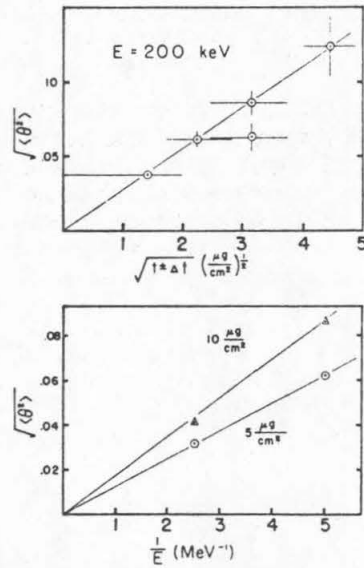


Fig. 4. Experimentally determined root-mean-square scattering angles for iron on carbon as a function of foil thickness and beam energy.

roughly proportional to  $t^{1/2}E^{-1}$ . In the worst cases, observations at a large distance from the foil had to be corrected by as much as 20% to account for ions which had scattered too far. However, these corrections had a negligible effect on the value of the lifetime.

Another correction was made for the change in velocity as a result of energy loss in the foil. Only the electronic stopping term in the theoretical analysis of Lindhard et al.<sup>5</sup> was used because the particles observed had not undergone large angle nuclear scatterings. The energy loss correction was increased by some 30% in view of the experimental results of Fastrup et al.<sup>6</sup>

TABLE I  
Fe II lifetime measurements.

$\lambda$ (Å)	Multiplet no. <sup>a)</sup>	Lifetime (nsec)	
		$\tau_{\text{CIT}}$	$\tau_{\text{ref. 7}}$
2592.78	318 u	4.48 ± 0.4	4.5 ± 0.3
2625.49	318 u	4.64 ± 0.4	4.5 ± 0.3
2550.02	240 u	(3.6 ± 0.8)	3.8 ± 0.6
2550.68	240 u		
2666.63	263 u	3.80 ± 0.3	4.3 ± 0.3
2664.66	263 u	4.26 ± 0.3	
2753.29	235 u	5.00 ± 0.3	4.8 ± 0.3
2767.50	235 u	(4.6 ± 0.8)	4.8 ± 0.3

There was considerable uncertainty in both these foil-dependent corrections because the foil thickness was known only to ± 40%. However, measurements of the same lifetime with foils of both 5 and 10  $\mu\text{g}/\text{cm}^2$  thickness gave essentially identical results. The data were fitted as the sum of two exponentials with a non-linear least squares computer program which minimized the following function:

$$\chi^2 = \sum_i \left[ \frac{x_{i,\text{data}} - x_{i,\text{calculated}}}{(\text{statistical error})_i} \right]^2$$

The r.m.s. deviation of measurements taken over a range of energies from 200 to 400 keV was at most ± 8% and showed no significant dependence upon energy. The values for the lifetimes, averaged over all measurements, are shown in table 1, column 3. There is good agreement with the results of Andersen<sup>7)</sup> as shown in table 1, column 4. The two values in parentheses are the results of preliminary measurements, but, because of the good agreement with ref. 7, they have been included.

#### 4. Transition probabilities

If a level decays by several channels, the lifetime is related to the transition probabilities,  $A_i$ , of the various channels by the relation:

$$1/\tau = A = \sum_i A_i \quad (\text{summed over all decays}).$$

If relative transition probabilities are available, then measurement of the lifetime permits normalization of all the  $A_i$ . For Fe II, relative transition probabilities can be calculated from the table of relative oscillator strengths published by Warner<sup>4)</sup>. This does not give oscillator strengths for all known branches with  $\lambda > 2500$  Å nor for any of those with  $\lambda < 2500$  Å. It is probably valid to assume that the omitted branches with  $\lambda > 2500$  Å are weak but Moore<sup>8)</sup> lists some strong branches at shorter wavelengths (see table 2).

Some comparison with the results of Warner<sup>4)</sup> is possible. We have  $1/\tau_{\text{CIT}} = A_{\text{CIT}}$  and

$$A_{\text{W}} = \sum_{(\text{all branches})} (A_i)_{\text{Warner}} \geq \sum_{(\text{some branches})} (A_i)_{\text{Warner}}$$

The known branches from ref. 8 and the oscillator strengths from ref. 4 are given in table 2. The fact that oscillator strengths for some decays are not known means that we can calculate only a lower limit to the total transition probability using the results of

TABLE 2

Possible decay modes for the levels whose lifetimes were measured. The level designations, multiplet numbers and intensities are from Moore<sup>7)</sup>. The wavelengths of the lines for the lifetimes were measured are marked with an asterisk. Decay modes for the preliminary measurements have not been included.

Upper level	Lower level	Multiplet	$\lambda$ (Å)	Intensity	$\log_{10} gf$ from Warner <sup>4)</sup>
$z^2K^0_{15/2}$	$a^2I_{13/2}$	318 u	2592.78*	9	0.82
$z^2K^0_{13/2}$	$a^2I_{11/2}$	318 u	2625.49*	9	0.78
	$a^2I_{13/2}$	318 u	2623.13	4	
$y^2G^0_{9/2}$	$a^2F_{7/2}$	263 u	2664.67*	10	0.48
	$b^2F_{7/2}$	98	3044.84	5	-1.17
	$c^2F_{7/2}$	168	5019.48	0	
	$a^2G_{9/2}$	93 u	2040.69	25	
	$b^2G_{7/2}$	278 u	2934.49	3	
	$b^2G_{9/2}$	278 u	2902.46	5	-1.01
	$c^2G_{9/2}$	120	3187.29	8	-0.39
	$b^2H_{9/2}$	239 u	2598.03	2	
	$b^4D_{7/2}$	85	2997.75	tr	
	$b^4F_{9/2}$	182 u	2369.23	1	
	$b^4F_{7/2}$	182 u	2379.00	2	
	$a^4G_{9/2}$	205 u	2561.58	1	-1.55
	$a^4G_{7/2}$	205 u	2573.21	5	-0.63
	<del><math>a^4H_{11/2}</math></del>	<del>167 u</del>	<del>2303.25</del>	<del>1</del>	<del>0.63</del>
	$a^2I_{11/2}$	107	3131.72	4	-1.33
$y^2G^0_{7/2}$	$a^2F_{5/2}$	263 u	2666.63*	10	0.40
	$a^2F_{7/2}$	263 u	2645.08	3	-0.90
	$b^2F_{5/2}$	98	3002.33	5	
	$c^2F_{5/2}$	168	4953.98	0	-1.85 *
	$a^2G_{7/2}$	93 u	2051.03	25	
	$a^2G_{9/2}$	93 u	2029.18	8	
	$b^2G_{7/2}$	278 u	2910.76	4	
	$b^2G_{9/2}$	278 u	2879.24	3	-1.14
	$c^2G_{7/2}$	120	3162.80	8	-0.68
	$b^2H_{9/2}$	239 u	2579.41	3	-0.88
	$a^2G_{7/2}$	205 u	2554.95	1	-1.21
	$a^2G_{5/2}$	205 u	2559.77	5	-0.51
	$a^4H_{9/2}$	167 u	2296.66	0	
$z^2I^0_{11/2}$	$a^2H_{9/2}$	117 u	2388.39	3	
	$b^2H_{9/2}$	235 u	2753.29*	12	0.58
	$a^2I_{11/2}$	105	3360.10	3	-1.33
	<del><math>a^2I_{9/2}</math></del>	<del>105</del>	<del>3356.24</del>	<del>tr</del>	
	$a^4G_{9/2}$	201 u	2712.39	6	-0.47
	$a^4G_{11/2}$	201 u	2684.94	3	
	$a^4H_{9/2}$	164 u	2433.50	4	
	$a^4H_{13/2}$	164 u	2414.08	1	

## II. LIFETIMES AND TRANSITION PROBABILITIES

\* from Warner (1968)

TABLE 3

Comparison of total transition probabilities with the results of Warner<sup>4)</sup> and Warner and Cowley<sup>9)</sup>. The column headings are explained in the text. Note that the values in the last four columns are lower limits. Parentheses indicate results of preliminary measurements (see text).

$\lambda$ (Å)	Transition	EP (cm <sup>-1</sup> )	$A_{CIT}$ ( $\times 10^8$ sec <sup>-1</sup> )	$A_w$ ( $\times 10^8$ sec <sup>-1</sup> )	$\frac{A_w}{A_{CIT}}$	$\frac{A_w'}{A_{CIT}}$	$\frac{A_{wc}}{A_{CIT}}$
2592.78	a <sup>2</sup> I <sub>13/2</sub> -z <sup>2</sup> K <sub>15/2</sub> <sup>0</sup>	71433	2.24	≥ 4.10	≥ 1.82	≥ 67.5	≥ 0.338
2625.49	a <sup>2</sup> I <sub>11/2</sub> -z <sup>2</sup> K <sub>13/2</sub> <sup>0</sup>	70987	2.16	4.16	1.93	68.3	0.368
2550.02	b <sup>2</sup> H <sub>9/2</sub> -z <sup>2</sup> H <sub>9/2</sub> <sup>0</sup>	65556	(2.78)	4.51	(1.62)	(30.8)	(0.332)
2550.68	b <sup>2</sup> H <sub>11/2</sub> -z <sup>2</sup> H <sub>11/2</sub> <sup>0</sup>	65364		3.98	(1.43)	(26.6)	(0.292)
2666.63	a <sup>2</sup> F <sub>5/2</sub> -y <sup>2</sup> G <sub>7/2</sub> <sup>0</sup>	65110	2.63	(3.82)	1.49	27.1	0.314
2664.66	a <sup>2</sup> F <sub>7/2</sub> -y <sup>2</sup> G <sub>9/2</sub> <sup>0</sup>	64832	2.35	(3.91)	1.63	28.0	0.326
2753.29	b <sup>2</sup> H <sub>9/2</sub> -z <sup>2</sup> I <sub>11/2</sub> <sup>0</sup>	62662	2.00	3.08	1.54	21.3	0.338
2767.50	b <sup>2</sup> H <sub>11/2</sub> -z <sup>2</sup> I <sub>13/2</sub> <sup>0</sup>	62293	(2.18)	≥ 2.92	(≥ 1.32)	(≥ 17.7)	(≥ 0.264)

Warner<sup>4)</sup>. The ratio  $A_w/A_{CIT}$  is given in table 3, column 6.

There has been some discussion in the literature of a normalization function used by Warner<sup>4)</sup>. This is a function,  $C(\chi)$ , of the excitation potential,  $\chi$ , of the upper level which was applied to the oscillator strengths for  $\chi \geq 6$  eV  $\approx 48000$  cm<sup>-1</sup> in order to give agreement between observed and calculated oscillator strengths. The values from Warner<sup>4)</sup> without this correction are compared with our results in table 3, column 7 as  $A_w'/A_{CIT}$ . Warner and Cowley<sup>9)</sup> modified  $C(\chi)$  for Fe II, and transition probabilities ( $A_{wc}$ ) calculated from their  $gf$  values are also compared with our results in table 3, column 8. Neither correction yields values in agreement with experiment although the discrepancy between our work and that of Warner and Cowley<sup>9)</sup> may lessen as more branches are added to the sums.

The present lifetime measurements are for levels with a rather limited range of excitation potential;  $62000$  cm<sup>-1</sup>  $\leq \chi \leq 72000$  cm<sup>-1</sup>. As the normalization function is dependent on  $\chi$ , it would be interesting to measure lifetimes of levels with a broader range of excitation potentials. However, lower levels tend to exhibit repopulation by cascading which makes lifetime measurements difficult. The oscillator strengths for most of the lines studied by Baschek et al.<sup>2)</sup> confirm that the normalization function of Warner and Cowley<sup>9)</sup> is approximately correct for  $\chi \approx 44000$  cm<sup>-1</sup>.

In order to resolve some of the confusion we are attempting to measure the branching for the various decays which depopulate our upper levels. These branching ratios, combined with the lifetime measurements, will give absolute transition probabilities.

Whaling et al.<sup>1)</sup> discuss similar measurements for Fe I. The absolute transition probabilities will be independent of other work and thus will normalize the relative values used in solar iron abundance calculations based on Fe II.

#### References

- 1) W. Whaling, M. Martinez-Garcia, D. L. Mickey and G. M. Lawrence, Proceedings of this conference.
- 2) B. Baschek, T. Garz, H. Holweger and J. Richter, *Astron. Astrophys.* 4 (1970) 229.
- 3) P. L. Smith and W. Whaling, *Phys. Rev.* 188 (1969) 36.
- 4) B. Warner, *Mem. R. Astron. Soc.* 70 (1967) 165.
- 5) J. Lindhard, M. Scharff and H. E. Shiot, *Kgl. Danske Vid. Selsk. Mat.-Fys. Medd.* 33, no. 14 (1963).
- 6) B. Fastrup, P. Hvelplund and C. A. Sautter, *Kgl. Danske Vid. Selsk. Mat.-Fys. Medd.* 35, no. 10 (1966).
- 7) T. Andersen, University of Aarhus, Aarhus, Denmark, private communication.
- 8) C. E. Moore, *An ultraviolet multiplet table*, U.S. Nat. Bur. Std. Circular 488 (1950); and *A multiplet table of astrophysical interest*, rev. ed. (Princeton University Observatory, 1945).
- 9) B. Warner and C. R. Cowley, *J. Quant. Spectr. Radiative Transfer* 7 (1967) 751.

#### Discussion

BICKEL: Have your angular distributions been corrected for depth of focus?

SMITH: No. However, because there is some discrepancy between our results and those of other groups, I should point out that we have quoted the r.m.s. scattering angle rather than the angular width of the beam profile.

BERRY: With or without correction factors these results do not agree with our angular distribution measurements.

Note added in proof by Smith: Consideration of the optical system used showed that no correction for the depth of focus was necessary.

## APPENDIX C – OPTICAL EQUIPMENT AND COMPONENTS

## C.1 LENSES

The lenses used throughout the work described were quartz-lithium fluoride\* achromats designed by Dr. R. B. King (Caltech). The design focal length was 18.37 cm with a maximum aperture of 50 mm. The construction parameters and the focal length as a function of wavelength are shown in Fig. 12. The measured focal length was  $18.3 \pm 0.1$  cm.

## C.2 FILTERS

Some portions of the efficiency calibration and branching ratio measurements required the use of filters to eliminate scattered light and unwanted orders. Glass and gelatin color filters<sup>†</sup> and multilayer-dielectric interference filters<sup>‡</sup> were used. When necessary, these filters were calibrated for transmission as a

---

\* Quartz; Type 151, General Electric Co., Willoughby, Ohio 44094.  
LiF; The Harshaw Chemical Co., Crystal-Solid State Department.

† Corning Glass Works, Optical Products Department, Corning, N. Y. 14830.

SCHOTT - Jena Glaswerk Schott + Gen., Mainz, West Germany.  
Eastman Kodak Co., Rochester, N. Y. 14650.

‡ Corion Instrument Corp., Waltham, Mass.  
Baird-Atomic Corp., Bedford, Mass. 01730.  
Optics Technology Inc., Palo Alto, Calif.

function of wavelength. The instruments used for this purpose were two Guilford spectrophotometers, Model 240, located in the Norman Church Laboratory for Chemical Biology at Caltech. These instruments read absorbance directly, where absorbance =  $\log_{10}(I_0/I)$ . These measurements were checked by observing, with a spectrometer, the Fe spectrum from the hollow cathode discharge. The filters were put into the optical path and the change in observed intensity was noted as a function of wavelength. For the broad-band color filters, with  $T$  = filter transmission,

$$\Delta T = |T_{\text{spectrophotometer}} - T_{\text{spectrometer}}| \leq 0.04 \quad (\text{C-1})$$

for wavelength ranges such that  $T \geq 0.10$ . Transmissions, as measured by either method, are probably accurate to within  $\pm 5\%$  for  $T \geq 0.6$ , the region where the filters are most used. The transmission curve for the Corning 7-54 filter, which was the most frequently used, is shown in Fig. 13.

The narrow band interference filters are very sensitive to correct alignment. Both the peak wavelength and the half width are dependent upon the angle of incidence. In addition, the peak transmission is of the order of 0.1 to 0.3. This is lower than that for the color filters and so transmission measurements made with the spectrometer are somewhat more difficult because of the decreased signal-to-noise ratio. The transmission values measured with a Guilford spectrophotometer and measured with the spectrometer

usually agreed to within  $\pm 10\%$  at the peak but often differed by as much as a factor 2 when  $T/T_{\text{maximum}} \leq 0.02$ .

### C.3 THE STANDARD LAMP\*

An incandescent tungsten ribbon-filament lamp was used as a standard of spectral radiance for  $2500 \text{ \AA} \leq \lambda \leq 6000 \text{ \AA}$ . The lamp was a General Electric Type 30A/T24/17 with an SR-8A filament. It was calibrated for operation at a current of 35 A a. c. by the Eppley Laboratory Inc., Newport, R.I. The calibration was made by comparing the lamp to two standards which in turn were calibrated against two National Bureau of Standards (NBS) lamps. The calibration of the latter could be traced to comparison with a blackbody as described by Stair *et al.* (1960). The calibration supplied by Eppley was expressed in terms of monochromatic brightness (microwatts  $(\text{cm}^2 \text{ of source})^{-1} (\text{steradian})^{-1} (\text{nanometer})^{-1}$ ) versus wavelength at various wavelength intervals. For convenience, this table was converted to monochromatic photon intensity (photons  $(\text{second})^{-1} (\text{cm}^2 \text{ of source})^{-1} (\text{steradian})^{-1} (\text{nanometer})^{-1}$ ). These data are shown in Fig. 14.

The lamp power supply and the auxiliary equipment used to calibrate the ammeters are shown in Fig. 15. The r. m. s. voltmeter was calibrated by R. G. Marcle (Caltech) to  $\pm 0.1\%$ .

---

\* See Drummond (1970) for discussions of precision radiometry.

After calibration, it was found that the lamp current could be repeatedly set to within  $\pm 0.2\%$  of the desired value of 35 A. This accuracy was necessary because it was found experimentally that small changes in the lamp current,  $c$ , had a significant effect on the photon intensity,  $N$ ;

$$\frac{dN}{N} \approx \frac{3.5 \times 10^4}{\lambda(\text{\AA})} \frac{dc}{c} . \quad (N = N(\lambda)) \quad (\text{C-2})$$

According to Stair et al. (1960), the maximum uncertainty in the calibration of the NBS standards ranges from about 8% at 2500 Å to about 3% at the longest wavelengths. It was assumed that the calibration provided by Eppley was correct to within these limits.

Eppley suggests an upper limit of 50 hours operation of these lamps at 35 A. After that time, the lamp should be recalibrated. In order to accomplish this, the laboratory purchased two such lamps with Eppley serial numbers 1130 and 1153. No. 1153 is used as a primary standard and No. 1130 is compared to it after 50 hours of use in order to detect any changes. Martinez had used lamp 1130 for some unknown time so it was judged that recalibration prior to our use was necessary.

The relative number of photons from the lamp seen by a detection system is  $n(\lambda) = I(\lambda) f(\lambda) \epsilon(\lambda) \Omega$  where the functions are defined in Appendix D. If two lamps are compared by using a given monochromator and filter then

$$\frac{n_1(\lambda)}{n_2(\lambda)} = \frac{I_1(\lambda) f(\lambda) \epsilon(\lambda) \Omega_1}{I_2(\lambda) f(\lambda) \epsilon(\lambda) \Omega_2} \quad (\text{C-3})$$

or, as  $\Omega_1 = \Omega_2$ ,

$$\frac{n_1(\lambda)/I_1(\lambda)}{n_2(\lambda)/I_2(\lambda)} = 1. \quad (\text{C-4})$$

If the geometry is changed somewhat, the ratio will not be 1, but will be constant as a function of wavelength.

The results of such a comparison are shown in Fig. 16. Lamp 1130 has increased its output, compared to the calibration values, by 13% at 2500 Å relative to the output in the visible range. This can be compared to the maximum uncertainty of 8% quoted by Stair et al. (1960). This discrepancy can be attributed only to aging of lamp 1130. The condition of lamp 1130 when used by Martinez is not known. Consequently, any deviation between his results and this work for the region  $2500 \text{ \AA} \leq \lambda \leq 3400 \text{ \AA}$  could be due to this discrepancy.

#### C. 4 McPHERSON SPECTROMETER SYSTEM\*

Each spectrometer was used with some particular auxiliary optical equipment. The entire spectrometer 'system' was calibrated (see Appendix D) and used as a unit.

The McPherson system is shown in Fig. 17 and consisted of a lens, a McPherson Model 218 spectrometer,<sup>†</sup> and a photomultiplier tube. The lens, described in Appendix C.1, was used to focus the image of the source onto the entrance slit. The spectrometer is of the Czerny-Turner type, with a focal length of 0.3 m and an aperture of f/5.3. The only moving part is the grating which rotates about an axis parallel to the grooves in order to change the wavelength. The grating used had 2400 lines/mm blazed at 3000 Å and was overcoated with MgF<sub>2</sub> to increase reflectivity in the ultraviolet. The reciprocal dispersion was 13.3 Å/mm. The resolving power was limited by the slit widths (see Eq. 4-1), whereas the wavelength resolution was limited to 0.3 Å by irregularities in the scanning mechanism.

---

\* The description of this instrument and of the Rowland Spectrometer (see Sect. C.5) as spectrometers or as monochromators is rather arbitrary but depends somewhat upon how they are being used, a spectrometer being used to measure spectral wavelengths and a monochromator being used to isolate and study a particular line. Both instruments were used in both roles.

<sup>†</sup> McPherson Instrument Corp., Acton, Mass.

An EMI 6256S photomultiplier tube\* was mounted at the exit slit. The tube was used in the photon counting mode and was cooled to dry-ice temperatures to reduce dark noise to one or two counts per second. In order to avoid condensation of water vapor on the window of the cooled tube, a light pipe consisting of a glass cylinder 25 mm long by 10 mm diameter was used. The internal surface was 'silvered' with aluminum, the volume was filled with dry argon at atmospheric pressure and the ends were closed with 1/32 inch thick fused quartz disks. The photomultiplier socket and dynode resistor chain were heated to prevent condensation which might cause high-voltage breakdown.

#### C.5 ROWLAND SPECTROMETER SYSTEM

The Rowland spectrometer system, which is shown in Fig. 3, consisted of a 6.65 m, f/48 Rowland mount spectrograph, an achromatic lens (see Appendix C.1), a photomultiplier tube, a front-surface mirror and a 3 mm thick quartz disc which formed the window of the hollow cathode source (see Appendix C.7). As the optical properties of all these components were involved in the relative intensity measurements, the entire system was calibrated and used as a unit. The grating has 600 lines/mm blazed at 3000 Å in second order. The exit slit is fixed in size at 25 mm by 25 μ. The reciprocal dispersion is 1.253 Å/mm in second order. Measured line widths

---

\* Gencom Division, Varian/EMI, Plainview, N. Y., 11803.

of less than 40 mÅ were obtained at 3000 Å in second order; roughly what would be expected from Eq. 4-1. This corresponds to a resolving power,  $\lambda/\Delta\lambda$ , of  $.75 \times 10^5$ . The theoretical resolving power is  $1.66 \times 10^5$ .\* A dry-ice cooled EMI 9526B photomultiplier tube was used as a photon detector. As with the McPherson system, the base was heated and the tube face was protected from condensation with a light pipe. More information about the Rowland spectrometer is given by Ashenfelter (1967).

#### C.6 OPTICAL ALIGNMENT OF THE ROWLAND SPECTROMETER

Measurements with the Rowland spectrometer usually required several additional optical elements. Because the acceptance angle of the instrument is only  $1/48$  radians ( $\approx 1.2^\circ$ ), accurate alignment was required to ensure that all components were fully illuminated.

A helium-neon laser was used to determine the optic axis. The spectrometer was adjusted to detect the laser wavelength and then the phototube and exit slit assembly were removed as a unit. The laser beam passed through the center of the entrance slit onto the center of the grating. The position of the emergent beam at the exit carriage was marked. Then the direction of the laser beam was reversed so that it entered at the exit slit carriage, hit the center of the grating and passed through the center of the entrance slit.

---

\* A discussion of grating spectrometer parameters is given by Jenkins and White (1957), Chapter 17.

This beam now defined the optic axis and the various components were centered on this axis. When alignment was completed, time exposure Polaroid photographs were taken to confirm that the grating was fully illuminated.

### C.7 HOLLOW CATHODE SOURCE

The light source for the branching ratio measurements was a hollow cathode discharge tube, a diagram of which is shown in Fig. 18. The cathode was a cylinder of spectroscopically pure iron,<sup>\*</sup> 52 mm long and 10 mm diameter, with a 3 mm diameter canal along its axis. Surrounding the cathode cylinder was a water-cooled aluminum body. No temperature measurements were made but it was observed that the cathode did not glow red during operation. The anode, an open-ended, thin-walled, stainless-steel cylinder, 25 mm long and 50 mm diameter, was concentric with the cathode. The distance to the quartz end-window was 15 cm; long enough to keep deposit of sputtered iron to a minimum.

Because the cathode temperature is low, it is believed that the iron atoms are sputtered off by collisions of the carrier gas ions with the cathode (Tolansky, 1947). Ionization and excitation then take place through ion and electron bombardment. The iron atoms constitute an impurity in the carrier gas. Several parameters were

---

\* Jarrell-Ash, Waltham, Mass.; sample No. JM848.

varied in order to determine the optimum operating conditions. These included cathode diameter, gas type and pressure, and discharge current. A small cathode diameter (3 mm) resulted in a brighter discharge than did the larger cathode (11 mm) tried initially. This is consistent with the results of Tolansky (1947) who believed that the intensity was proportional to the current density for the cathode. Both neon and argon were found to give satisfactory results but helium, probably because of its low mass, produced a relatively weak iron spectrum. For the 3 mm diameter cathode, gas pressure and discharge current were varied in order to maximize the signal-to-noise ratio. For argon, this was achieved with pressures of about 2.5 to 3 torr and the highest practical currents. The currents were limited to less than 600 mA in order to avoid self absorption (see Sect. 4.6). For neon, pressures of about 4 torr or higher were required to maintain the discharge so this pressure was used at all times. The pressure was measured with an oil manometer.

The gas inlet line and the pumping line were passed through a dry-ice and alcohol mixture in the case of argon or liquid nitrogen in the case of neon. This was intended to reduce contaminant elements in the discharge which would cause spurious lines. The only lines observed that did not come from iron or the carrier gas were  $N_2$  molecular bands. The gas flow through the tube was held at 2 to 3  $cm^3$ /minute (NTP).

The discharge was powered by a 1500 V motor-generator with a 3000  $\Omega$  ballast resistor in series to provide stability. Typically, the discharge current was about 460 mA, providing about 1200 V drop in the ballast and a 300 V drop across the discharge.

## APPENDIX D – SPECTROMETER CALIBRATION

## D. 1 INTRODUCTION

In order to determine the relative intensities or branching ratios (see Sec. 2.2) of the decays from a given atomic level, the relative efficiency,  $\epsilon(\lambda)$ , of the detection equipment must be obtained as a function of wavelength. Two separate detection systems were used in this work. They have been described in Appendix C and will be referred to as the McPherson system and the Rowland system. The calibration of both systems was rather similar, so the techniques will be described in some detail for the Rowland system. Difficulties unique to the other system will be pointed out.

The simplest way to calibrate a detecting system is to observe with it a standard light source of known intensity as a function of wavelength (see Drummond, 1970). The most common sources used in this fashion are tungsten-filament lamps and carbon arcs. Unfortunately, the emission of the former is very weak for wavelengths below 3000 Å (see Fig. 14), while carbon arcs are difficult to use in a reproducible fashion, the output being dependent upon the construction parameters of the lamp (Hennes and Dunkelman, 1967). Consequently, although a standard lamp was used for most measurements, an alternate technique was used for  $1900 \text{ Å} \leq \lambda \leq 2500 \text{ Å}$ . In this range the relative efficiencies of the systems were compared to that of a detector of known efficiency, a sodium salicylate coated

photomultiplier.

## D. 2 PREVIOUS WORK

Previous users of the two spectrometer systems had made some relative efficiency measurements (Martinez). The efficiency calibration for the McPherson system with the 2400 line/mm grating in second order covered the range from 1900 Å to 5000 Å. This calibration was checked, using the standard lamp, for  $2500 \text{ Å} \leq \lambda \leq 4000 \text{ Å}$ .

The relative efficiency calibration of the Rowland spectrometer system had a lower limit of 2800 Å (Martinez). This was extended to 2250 Å, and the calibration through to 4000 Å was checked in second order while the first order calibration was checked for  $3000 \text{ Å} \leq \lambda \leq 6000 \text{ Å}$ . Comparison with the results of Martinez is given in Sect. D. 3.

## D. 3 EFFICIENCY CALIBRATION FOR $\lambda \geq 2500 \text{ Å}$

The equipment used to calibrate the Rowland spectrometer for  $\lambda \geq 2500 \text{ Å}$  is shown in Fig. 3. A listing of the electronic components is given in Table 1. Because of the small angles involved, alignment was rather critical (see Appendix C. 6), but somewhat less care had to be taken with the linear dimensions. However, an effort was made to keep the distances between components roughly the same for both calibration and use in branching ratio measurements.

A description of the standard lamp is given in Appendix C. 3. A magnification of about 4 ensured that the image of the source was larger than the entrance slit. The length of the slit was 10 mm, and the width was varied depending upon the photon intensity in the wavelength region being observed. The relative detection efficiency, as a function of wavelength, should not be dependent upon the slit size. In order to avoid errors from spectrometer slit widths that might deviate from the values indicated on the micrometer dial, portions of the wavelength range were measured with a constant slit width. If it was necessary to change the slit width in order to calibrate an adjacent wavelength range, some overlapping measurements were made.

The photon intensity of the standard lamp at  $6000 \text{ \AA}$  is  $10^4$  times that at  $2500 \text{ \AA}$  (see Fig. 14). Consequently, light scattered in the spectrometer was a considerable problem when working at shorter wavelengths. To eliminate this scattered light, it was necessary to use blocking filters of known transmission (see Appendix C. 2). The only interference filter used in this manner was the Baird-Atomic  $2537 \text{ \AA}$  filter. The absolute transmission of this filter was known to  $\pm 10\%$  for  $2450 \text{ \AA} \leq \lambda \leq 3000 \text{ \AA}$ .

The relative number of photons counted by the spectrometer system per unit time is, as a function of wavelength,

$$n(\lambda) = I(\lambda) f(\lambda) \epsilon(\lambda) \Omega \quad (\text{D-1})$$

where

$I(\lambda)$  = the relative intensity of the source  
(photons/(second  $\cdot$  cm<sup>2</sup> of source  $\cdot$  steradian  $\cdot$  Å)),

$f(\lambda)$  = the transmission of the filter,

$\epsilon(\lambda)$  = relative detection efficiency of the spectrometer system (recall that this value includes the transmission or reflectivity of any optical components included in the 'system' as well as the properties of the photomultiplier tube and spectrometer itself), and

$\Omega$  = a geometrical factor that determines the fraction of the photons leaving the lamp which enter the slits of the spectrometer.

Since only the relative efficiency as a function of wavelength is needed, it is not necessary to know the value of  $\Omega$ . Clearly,

$$\epsilon(\lambda) = \frac{n(\lambda)}{I(\lambda) f(\lambda) \Omega} \quad (\text{D-1}')$$

The system was calibrated in first order from 3000 Å to 6000 Å. The slit width was chosen to keep the maximum counting rate below 25 kHz. At this rate, the measured counting losses due to pile up in the electronics was less than 2%. The results are shown in Fig. 19, along with the results of Martinez. The agreement is good, discrepancies being less than 5% for all wavelengths. The relative detection efficiency is probably accurate to

$\pm 10\%$  for  $3500 \text{ \AA} \leq \lambda \leq 6000 \text{ \AA}$  and  $\pm 20\%$  for  $3000 \text{ \AA} \leq \lambda \leq 3500 \text{ \AA}$ .

The larger uncertainty at short wavelengths is a consequence of the use of the 7-54 filter to eliminate scattered light.

The Rowland system was calibrated in second order from  $2500 \text{ \AA}$  to  $3600 \text{ \AA}$  using the standard lamp. The slit width was constant throughout. In order to eliminate most scattered light, both a Corning 7-54 and a Baird-Atomic  $2537 \text{ \AA}$  interference filter were used. The results are shown in Fig. 20. The error limits are given by

$$\Delta\epsilon(\lambda) = \sqrt{(\Delta n(\lambda))^2 + (\Delta f_{7.54}(\lambda))^2 + (\Delta f_{2537}(\lambda))^2}, \quad (\text{D-2})$$

where  $\Delta n(\lambda)$  is the root mean square deviation from the mean of the various measurements of  $n(\lambda)$ , and  $\Delta f_i(\lambda)$  is an estimate of the uncertainty in the measured transmission of filter  $i$  at  $\lambda$  (see Appendix C. 2). The possible error in the lamp calibration (see Appendix C. 3) has not been included. The measurements were repeated three times with consistent results. Values obtained for  $\lambda$  3150, 3300 and  $3650 \text{ \AA}$  using no filters were also consistent. Comparison with the results of Martinez will be discussed in Sect. 4 of this Appendix.

The calibration of the McPherson system was completed by Martinez but a check of his measurements was made for  $2500 \text{ \AA} \leq \lambda \leq 4000 \text{ \AA}$  using the standard lamp. The technique was essentially the same as for the Rowland spectrometer calibration in this region, except that some additional concern had to be given to ensuring that

the grating was fully illuminated. In fact, it is desirable, when using a spectrometer, to overfill the grating with light. When this is done, the results are, firstly, independent of any localized irregularities in the surface reflectivity of the grating and, secondly, independent of the variation in the solid angle subtended by the grating as the wavelength observed is changed. (The variation in solid angle is independent of wavelength for the Rowland mounting.)

The McPherson grating was  $\geq 90\%$  illuminated. It is physically impossible to overfill the grating using only one of the 18.4 cm focal length achromats and the geometry was such that two lenses could not be used. However, the geometry used in the calibration was the same as when the measurements were made, so the efficiency results are certainly valid.

The results of these measurements are shown in Fig. 21, along with the results of Martinez. A Corning 7-54 filter was used to eliminate scattered light. The 7-54 filter used by Martinez was not compared to the 7-54 filter used in this work so some of the discrepancy could be attributed to errors in filter calibration. No adjustment has been made to account for possible changes in the output of the standard lamp below 3400 Å (see Appendix C.6). The difference between the curves is less than 10% at all wavelengths and is within the error limits for the points from this work. The latter were calculated from

$$\Delta\epsilon(\lambda) = \sqrt{(\Delta n)^2 + (\Delta f)^2}, \quad (D-3)$$

where the various functions have been defined earlier in this section.

#### D. 4 EFFICIENCY CALIBRATION FOR $\lambda \leq 2500 \text{ \AA}$

The output of the standard lamp below  $2500 \text{ \AA}$  is too low to be of use, and consequently Eppley does not provide calibration points in this region (see Fig. 14). Since there are no satisfactory alternative sources with known output as a function of wavelength\*, it was necessary to compare the spectrometer systems with another detector system of known sensitivity.

The phosphor, sodium salicylate ( $\text{NaC}_7\text{H}_5\text{O}_3$ ), is a luminescent converter of constant efficiency as a function of wavelength. In other words, the ratio of emitted photons (which are all within a small range of wavelengths) to absorbed photons is nearly constant for a range of input photon wavelengths from at least  $1000 \text{ \AA}$  to  $3000 \text{ \AA}$  (Samson, 1967). Although some workers claim to have seen variations in yield, the variations are fairly small ( $\leq 10\%$ ) for  $\lambda \leq 3000 \text{ \AA}$  (Hennes and Dunkelman, 1967). Following this last reference, the sodium salicylate was dissolved in methyl alcohol and sprayed onto a 1 inch by 1/16 inch quartz disk which weighed about 1.87 g. The measurements were performed twice, with  $11.37 \mu\text{g}$  ( $2.25 \mu\text{g}/\text{cm}^2$ ) and  $21.17 \mu\text{g}$  ( $4.18 \mu\text{g}/\text{cm}^2$ ) coatings. These are within the optimum range given by Hennes and Dunkelman (1967).

---

\* A new, high-accuracy, spectral radiance standard has been developed by the National Bureau of Standards. This standard is calibrated to better than  $\pm 3\%$  for  $2250 \text{ \AA} \leq \lambda \leq 2 \mu$  (see Kostkowski *et al.*, 1970).

The emission spectrum of sodium salicylate is peaked at 4200 Å and has a half-width of about 800 Å. A Kodak Wratten filter #35 matches this spectrum and was used as a protection against detection of unwanted radiation. The filter was fixed to the face of a Dumont 6291 phototube, and the coated quartz was fixed to the filter with Dow-Corning #20057 optical coupling grease. Figure 22 shows a schematic diagram of the assembly. The photomultiplier tube base was designed for current measurement, and the high-voltage was chosen to be -1100 V to maximize the signal to dark-current ratio.

A source of monochromatic radiation was constructed from a continuous source and the McPherson spectrometer as a wavelength selector. The apparatus is shown schematically in Fig. 22. The lamp was an Osram high-pressure xenon arc lamp, XBO-162, powered by a Einbauszundgerat ZIF 1 supply designed especially for this lamp. A fan kept the lamp from overheating and an exhaust hood removed the ozone produced by the ultraviolet radiation. No irregularities were observed in the continuous spectrum of this lamp for  $2000 \text{ \AA} \leq \lambda \leq 3600 \text{ \AA}$ .

In order to reduce scattered light in the output of the McPherson spectrometer, interference filters were used at the entrance slit. Because this calibration was made relative to a detector of known sensitivity, quantitative values for the lamp output and filter transmission were not needed. This monochromatic source (xenon lamp + interference filter + spectrometer) was then observed by the sodium salicylate and photomultiplier, giving an output

current  $i(\lambda)$ . Then the photomultiplier assembly was moved and the same source was observed by the Rowland spectrometer system.

The relative efficiency of the latter system is given by

$$\epsilon(\lambda) = \frac{n(\lambda)}{i(\lambda)} \quad (\text{D-4})$$

where  $n(\lambda)$  is the count rate measured by the Rowland system.

The results are shown in Fig. 20. This figure shows

- i) the efficiency calibration for  $2500 \text{ \AA} \leq \lambda \leq 3650 \text{ \AA}$  done using the standard lamp,
- ii) the efficiency calibration for  $2250 \text{ \AA} \leq \lambda \leq 3200 \text{ \AA}$  made with sodium salicylate, and
- iii) the efficiency calibration obtained by Martinez.

In the region of overlap, comparison between i) and ii) is quite good.

There seems to be a systematic discrepancy of less than  $\pm 15\%$  with the results of Martinez. Probable error limits of

- i)  $\pm 10\%$  for  $2900 \text{ \AA} \leq \lambda \leq 3500 \text{ \AA}$ ,
- ii)  $\pm 20\%$  for  $2500 \text{ \AA} \leq \lambda \leq 2900 \text{ \AA}$ , and
- iii)  $\pm 25\%$  for  $2250 \text{ \AA} \leq \lambda \leq 2500 \text{ \AA}$

were assigned for use in transition probability calculations (see Table 4 ).

For the McPherson system, the calibration for  $2000 \text{ \AA} \leq \lambda \leq 2500 \text{ \AA}$  given by Martinez was used. Repetition of his measurements was impossible because of the unavailability of a second, high-quality spectrometer to be used as a wavelength selector in the sodium

salicylate method. The assumption that the efficiency had not changed significantly with time is probably valid, although the reflectivity of the three reflecting surfaces is possibly somewhat time dependent. The implications of this possible systematic error are discussed in Sect. 5.5.

#### D. 5 EFFICIENCY CALIBRATION CHECK

The relative intensities of two groups of lines were observed with both systems (see Sect. 4.4 and Table 3 ). Then,

$$I_i(\lambda) = N(\lambda) A(\lambda) \epsilon_i(\lambda) \Omega_i \quad (\text{D-5})$$

where the subscript  $i$  refers to a given spectrometer system and

$I_i(\lambda)$  is the number of photons observed per unit time,

$N(\lambda)$  is the population of the upper state,

$A(\lambda)$  is the transition probability,

$\epsilon_i(\lambda)$  is the spectrometer system detection efficiency, and

$\Omega_i$  is a geometrical factor, not dependent upon wavelength.

For two spectrometers viewing the same lines

$$\frac{I_M(\lambda)}{I_R(\lambda)} = \frac{\epsilon_M(\lambda) \Omega_M}{\epsilon_R(\lambda) \Omega_R} \quad \left( \begin{array}{l} M = \text{McPherson} \\ R = \text{Rowland} \end{array} \right) \quad (\text{D-6})$$

or

$$\frac{(I_M(\lambda)/\epsilon_M(\lambda))}{(I_R(\lambda)/\epsilon_R(\lambda))} \equiv \frac{(\text{Relative Intensity})_M}{(\text{Relative Intensity})_R} = \text{constant} \quad (\text{D-7})$$

for a given upper level. The data are given in Table 3. For each upper level, the value of  $RI_M/RI_R$  is a constant within the limit of the experimental uncertainty. Determination of these experimental uncertainties is discussed in Sect. 4.5.

## REFERENCES

1. L. H. Aller, Astrophysics - The Atmospheres of the Sun and Stars, 2nd ed., (Rowland Press, New York, 1963).
2. T. Anderson, Institute of Chemistry, University of Aarhus, Aarhus, Denmark, private communication (1970).
3. R. C. Ashenfelter, Ph.D. Thesis, California Institute of Technology (1967).
4. B. Baschek, T. Garz, H. Holweger, and J. Richter, *Astron. and Astrophys.* 4, 229 (1970).
5. S. Bashkin, ed., Proceedings of the Conference on Beam Foil Spectroscopy (Gordon and Breach, New York, 1968a).
6. S. Bashkin, *Applied Optics* 7, 2341 (1968b).
7. S. Bashkin, 'Beam Foil Spectroscopy', Chapter 4 of New Uses for Low Energy Accelerators, National Academy of Sciences (1968c).
8. W. S. Bickel, *Appl. Opt.* 6, 1309 (1967).
9. W. S. Bickel, *Appl. Opt.* 7, 2367 (1968).
10. J. M. Bridges and W. L. Wiese, *Astrophys. J.* 161, L71 (1970).
11. R. Cayrel and J. Jugaku, *Annales D'Astrophysique* 26, 495 (1963).
12. E. U. Condon and G. H. Shortley, The Theory of Atomic Spectra (Cambridge, 1967).
13. C. H. Corliss and W. R. Bozman, *Natl. Bur. Std. Monograph*, No. 53 (1962).
14. C. H. Corliss and J. L. Tech, *Natl. Bur. Std. Monograph*, No. 108 (1968).

15. C. H. Corliss and B. Warner, *Astrophys. J. Suppl. Ser.* 8, 395 (1964).
16. C. H. Corliss and B. Warner, *J. Res. Natl. Bur. Std.* 70A, 325 (1966).
17. R. D. Cowan and G. H. Dieke, *Rev. Mod. Phys.* 20, 418 (1948).
18. A. J. Drummond, ed., *Advances in Geophysics* 14 (1970).
19. B. Fastrup, P. Hvelplund and C. A. Sautter, *Klg. Danske Vid. Selsk. Mat.-Fys. Medd.* 35, No. 10 (1966).
20. E. W. Foster, *Rept. Progr. Phys.* 27, 469 (1964).
21. T. Garz, H. Holweger, M. Kock and J. Richter, *Astron. and Astrophys.* 2, 446 (1969).
22. T. Garz and M. Kock, *Astron. and Astrophys.* 2, 274 (1969).
23. L. Goldberg, A. E. Müller and L. H. Aller, *Astrophys. J. Suppl.* 5 (1960).
24. G. L. Grasdalen, M. Huber and W. H. Parkinson, *Astrophys. J.* 156, 1153 (1969).
25. N. Grevesse and J. P. Swings, *Astron. and Astrophys.* 2, 28 (1969).
26. H.-G. Groth, *Z. Astrophys.* 51, 231 (1961).
27. G. R. Harrison, M. I. T. Wavelength Tables (Revised) (M. I. T., Cambridge, Mass., 1969).
28. J. Hennes and L. Dunkelman, 'U. V. Technology' in The Middle Ultraviolet: Its science and technology, A. E. S. Green, ed. (Wiley and Sons, Inc., New York, 1967).
29. L. Heroux, *Appl. Opt.* 7, 2351 (1968).
30. H. Hubenet, ed., Abundance Determinations in Stellar Spectra, (Academic Press, New York, 1966).
31. P. Hvelplund and B. Fastrup, *Phys. Rev.* 165, 404 (1968).

32. P. Hvelplund, E. Laegsgard, J. O. Olsen and E. H. Pederson, *Nucl. Inst. and Meth.* 90, 315 (1970).
33. J. T. Jeffries, 'The Solar Abundance of Iron' in Abundance Determinations in Stellar Spectra, H. Hubenet, ed., (Academic Press, New York, 1966).
34. F. A. Jenkins and H. E. White, Fundamentals of Optics (McGraw Hill Book Co., New York, 1957).
35. H. J. Kostkowski, D. E. Erminy and A. T. Hattenburg, *Advances in Geophysics* 14, 111 (1970).
36. L. Kuzmickyte and K. Uspalis, *Lietuvos Fizikos Rinkiny* 10, 59 (1970).
37. Wm. N. Lennard, California Institute of Technology, private communication (1972).
38. J. Lindhard, M. Scharff and H. E. Shiott, *Kgl. Danske Vid. Selsk. Mat.-Fys. Medd.* 33, No. 14 (1963).
39. G. D. Magnuson, C. E. Carlston, P. Mahadevan and A. R. Comeaux, *Rev. Sci. Inst.* 36, 136 (1965).
40. M. Martinez-Garcia, Ph. D. Thesis, California Institute of Technology (1971).
41. M. Martinez-Garcia and W. Whaling, *Bull. Am. Phys. Soc.* 16, 107 (1971).
42. M. Martinez-Garcia, W. Whaling, D. L. Mickey and G. M. Lawrence, *Astrophys. J.* 165, 213 (1971).
43. W. F. Meggers et al., *Nat. Bur. Std. Monograph*, No. 32 (1961).
44. C. E. Moore, A Multiplet Table of Astrophysical Interest, rev. ed. (Princeton University Observatory, 1945).
45. C. E. Moore, An Ultraviolet Multiplet Table, *Natl. Bur. Std. Circular* 488 (1950).
46. C. E. Moore, M. G. J. Minnaert and J. Houtgast, The Solar Spectrum 2935 Å - 8770 Å, *Natl. Bur. Std. Monograph* 61 (1966).

47. J. C. Pecker and S. R. Pottasch, *Astron. and Astrophys.* 2, 81 (1969).
48. S. R. Pottasch, *Bull. Astr. Inst. Netherlands* 19, 113 (1967).
49. O. Roder, *Z. Astrophys.* 55, 38 (1962).
50. J. E. Ross, *Nature* 225, 610 (1970).
51. J. E. Ross, University of California at Los Angeles, private communication (1972).
52. J. A. R. Samson, Techniques of Vacuum Ultraviolet Spectroscopy (Wiley and Sons, Inc., New York, 1967).
53. P. L. Smith and W. Whaling, *Phys. Rev.* 188, 36 (1969).
54. R. Stair, R. G. Johnston, and E. W. Halbach, *J. Res. Natl. Bur. Std.* 64A, 291 (1960).
55. J. O. Stoner and J. A. Leavitt, *Appl. Phys. Lett.* 18, 268 (1971).
56. A. R. Striganov and N. S. Sventitskii, Tables of Spectral Lines of Neutral and Ionized Atoms (IFI/Plenum Press, New York, 1968).
57. S. Tolansky, High Resolution Spectroscopy (Methuen and Co., London, 1947).
58. H. C. Urey, *Quart. J. Roy. Astro. Soc.* 8, 23 (1967).
59. B. Warner, *Mem. Roy. Astron. Soc.* 70, 165 (1967).
60. B. Warner, *Mon. Not. Roy. Astron. Soc.* 138, 229 (1968).
61. W. Whaling, 'Atomic Lifetime Measurements', Chapter 5 of New Uses for Low Energy Accelerators, National Academy of Sciences (1968).
62. W. L. Wiese, in Methods of Experimental Physics, Vol. 7A, B. Bederson and W. L. Fite, eds. (Academic Press, New York, 1968).

63. G. L. Withbroe, *Astrophys. J.* 156, 1177 (1969).
64. S. J. Wolnik, R. O. Berthel and G. W. Wares, *Astrophys. J.* 166, L31 (1971).

## TABLE 1

Listing of electronic equipment used in this work. The equipment used for the lifetime measurements is listed in Part 1 of the Table. The equipment used for the efficiency calibration and branching ratio measurements is listed in Part 2 of the Table. (refer to pages 15, 28, 30, 85)

TABLE 1  
ELECTRONICS

Description	Manufacturer	Model	Serial No.
<u>Part 1: Lifetime Measurements</u>			
Spectrometer PMT high voltage	Fluke	412B	3345
Monitor PMT high voltage	Fluke	405	886
Preamplifier	Tennelec	100C	172
Preamplifier power	Tennelec	900	273
Amplifier-discriminator	Hamner	N328	82
Current integrator	Elcor	A308C	10-1068
Scalers	RIDL	49-28 49-30	U3534 H6538
<u>Part 2: Efficiency Calibration and Branching Ratio Measurements</u>			
Rowland spectrometer PMT high voltage	Fluke Fluke	412B 402M	635 389
Preamplifier-discriminator	see Mickey <u>et al.</u> (1970)		
Scaler	ORTEC ORTEC	430 430	144 195
Timer-scaler	ORTEC	431	157
Log-linear count rate meter	Mechtronics	775	801007
Chart recorder	Moseley	680	192
Microammeter	Hewlett-Packard	425A	142-03534
Preamplifier	Tennelec	100A	215
Preamplifier power supply	Tennelec	901RM	45
Amplifier-discriminator	Hamner	N328	55

TABLE 2

Results of the beam-foil lifetime measurements in units of  $10^{-9}$  seconds for seven lines of Fe II. The beam energy and foil thickness are shown for each measurement. The multiplet numbers are from Moore (1950). Values in brackets are the results of rough measurements only. The uncertainties shown are those assigned by the curve fitting program. The mean values were calculated by taking an weighted average of all measurements and the uncertainty is the weighted r. m. s. deviation from the mean. The values of Anderson (1970) are included for comparison. (refer to pages 20, 25)

TABLE 2

	$\lambda(\text{\AA})$	$\left. \begin{matrix} 2550.02 \\ 2550.68 \end{matrix} \right\}$	2592.78	2625.49	2664.66	2666.63	2753.29	2767.50
	Multiplet	240u	318u	318u	263u	263u	235u	235u
Beam energy (keV)	Foil ( $\mu\text{g}/\text{cm}^2$ )							
200	5			$4.68 \pm .18$	$4.30 \pm .12$	$3.56 \pm .35$		
	5			$4.30 \pm .20$		$3.73 \pm .40$		
	5			$4.01 \pm .15$				
250	5		$4.71 \pm .12$				$4.81 \pm .30$	
	10		$3.82 \pm .22$					
300	5	$(3.6 \pm 1.0)$		$4.85 \pm .17$		$3.88 \pm .18$		$(4.6 \pm 1.0)$
	5			$4.84 \pm .15$				
375	5						$4.83 \pm .10$	
400	5			$5.17 \pm .13$	$4.18 \pm .12$	$3.83 \pm .27$		
	5			$4.62 \pm .13$				
	10		$4.25 \pm .18$					
$\tau_{\text{Mean}}$		$(3.6 \pm 1.0)$	$4.44 \pm .34$	$4.68 \pm .37$	$4.24 \pm .06$	$3.81 \pm .11$	$4.83 \pm .01$	$(4.6 \pm 1.0)$
$\tau_{\text{Anderson}}$		$3.8 \pm 0.6$	$4.5 \pm .3$	$4.5 \pm .3$	$4.3 \pm 0.3$		$4.8 \pm 0.3$	$4.8 \pm 0.3$

TABLE 3

Data used in the determination of the relative intensities of 3 lines with  $\lambda \leq 2250 \text{ \AA}$ . Using the McPherson spectrometer system, the relative intensity of these lines was compared to others from the same upper levels as shown in the Table. Then, the relative intensities of all lines with  $\lambda \geq 2250 \text{ \AA}$  were compared using the Rowland spectrometer. The transmission of the quartz end window is included in the calculation because it is not part of the McPherson spectrometer system. The reading error and calibration error (see Sect. 4) are given. Combined, they give the uncertainty in  $I_{\text{McPherson}}$ , which is given by

$$I_{\text{McPherson}} = \frac{\text{measured relative intensity}}{\epsilon(\lambda) (\text{quartz transmission})}$$

Relative intensities of lines measured with both systems are compared in order to put the values for lines with  $\lambda \leq 2250 \text{ \AA}$  on a relative scale consistent with other Rowland system measurements. (refer to pages 33, 93, 94)

TABLE 3

	Wavelength (Å)	Measured Relative Intensity	$\epsilon(\lambda)$	Quartz Transmission	Relative Intensity (I <sub>McPherson</sub> )	Reading Error (%)	Calibration Error (%)	Relative Intensity (I <sub>Rowland</sub> )	$\frac{I_{\text{Rowland}}}{I_{\text{McPherson}}}$	Uncertainty in McPherson Relative Intensity (%)
$y^2G^0_{9/2}$	2040	9.97	.24	.87	47.8	5	50	(1500)		50
	2753	13.2	1.25	.91	11.6	7	10	378	32.6	12
	2665	162.	1.18	.915	150.	10	10	5020	33.4	14
	2902	4.96	1.18	.92	4.56	10	10	128	27.9	14

$$\text{mean } \frac{I_{\text{Rowland}}}{I_{\text{McPherson}}} = 31.3$$

$$I_{\text{Rowland}} (2040 \text{ Å}) = 31.3 \times 47.8 = 1500$$

$y^2G^0_{7/2}$	2029	.965	.22	.87	5.04	15	50	(139)		52
	2050	6.59	.27	.87	28.1	5	50	(773)		50
	2560	15.	1.27	.91	13.0	10	10	397	30.5	14
	3163	4.29	1.47	.92	3.14	10	10	77	24.4	14

$$\text{mean } \frac{I_{\text{Rowland}}}{I_{\text{McPherson}}} = 27.5$$

$$I_{\text{Rowland}} (2029 \text{ Å}) = 27.5 \times 5.04 = 139$$

$$I_{\text{Rowland}} (2050 \text{ Å}) = 27.5 \times 13.0 = 773$$

## TABLE 4

Data used in the calculation of the branching ratios for the 38 lines studied in this experiment. The reading, consistency and calibration errors as well as the calculation of the uncertainty in the relative intensity and in the branching ratio are discussed in Sect. 4.5. In the column titled 'comments', 7-54 and 0-52 refer to Corning filters used in the relative intensity measurements, brackets indicate that the filter was used for some, rather than all of the measurements, and Ar or Ne imply that the relative intensity obtained using that gas in the hollow cathode was the only relative intensity used in the calculations.

(refer to pages 31, 32, 39, 92)

Upper Level (Moore, 1950)	Wavelength (Å)	Relative Intensity	Reading Error (%)	Consistency Error (%)	Calibration Error (%)	Uncertainty in Relative Intensity (%)	Uncertainty in Branching Ratio (%)	Branching Ratio ± Uncertainty (%)	Comments
$z^2K^o_{15/2}$	2593	100	0	0	0	0	.0	100.00 ± .00	
$z^2K^o_{13/2}$	2623	45	20	0	0	20	19.7	4.31 ± .85	7-54
	2625	1000	5	0	0	5	.9	95.69 ± .85	7-54
$y^2G^o_{9/2}$	2665	5020	10	9	20	22	14.2	63.70 ± 9.06	
	2040	1540	10	31	50	59	49.5	19.54 ± 9.67	
	2303	181	50	24	25	56	57.6	2.30 ± 1.32	
	2369	88	20	16	25	32	36.6	1.12 ± .41	
	2379	214	15	13	25	29	33.8	2.72 ± .92	
	2562	27	45	9	20	49	52.4	.34 ± .18	7-54
	2573	378	8	12	20	23	28.8	4.80 ± 1.38	
	2598	67	40	19	20	45	48.0	.85 ± .41	7-54
	2902	128	10	26	10	28	33.0	1.62 ± .54	(7-54)
	2934	44	40	56	10	57	59.5	.56 ± .33	
	2998	16	100	37	10	100	100.0	.20 ± .20	
	3045	37	25	13	10	27	32.5	.47 ± .15	7-54
	3132	40	30	18	10	32	36.5	.51 ± .19	(7-54)
	3187	95	10	15	10	18	25.6	1.21 ± .31	
5019	5	35	0	30	46	49.6	.06 ± .03	0-52	
$y^2G^o_{7/2}$	2667	2950	5	4	20	21	1.6	61.46 ± 7.16	
	2029	139	15	5	50	52	52.9	2.90 ± 1.53	
	2050	773	5	5	50	50	44.3	16.10 ± 7.13	
	2296	67	50	28	25	56	57.2	1.40 ± .80	
	2555	34	20	9	20	28	32.0	.71 ± .23	
	2560	397	5	3	20	21	24.2	8.27 ± 2.00	7-54
	2579	151	7	4	20	7	16.8	3.15 ± .53	
	2645	113	6	9	20	22	26.3	2.35 ± .62	Ar
	2879	53	15	3	15	21	25.9	1.10 ± .29	
	2911	10	45	15	10	46	48.5	.21 ± .10	Ne
	3002	33	20	7	10	22	26.9	.69 ± .19	
	3162	77	5	3	10	11	18.8	1.60 ± .30	
	4953	3	33	0	30	45	47.1	.06 ± .03	0-52
	$z^2I^o_{11/2}$	2388	2460	10	4	25	27	30.4	6.70 ± 2.04
2414		168	100	33	25	100	100.0	.46 ± .46	7-54
2433		1610	8	5	25	26	30.4	4.38 ± 1.33	
2684		77	30	21	20	36	39.9	.21 ± .08	7-54
2712		1870	5	5	20	21	26.5	5.09 ± 1.35	
2753		30400	5	4	20	21	4.3	82.75 ± 3.57	
3360		150	30	7	10	32	35.9	.41 ± .15	

TABLE 5

The absolute transition probability and the values of  $gf$  and  $\log_{10}(gf)$  calculated from the branching ratios and lifetimes measured in this experiment. (refer to page 43)

TABLE 5

UPPER LEVEL (Moore, 1950)	$\lambda$ (Å)	TRANSITION PROBABILITY ( $10^8 \text{ sec}^{-1}$ )	$gf$	$\log_{10} gf$
$z^2 K^o_{15/2}$	2593	2.2523 ± .2252	3.6326 ± .3633	.56 ± .00
$z^2 K^o_{13/2}$	2623	.0920 ± .0204	.1329 ± .0294	-.88 ± .08
	2625	2.0447 ± .2053	2.9573 ± .2969	.47 ± .00
$y^2 G^o_{9/2}$	2665	1.5025 ± .2612	1.5998 ± .2782	.20 ± .06
	2040	.4609 ± .2326	.2876 ± .1452	-.54 ± .17
	2303	.0542 ± .0317	.0431 ± .0252	-1.37 ± .20
	2369	.0263 ± .0100	.0222 ± .0084	-1.66 ± .14
	2379	.0640 ± .0226	.0543 ± .0192	-1.27 ± .13
	2562	.0081 ± .0043	.0080 ± .0042	-2.10 ± .18
	2573	.1131 ± .0345	.1123 ± .0343	-.95 ± .11
	2598	.0201 ± .0098	.0203 ± .0100	-1.69 ± .17
	2902	.0383 ± .0132	.0484 ± .0167	-1.32 ± .12
	2934	.0132 ± .0079	.0170 ± .0103	-1.77 ± .20
	2998	.0048 ± .0048	.0065 ± .0065	-2.19 ± .30
	3045	.0111 ± .0038	.0154 ± .0052	-1.81 ± .12
	3132	.0120 ± .0045	.0176 ± .0067	-1.76 ± .14
	3187	.0284 ± .0078	.0433 ± .0119	-1.37 ± .10
	5019	.0015 ± .0008	.0058 ± .0029	-2.24 ± .18
$y^2 G^o_{7/2}$	2667	1.6173 ± .2482	1.3798 ± .2118	.14 ± .05
	2029	.0762 ± .0410	.0376 ± .0203	-1.43 ± .18
	2050	.4238 ± .1924	.2136 ± .0970	-.67 ± .16
	2296	.0367 ± .0213	.0232 ± .0135	-1.64 ± .20
	2555	.0186 ± .0062	.0146 ± .0049	-1.84 ± .12
	2560	.2177 ± .0571	.1711 ± .0449	-.77 ± .09
	2579	.0828 ± .0162	.0660 ± .0129	-1.18 ± .07
	2645	.0620 ± .0174	.0520 ± .0146	-1.29 ± .10
	2879	.0291 ± .0081	.0289 ± .0080	-1.54 ± .10
	2911	.0055 ± .0027	.0056 ± .0028	-2.26 ± .17
	3002	.0181 ± .0052	.0196 ± .0056	-1.71 ± .10
	3162	.0422 ± .0090	.0506 ± .0108	-1.30 ± .07
	4953	.0016 ± .0008	.0048 ± .0023	-2.32 ± .17
$z^2 I^o_{11/2}$	2388	.1384 ± .0443	.1419 ± .0454	-.85 ± .12
	2414	.0094 ± .0094	.0099 ± .0099	-2.01 ± .30
	2433	.0906 ± .0290	.0964 ± .0309	-1.02 ± .12
	2684	.0043 ± .0018	.0056 ± .0023	-2.25 ± .15
	2712	.1052 ± .0298	.1392 ± .0394	-.86 ± .10
	2753	1.7098 ± .1862	2.3314 ± .2539	.37 ± .02
	3360	.0084 ± .0031	.0171 ± .0064	-1.77 ± .13

TABLE 6

Comparison between the results of this experiment  
and the values obtained by Warner. (refer to page 44)

TABLE 6

Upper Level	(Å)	$A_{\text{CIT}}$ ( $10^8 \text{ sec}^{-1}$ )	$A_{\text{Warner}}$	$\frac{A_{\text{Warner}}}{A_{\text{CIT}}}$
$z^2K^{\circ}_{15/2}$	2593	$2.2523 \pm .2252$	4.0700	$1.81 \pm .18$
$z^2K^{\circ}_{13/2}$	2625	$2.0600 \pm .2000$	4.1650	$2.02 \pm .20$
$y^2G^{\circ}_{9/2}$	2562	$.0081 \pm .0043$	.0290	$3.58 \pm 1.90$
	2573	$.1131 \pm .0345$	.2360	$2.09 \pm .64$
	2665	$1.5025 \pm .2612$	2.8370	$1.89 \pm .33$
	2902	$.0383 \pm .0132$	.0770	$2.01 \pm .69$
	3045	$.0111 \pm .0038$	.0490	$4.41 \pm 1.51$
	3132	$.0120 \pm .0045$	.0320	$2.67 \pm 1.00$
	3187	$.0284 \pm .0078$	.2670	$9.40 \pm 2.58$
$y^2G^{\circ}_{7/2}$	2667	$1.6234 \pm .2493$	2.9400	$1.81 \pm .28$
	2555	$.0187 \pm .0063$	.0790	$4.22 \pm 1.42$
	2560	$.2185 \pm .0574$	.3930	$1.80 \pm .47$
	2579	$.0831 \pm .0228$	.1650	$1.99 \pm .54$
	2645	$.0622 \pm .0175$	.1500	$2.41 \pm .68$
	3163	$.0424 \pm .0090$	.1740	$4.10 \pm .87$
$z^2I^{\circ}_{11/2}$	2712	$.1052 \pm .0298$	.2560	$2.43 \pm .69$
	2753	$1.7098 \pm .1862$	2.7880	$1.63 \pm .18$
	3360	$.0084 \pm .0031$	.0230	$2.74 \pm 1.01$

## TABLE 7

Brief description of the six experimental determinations of Fe II absolute transition probabilities discussed in Sect. 5.2. (refer to page 44)

TABLE 7

	<u>Source</u>	<u>Detector</u>	<u>Relative values</u>	<u>Normalization</u>
This work	Fe hollow cathode	spectrometer and photomultiplier with known detection efficiency; $\epsilon(\lambda)$ from standard lamp	branching ratios	lifetimes from beam-foil spectroscopy
Warner (1967)	emission lines from spark between Fe electrodes	photographic; $\epsilon(\lambda)$ from known f-values for Fe I lines	temperature from Fe I f-values; T and $\epsilon(\lambda)$ give relative values from plates	calculated f-values
Roder (1962)	emission lines in wall stabilized arc FeCl <sub>3</sub> + Ar	photographic; $\epsilon(\lambda)$ from carbon arc	temperature from Ar line intensities gives relative Fe I and relative Fe II f-values	Fe I from Bell et al.; Fe II/Fe I from Saha equation
Baschek et al. (1970)	emission lines in wall stabilized arc FeCl <sub>3</sub> + Ar	photographic; $\epsilon(\lambda)$ from carbon arc	temperature from Ar line intensity	Fe I values from Garz and Kock; Fe II/Fe I from Saha equation

Table 7 (Cont'd)

	<u>Source</u>	<u>Detector</u>	<u>Relative values</u>	<u>Normalization</u>
Grasdalen et al. (1969)	absorption lines in shock tube $\text{Fe}(\text{CO})_5 + \text{Ar}$	photographic; temperature from line reversal	equivalent widths measured; curve of growth analysis for relative f- values	known amount of $\text{Fe}(\text{CO})_5$ ; population densities determined from Saha and Boltzmann equations
Wolnik <u>et al.</u> (1971)	emission lines in shock tube $\text{Fe}(\text{CO})_5 + \text{Ar}$	photographic; $\epsilon(\lambda)$ from carbon arc; temperature measured with ultrasonic probe	curve of growth for relative f- values	known amount of $\text{Fe}(\text{CO})_5$ ; population densities determined from Saha and Boltzmann equations

TABLE 8

Wavelength, multiplet number, lower level excitation potential in eV and equivalent width in mÅ for the six lines listed in Moore (1966) for which transition probabilities were measured in this experiment.

(refer to page 57)

TABLE 8

wavelength (Å)	multiplet	$E_{\text{lower}}$ (ev)	equivalent width (mÅ)	comments
3131.71	107	4.08	51	Fe II, Ni I blend
3162.80	120	4.15	68	Fe II
3187.31	120	4.15	69	Fe II
3360.12	105	4.06		Fe II, NH molecular band, blend
4954.02	168	5.57	4	Fe II
5019.48	168	5.57	7.5	Fe II

## FIGURE 1

Hypothetical light decay curves for a transition  $j \rightarrow i$  when level  $j$  is repopulated by decays  $k \rightarrow j$ . Semi-logarithmic plots of  $n_j(t) = C_j \exp(-t/\tau_j) + C_k \exp(-t/\tau_k)$  for different choices of parameters  $C_j$ ,  $C_k$ ,  $\tau_j$  and  $\tau_k$  are shown. The intensity observed is proportional to  $n_j(t)$ . The dashed lines indicate that  $C_j$  or  $C_k$  is negative. (refer to page 13)

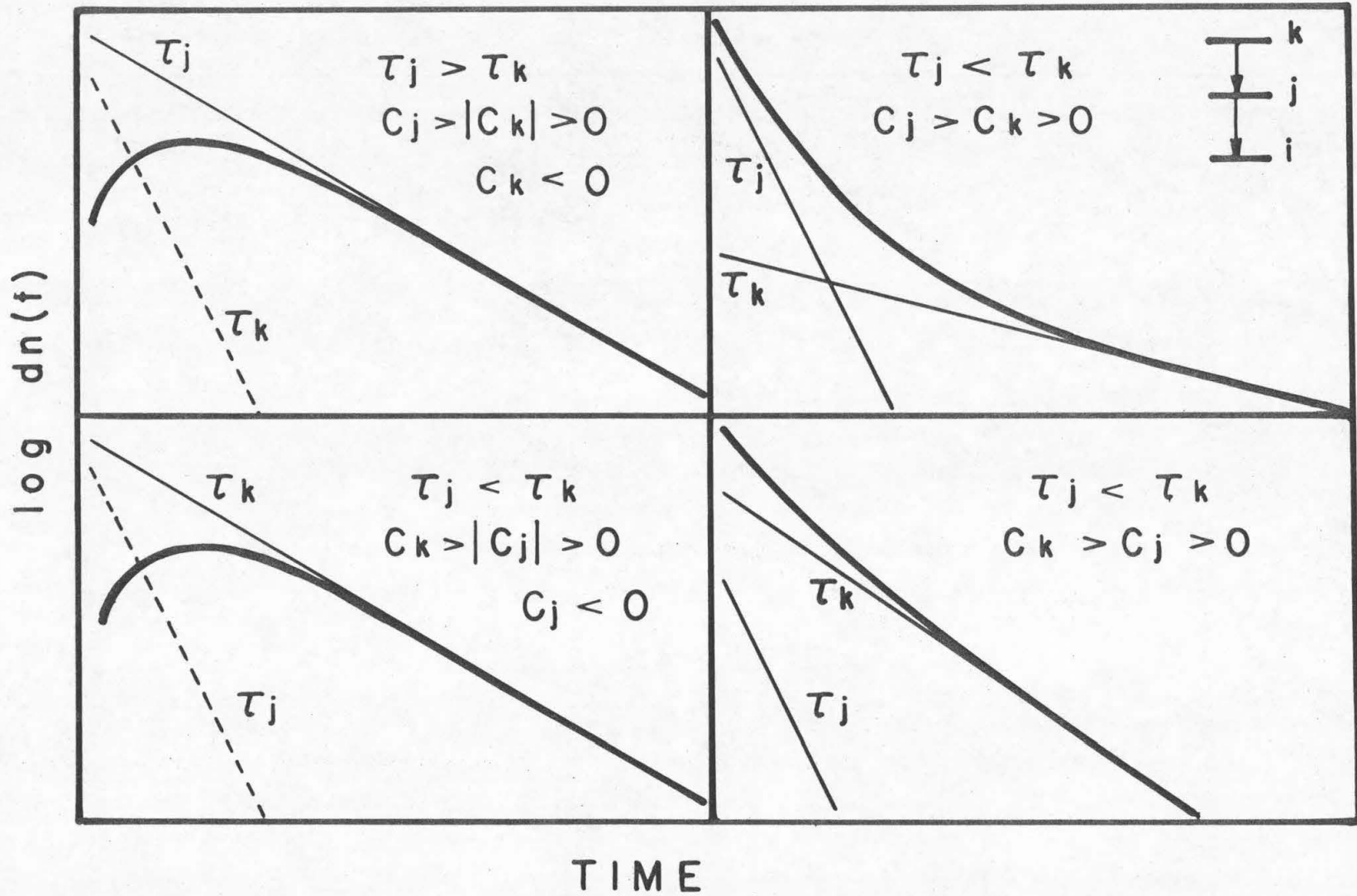
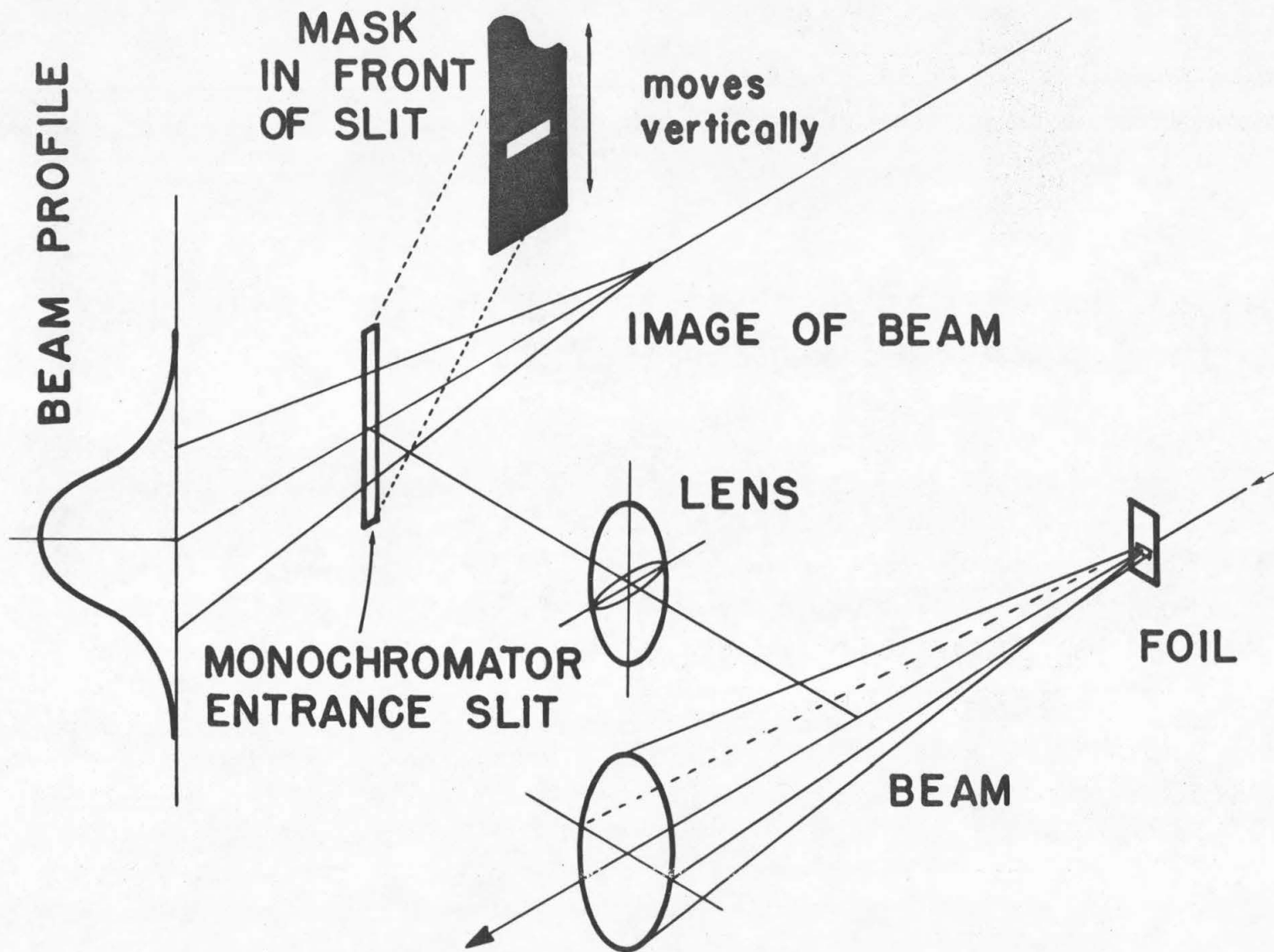


FIGURE 2

Schematic diagram of the apparatus used to determine the scattering of the ion beam by the foil. The beam profile was approximately Gaussian.  
(refer to page 22)



## FIGURE 3

Schematic diagram of the apparatus used with the Rowland spectrometer for measurement of the branching ratios. The mirror was rotated to observe the standard lamp in order to make the detection efficiency measurements. The end window of the hollow cathode source, the lens, the  $45^\circ$  mirror, and the spectrometer comprise the Rowland spectrometer system. The electronic equipment is listed in Table 1. The hollow cathode source is shown in more detail in Fig. 18. (refer to pages 27, 79, 85)

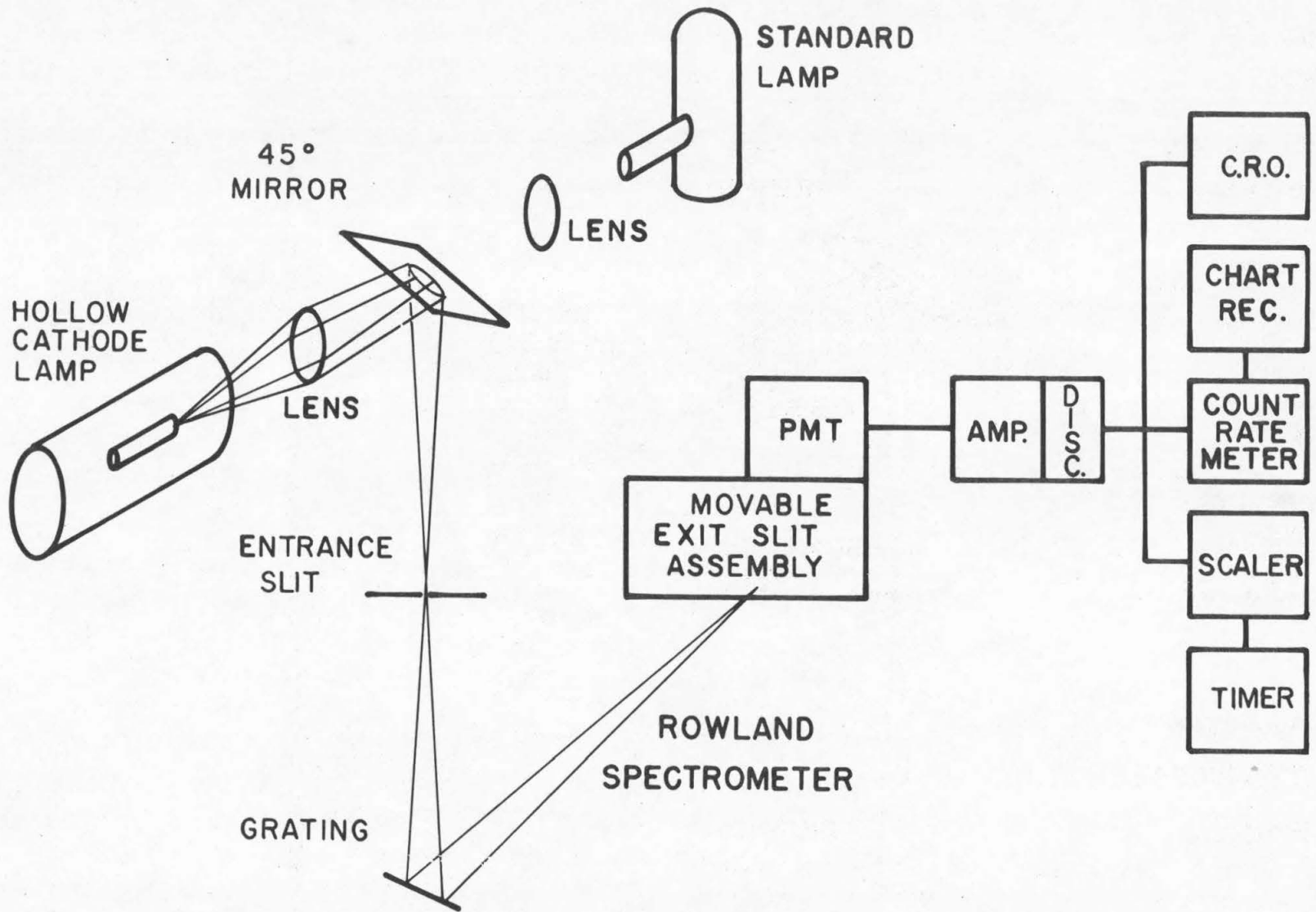
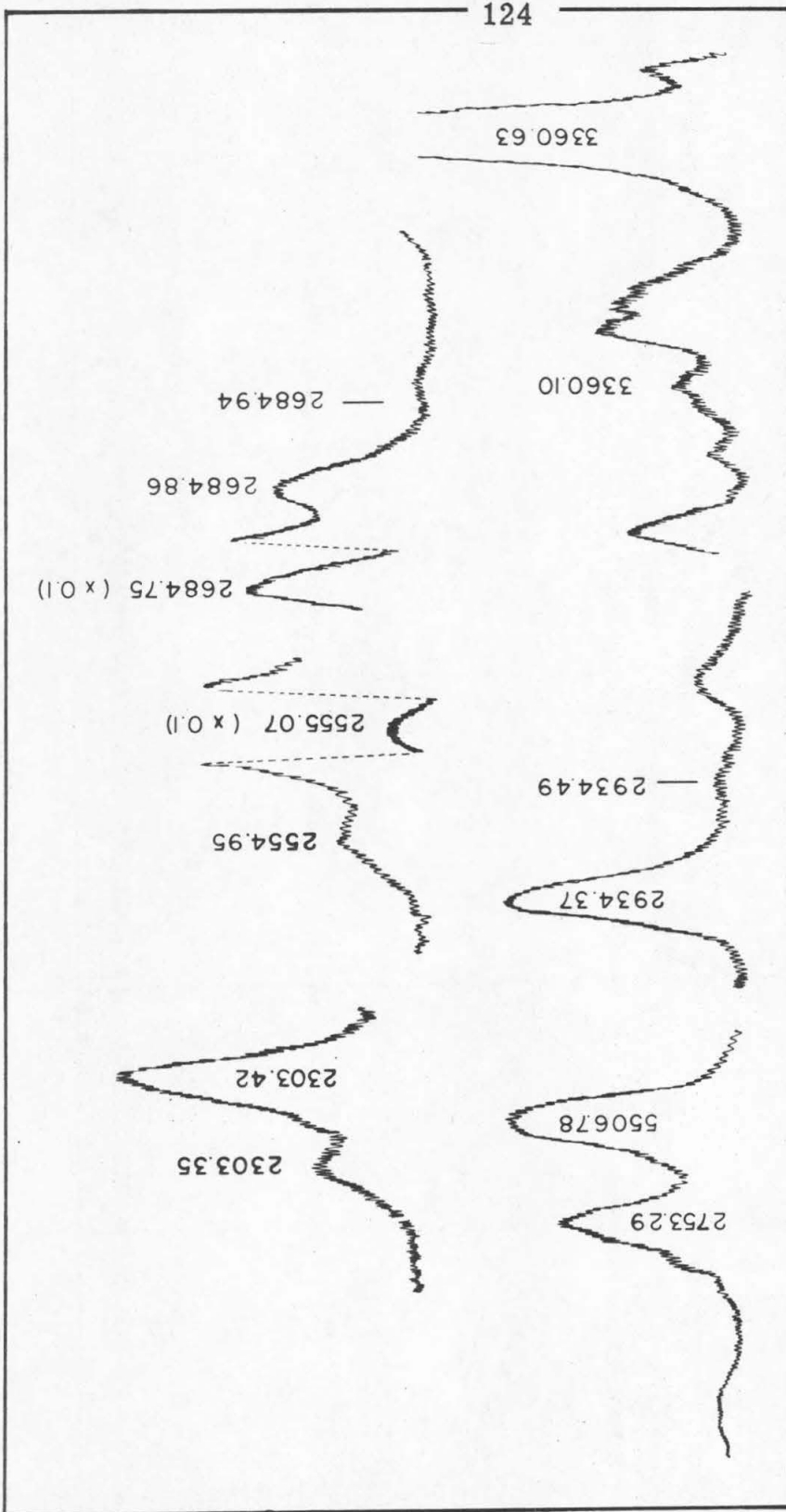


FIGURE 3

## FIGURE 4

Tracings of portions of the hollow cathode spectra. The original spectra have not been reproduced because they were marked during line identification procedure. The vertical scale is logarithmic with arbitrary units. Significant lines are marked. (refer to page 34).

FIGURE 4



## FIGURE 5

Ratios of observed relative intensities for two different operating conditions of the source plotted as a function of the transition probability. Three different upper levels were studied and the ratios were normalized to 1 for the strongest lines. The errors shown represent the uncertainty in the measurement of the line intensities when the lines were weakest, i. e., when the pressure and current were low. (refer to page 42)

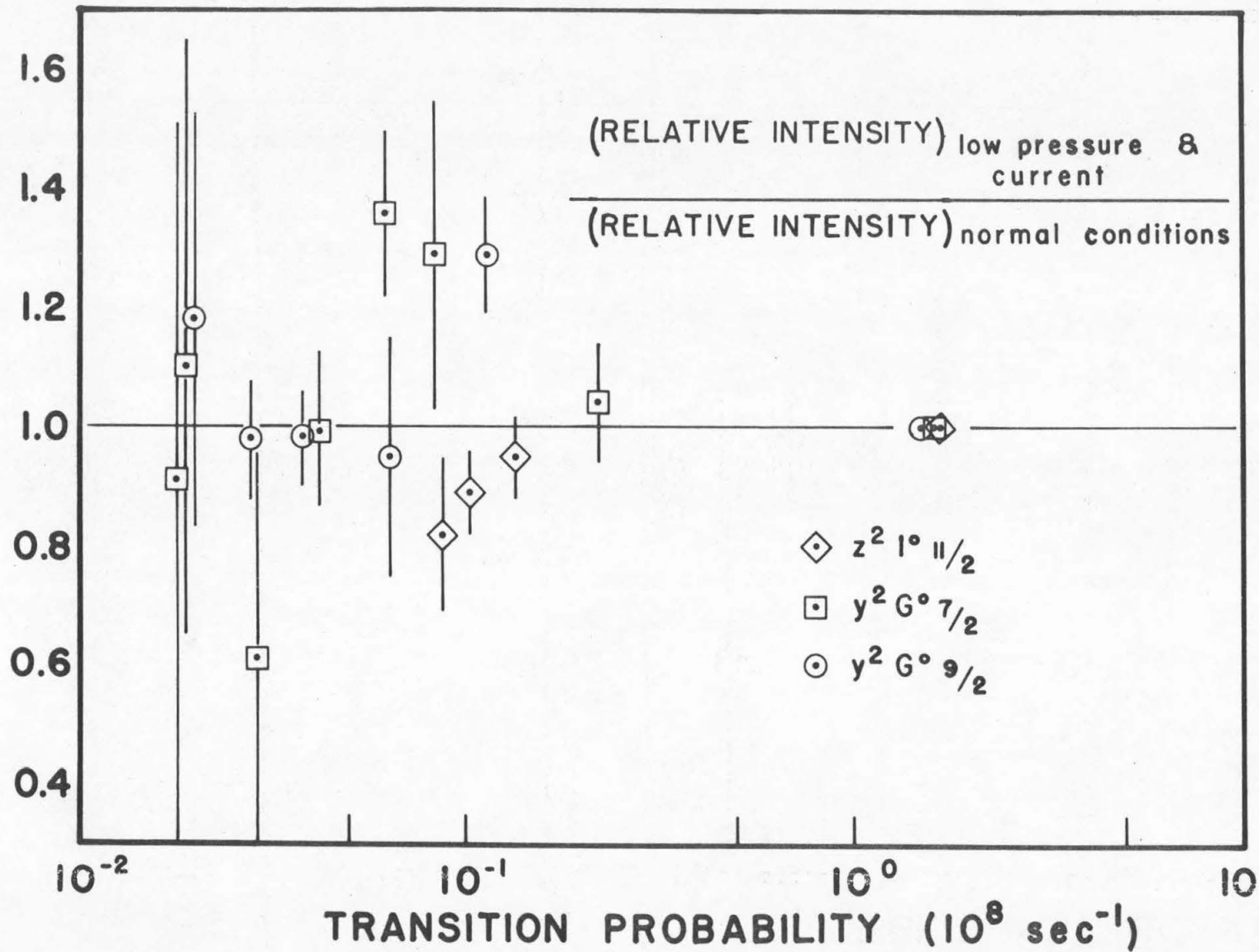


FIGURE 5

FIGURE 6

$\log_{10} \frac{A_W}{A_X}$  as a function of  $E_2$ , the energy of the upper level. Warner's results are compared to five other laboratory measurements. The values of  $A_W$  were obtained from the oscillator strengths published by Warner. (refer to pages 44-46)

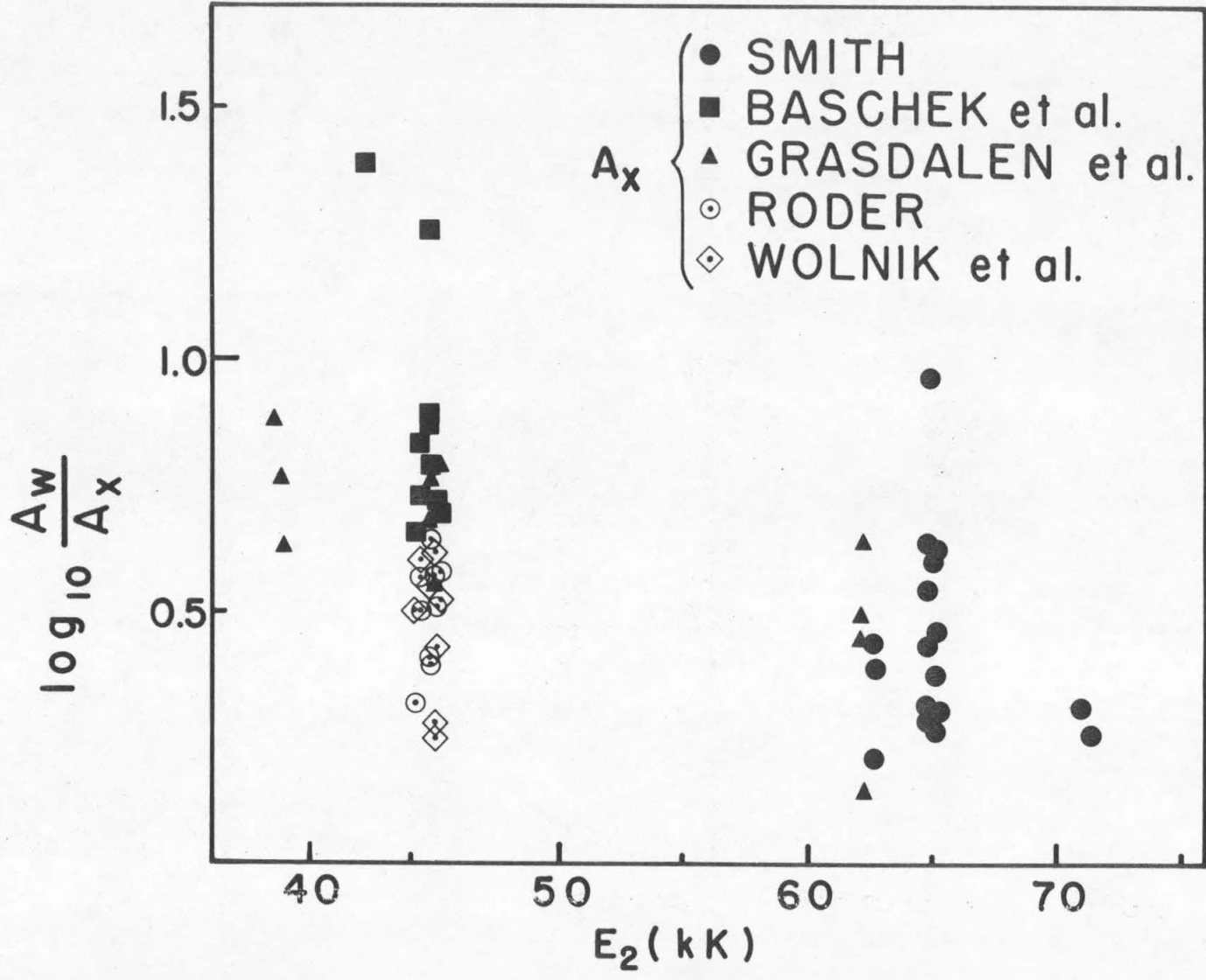


FIGURE 6

## FIGURE 7

$\log_{10} \frac{A'_W}{A_X}$  as a function of  $E_2$ , the energy of the

upper level. Warner's values are compared to five other laboratory measurements. The values of  $A'_W$  were obtained by removing the excitation potential dependent correction,  $C(E_2)$ , from Warner's data.  
(refer to pages 53, 54)

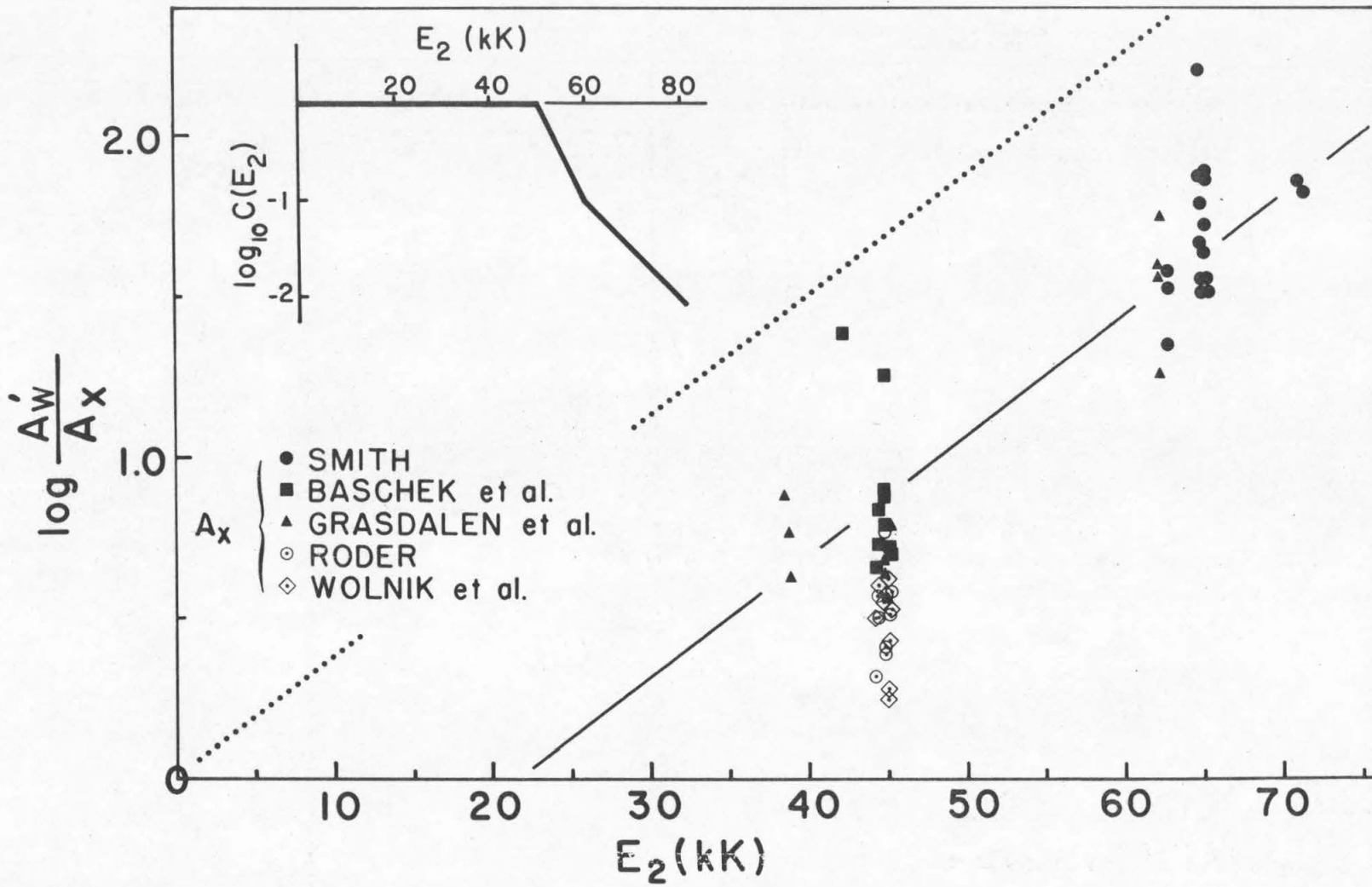


FIGURE 7

FIGURE 8

$\log_{10} \frac{A_W^*}{A_X}$  as a function of wavelength. Warner's

values are compared to values from five other laboratory measurements.  $A_W^*$  represents Warner's values corrected for his error in temperature and renormalized. The value of  $A_W^*$  for  $\lambda = 4954 \text{ \AA}$  is a point from an astrophysical analysis (Warner, 1968). (refer to page 56)

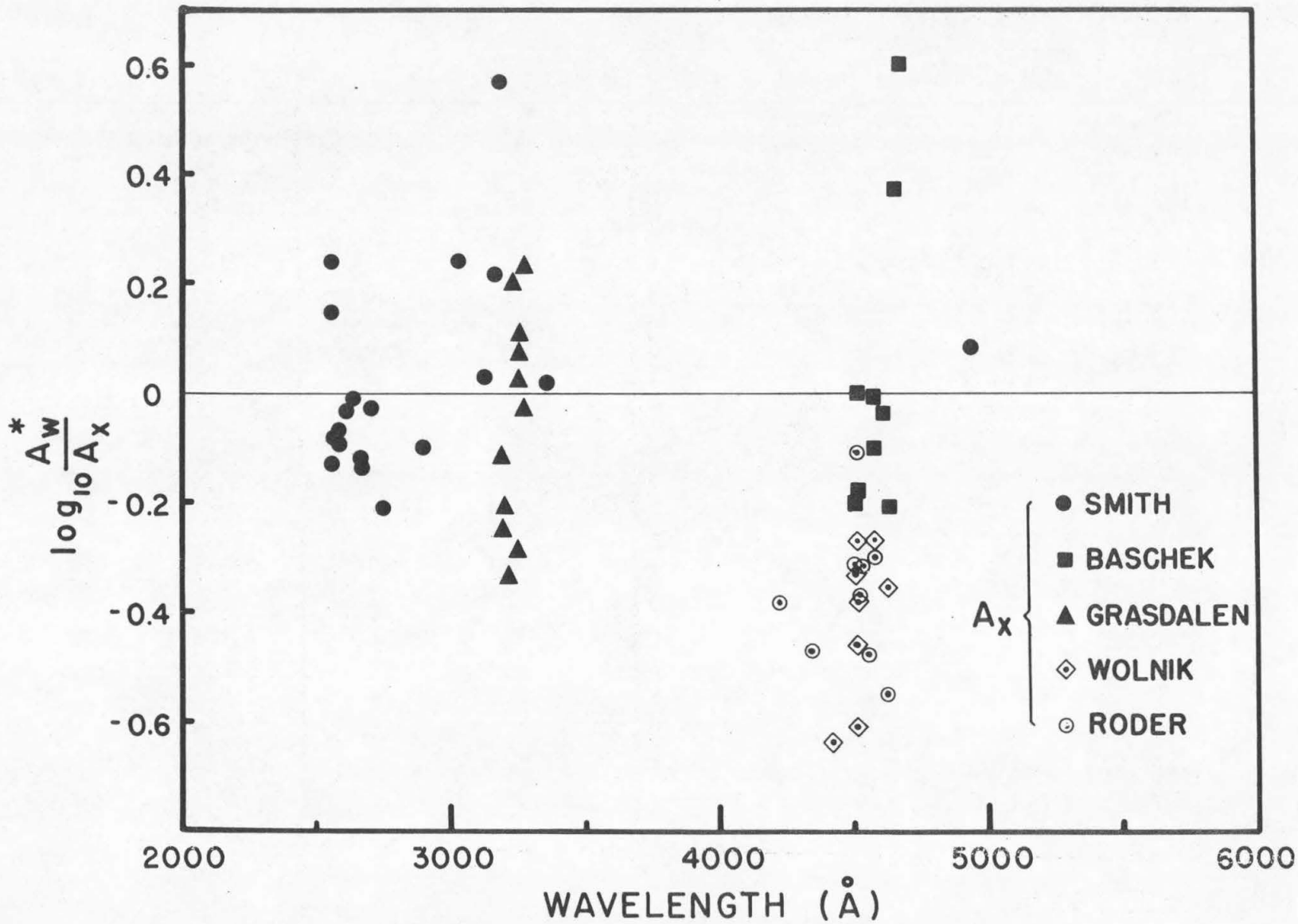


FIGURE 9

$\log_{10} \frac{A_W^*}{A_X}$  as a function of  $A_X$ . Warner's values

are compared to values from five other laboratory measurements.  $A_W^*$  represents Warner's values corrected for his error in temperature and renormalized. The experimental uncertainties in the results from our measurements are shown in this figure. (refer to pages 56, 62)

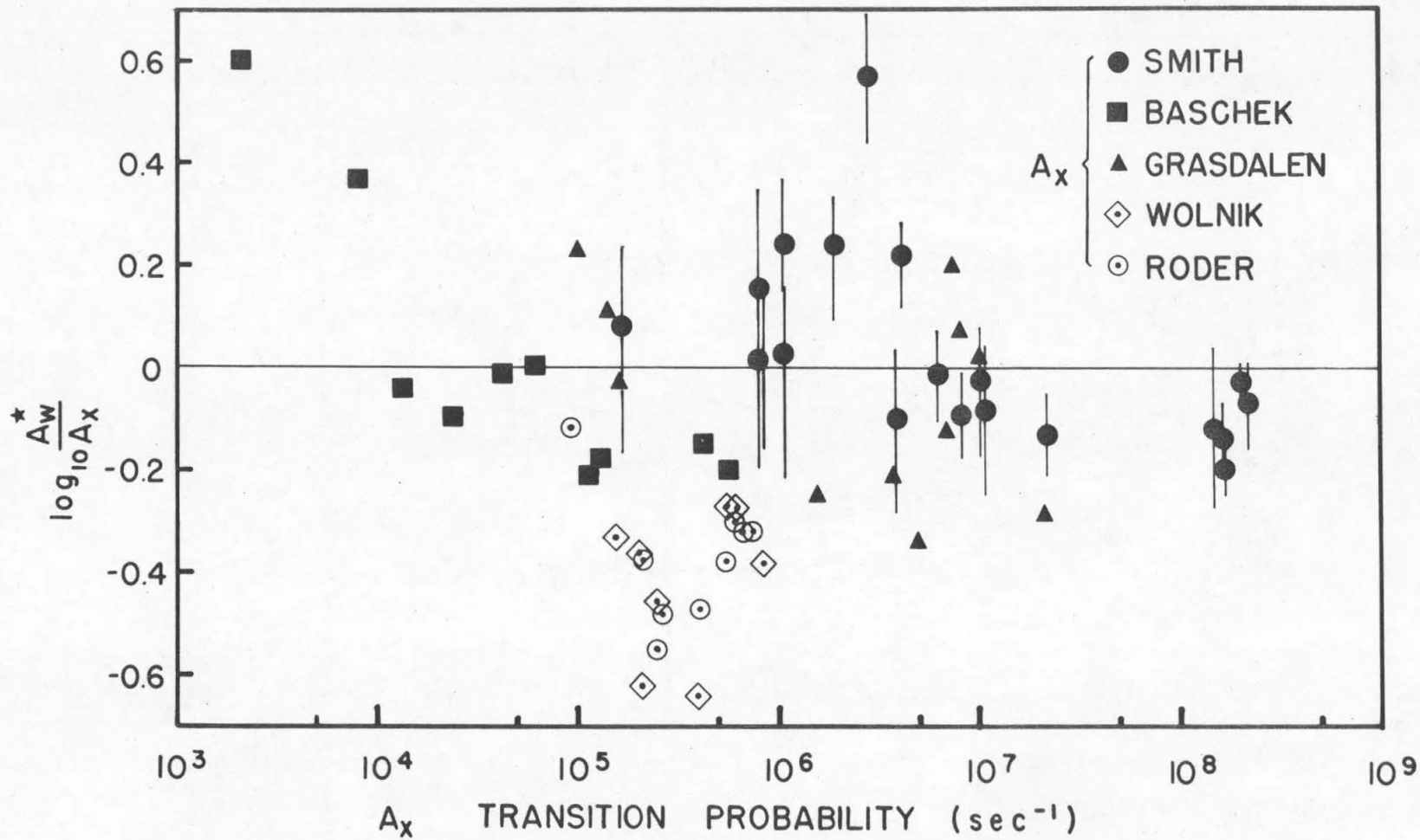


FIGURE 9

## FIGURE 10

Solar curve of growth for four lines for which the oscillator strength was determined in this experiment. Two points are shown as if they were on the weak line portion of the curve of growth. The solar iron abundance derived from each is shown. The abundance is given by

$$\log \frac{N_{\text{Fe}}}{N_{\text{H}}} = \log \left( \frac{W}{\lambda} \right) \quad \text{for } \log(gf\Gamma) = 0.$$

The abundance relative to  $10^{12}$  atoms of hydrogen is given by

$$\log N(\text{Fe}) \equiv \log \frac{N_{\text{Fe}}}{N_{\text{H}}} + 12.$$

(refer to page 58)

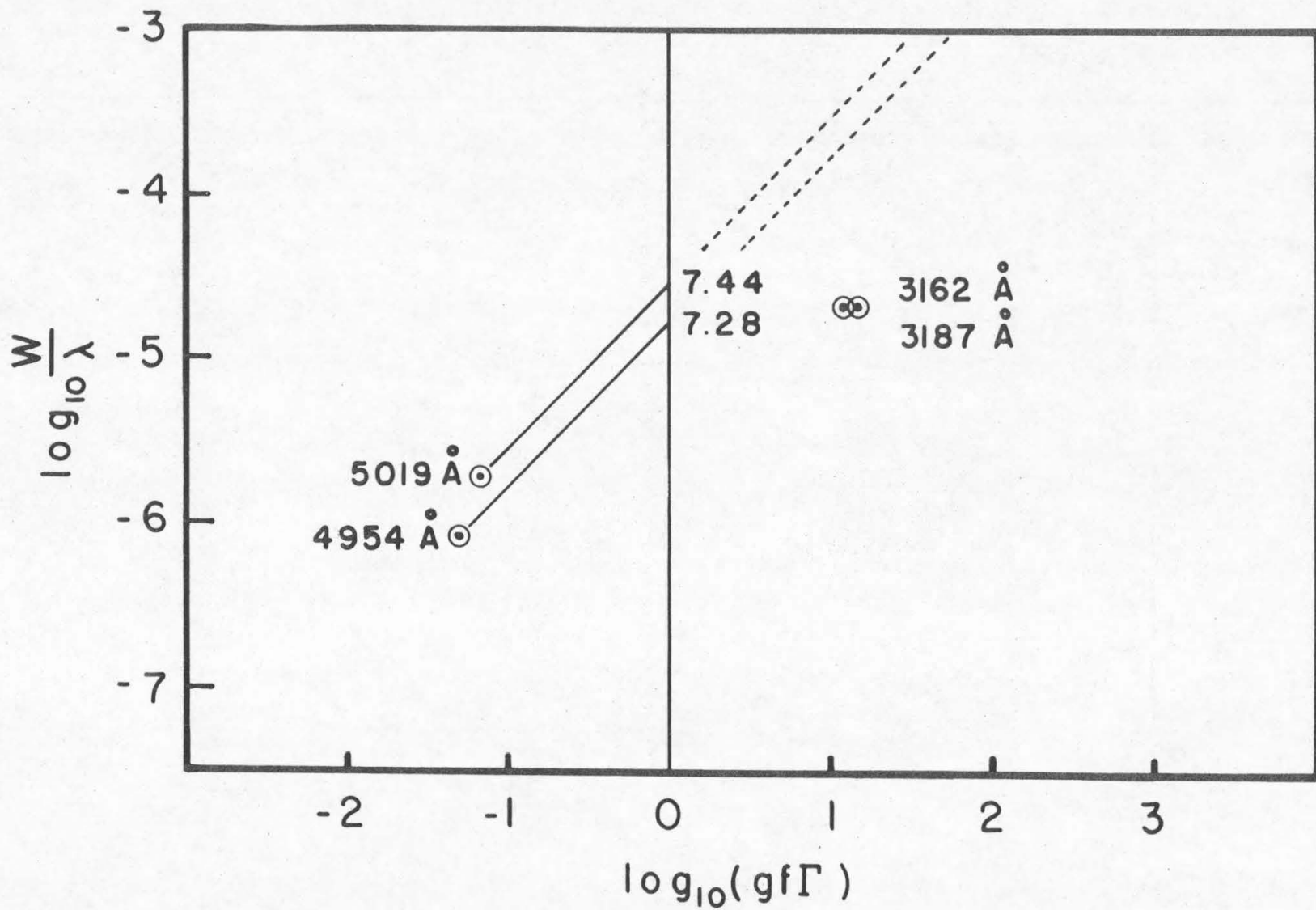


## FIGURE 11

Solar curve of growth plotted for the data given by Warner (1968) which has been corrected for Warner's error in temperature and renormalized. The square symbols are for lines measured by Warner (1967). The circles are for lines for which the oscillator strengths have been determined from observations of line intensities in stellar spectra. The solid symbols are for lines with  $E_2 < 56$  kK, and the open symbols are for lines with  $E_2 > 56$  kK. The abundance is given by the relation

$$\begin{aligned}
 \log N(\text{Fe}) &\equiv \log \frac{N_{\text{Fe}}}{N_{\text{H}}} + 12 \\
 &= \log \left( \frac{W}{\lambda} \right) + 12 \quad \text{for } \log (gf\Gamma) = 0 \\
 &= -4.72 + 12 \\
 &= 7.28.
 \end{aligned}$$

(refer to page 60)

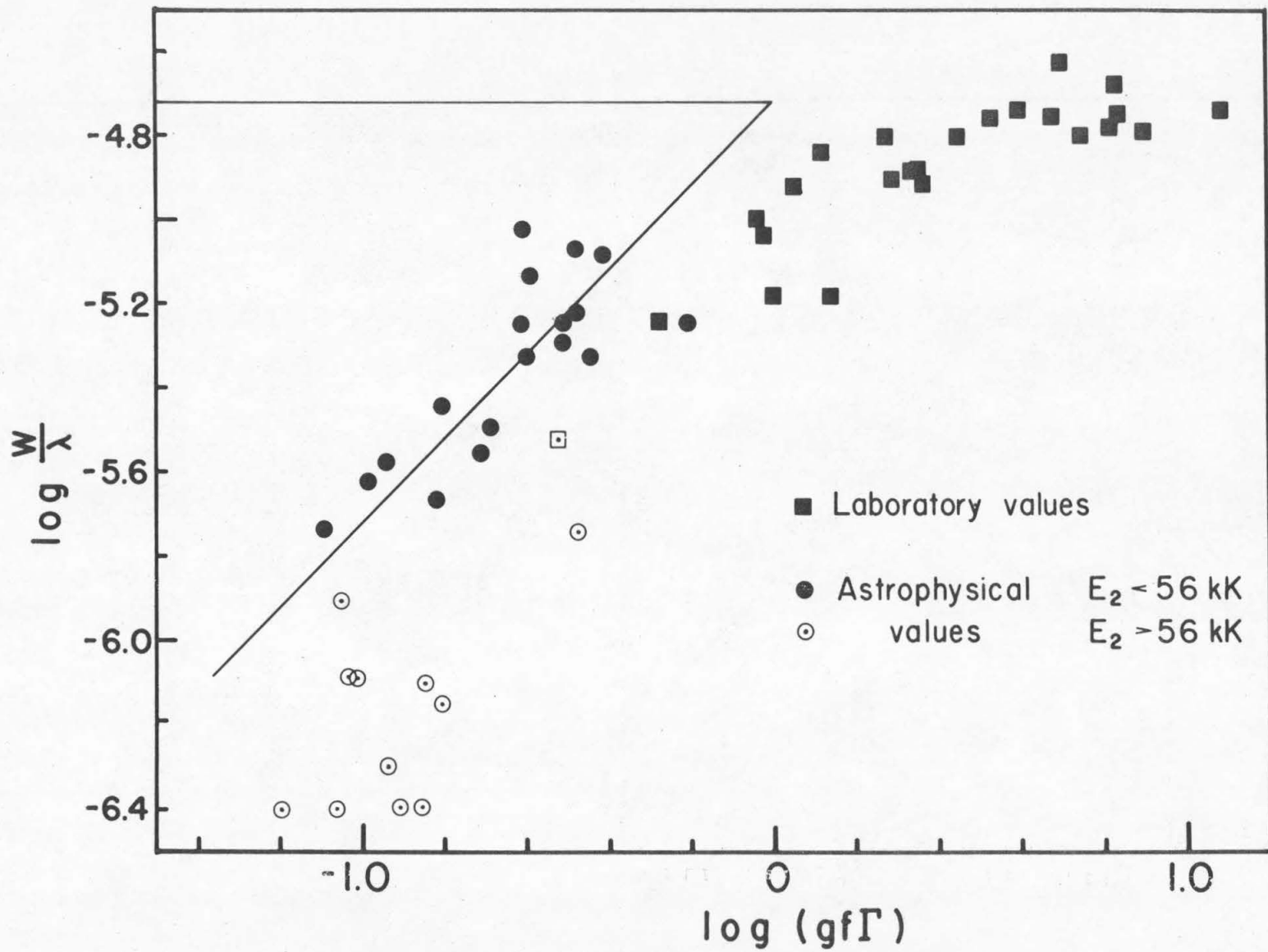


## FIGURE 12

a) Dimensions for the quartz-lithium fluoride achromats used in this experiment. The design focal length was 183.7 mm.

b) Calculated deviation from the design focal length. The measured focal length was  $183 \pm 1$  mm.  
(refer to page 73)

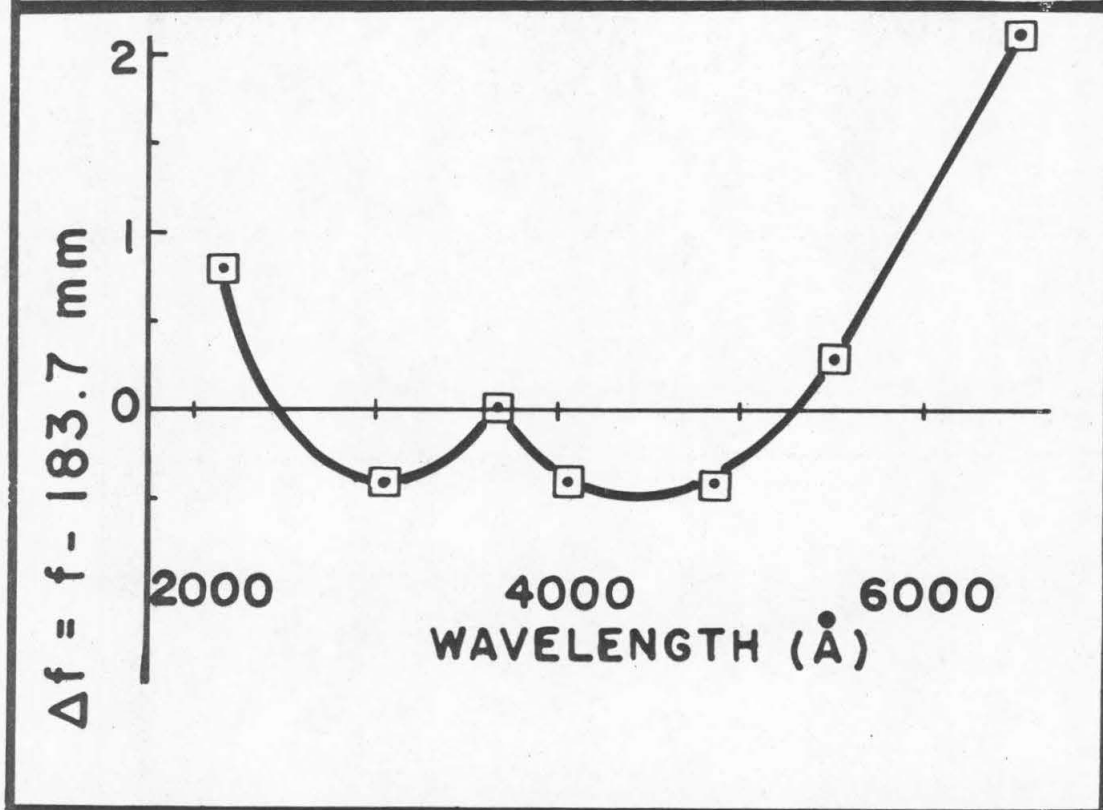
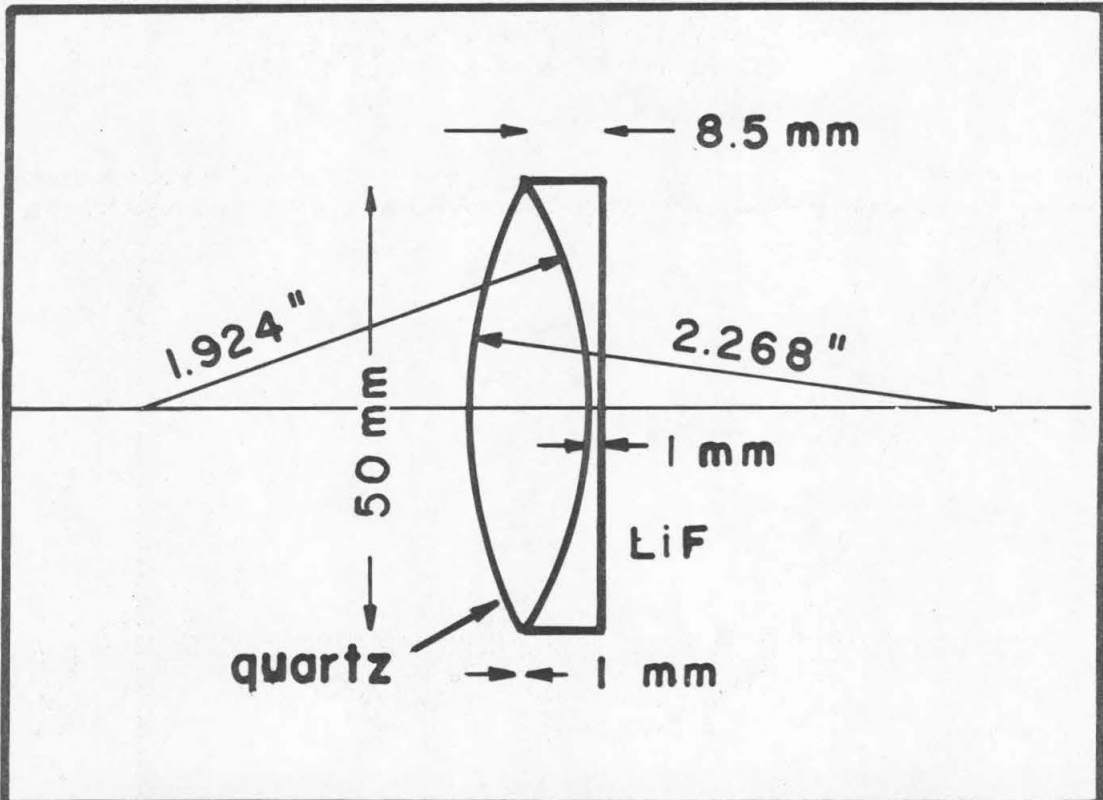


## FIGURE 13

Transmission of the Corning 7-54 filter used in this experiment. The circles represent values measured with a spectrophotometer, Guilford Model 240. The squares represent values obtained from observations of the Fe spectrum with a spectrometer; the filters were put into the optical path, and the change in observed intensity as a function of wavelength was noted. (refer to page 74)

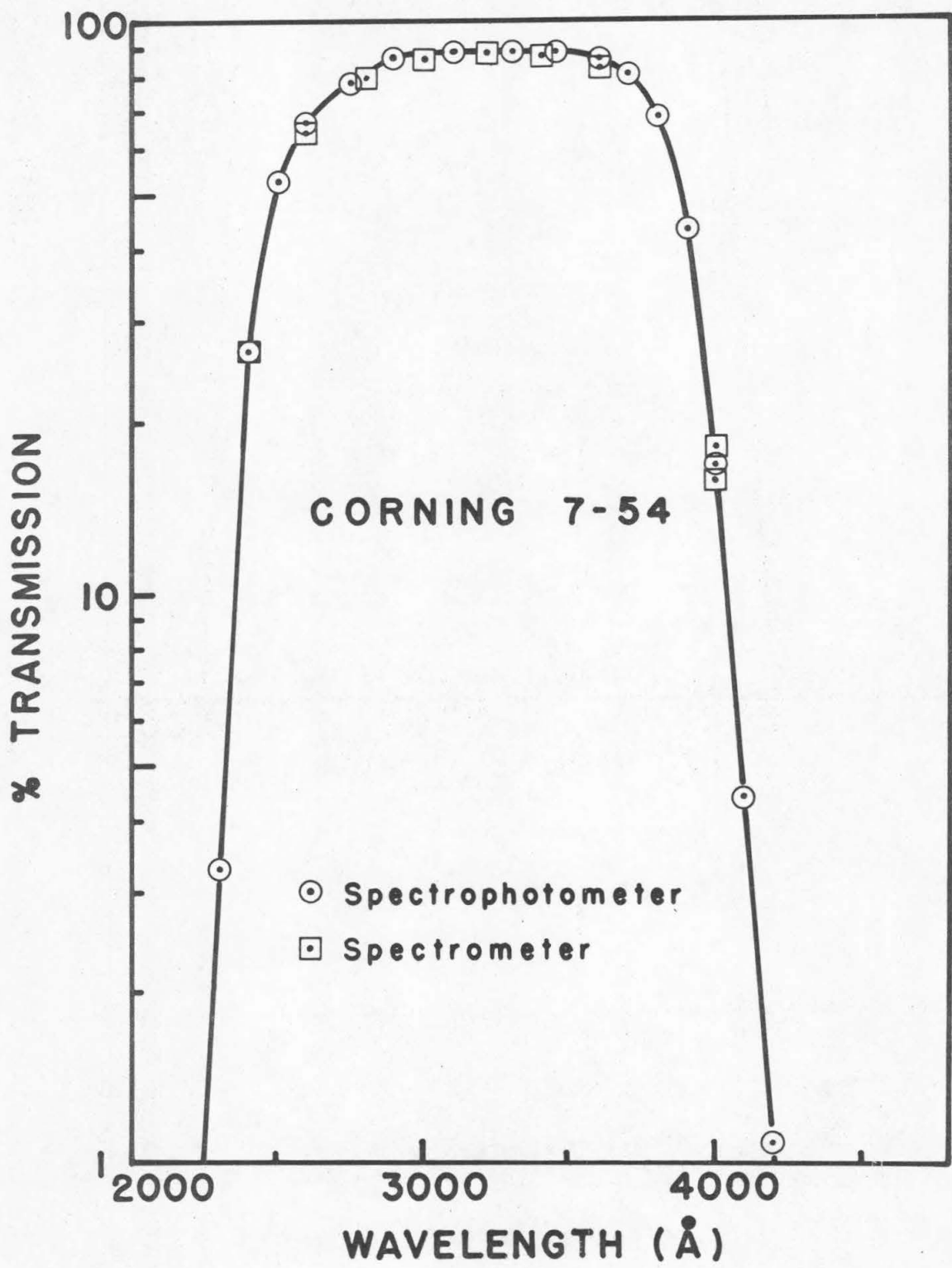


## FIGURE 14

Monochromatic photon intensity (photons per second per  $\text{cm}^2$  of source per steradian per Ångstrom) in arbitrary units for a GE 30A/T24/17 tungsten ribbon-filament lamp operated as 35 A a. c. The lamp was calibrated for use as a secondary intensity standard by the Eppley Laboratory Inc., Newport, R.I. (refer to pages 75, 84, 86, 90)

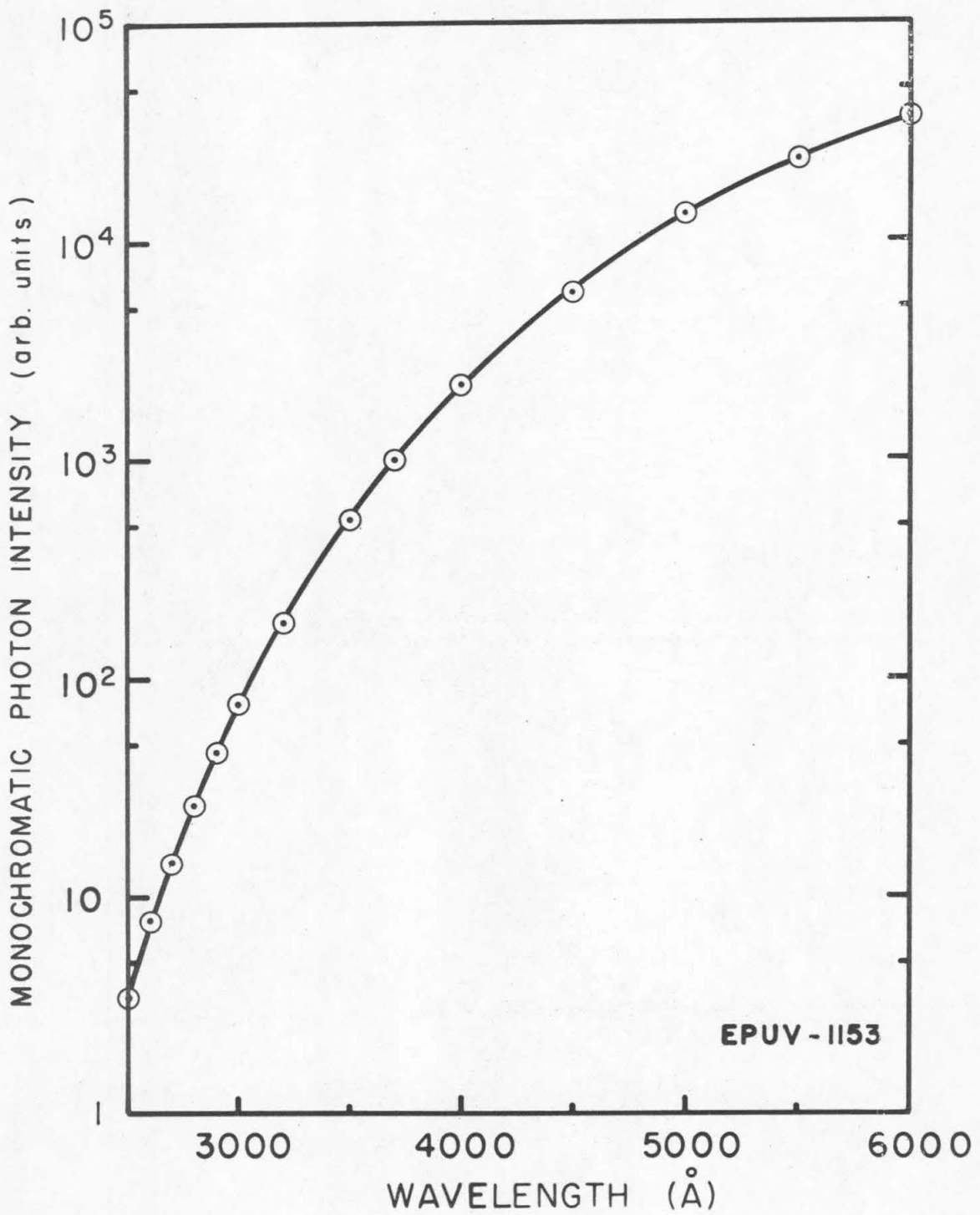


## FIGURE 15

Power supply for the standard lamp. The ammeters were calibrated to  $\pm 0.2\%$  at 35 Amperes. The supply is similar to that suggested by Stair et al. (1960).

$V_1, V_2$	115 V a. c., 5 A Variac
$T_1, T_2$	120 V/7.5 V, 25 A transformer
$T_3$	120 V/10 V, 10 A transformer
$T_4$	10:1 precision current transformer

The auxiliary equipment used to calibrate the ammeters is shown.

LOAD	carbon resistor or standard lamp
R	precision resistor; 0.0010013 (0.01%)
$V_{RMS}$	Hewlett-Packard 3000 A voltmeter
$V_D$	Fluke 881 AB digital voltmeter

(refer to page 75)

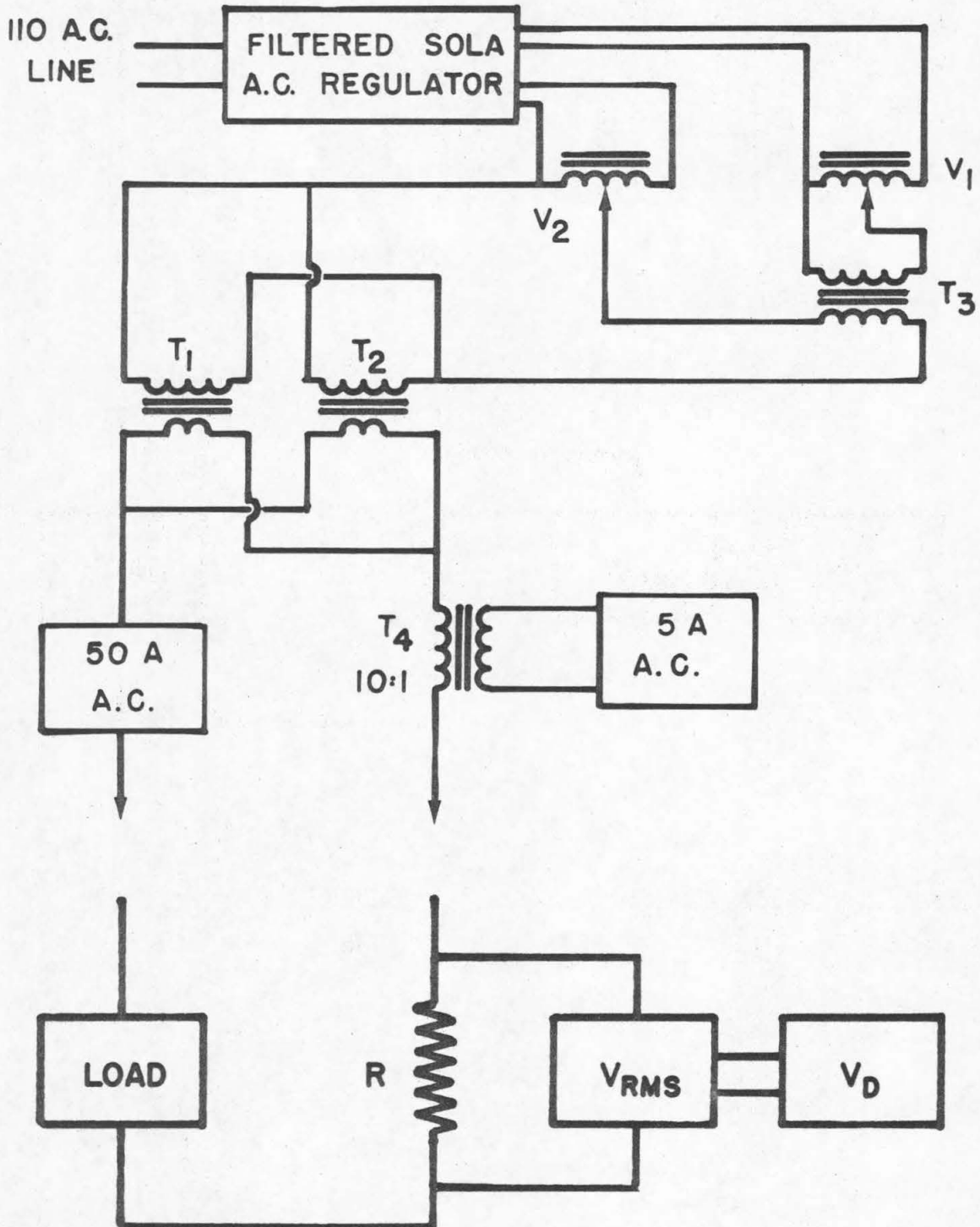
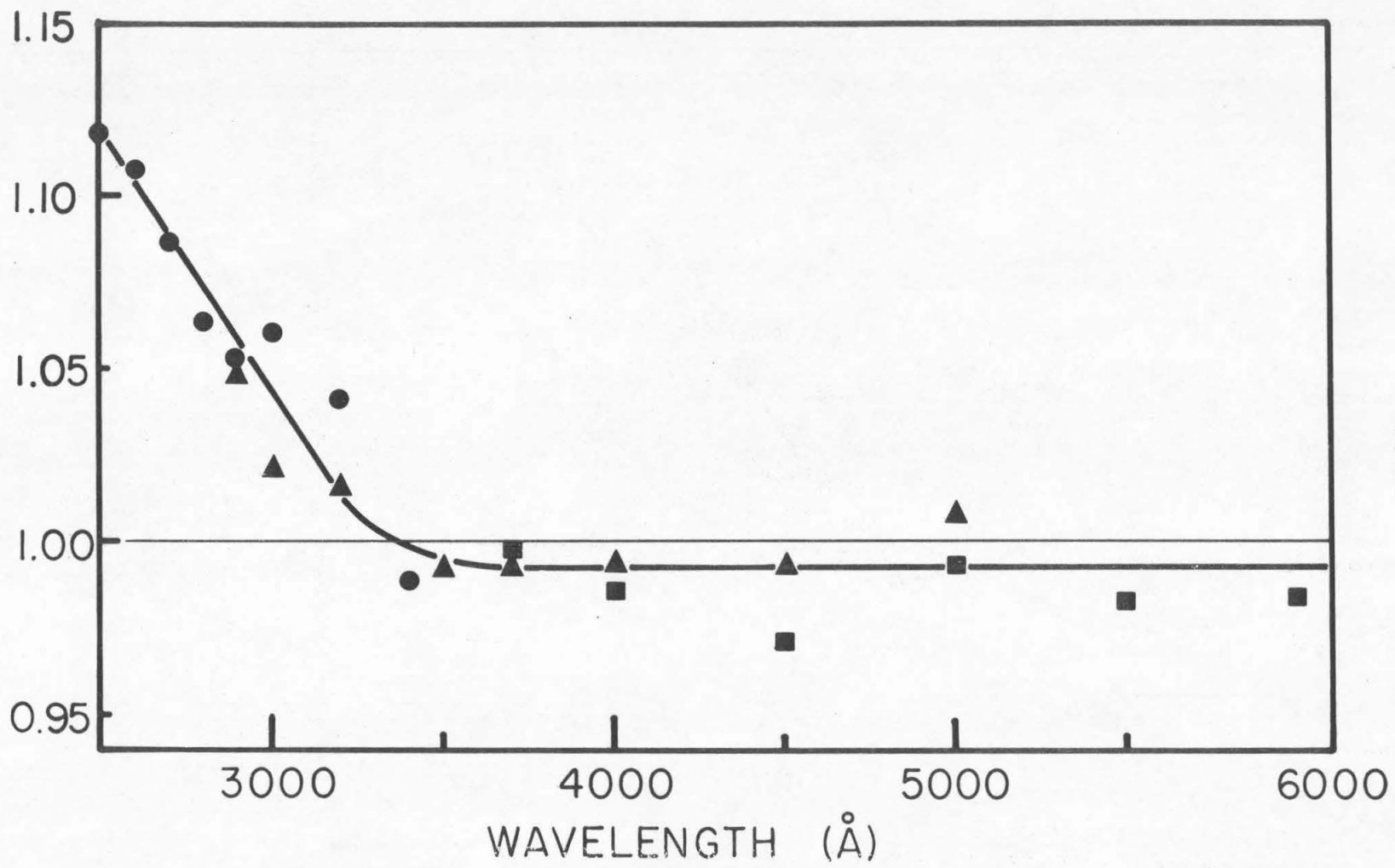


FIGURE 16

$\frac{n_1(\lambda)/I_1(\lambda)}{n_2(\lambda)/I_2(\lambda)}$  as a function of wavelength.  $n$  is the measured monochromatic photon intensity\* of a lamp;  $I$  is the monochromatic photon intensity given in the calibration by Eppley Lab. The subscripts 1 and 2 refer to lamps 1130 and 1156, respectively. The circles refer to data obtained using the 2400 line/mm grating in the McPherson Spectrometer with the Baird-Atomic 2537 Å interference filter and the Corning 7-54 filter to reduce scattered light. The triangles and squares refer to data obtained with the 2400 line/mm and the 1200 line/mm grating, respectively, but no filters. The deviation from unity in the ratio for  $\lambda > 4000 \text{ \AA}$  is a consequence of the fact that slight changes in geometry were made when switching from observation of one lamp to observation of the other. The figure shows that lamp 1130 has increased its output relative to the calibrated value at short wavelengths, if it is assumed that the output of lamp 1156 is correct. (refer to page 77)

---

\* Photons per second per  $\text{cm}^2$  of source per steradian per Ångstrom.



**FIGURE 17**

Schematic diagram of the McPherson spectrometer system and associated electronic equipment. A description of the latter may be found in Table 1. (refer to pages 63, 78)

FIGURE 17

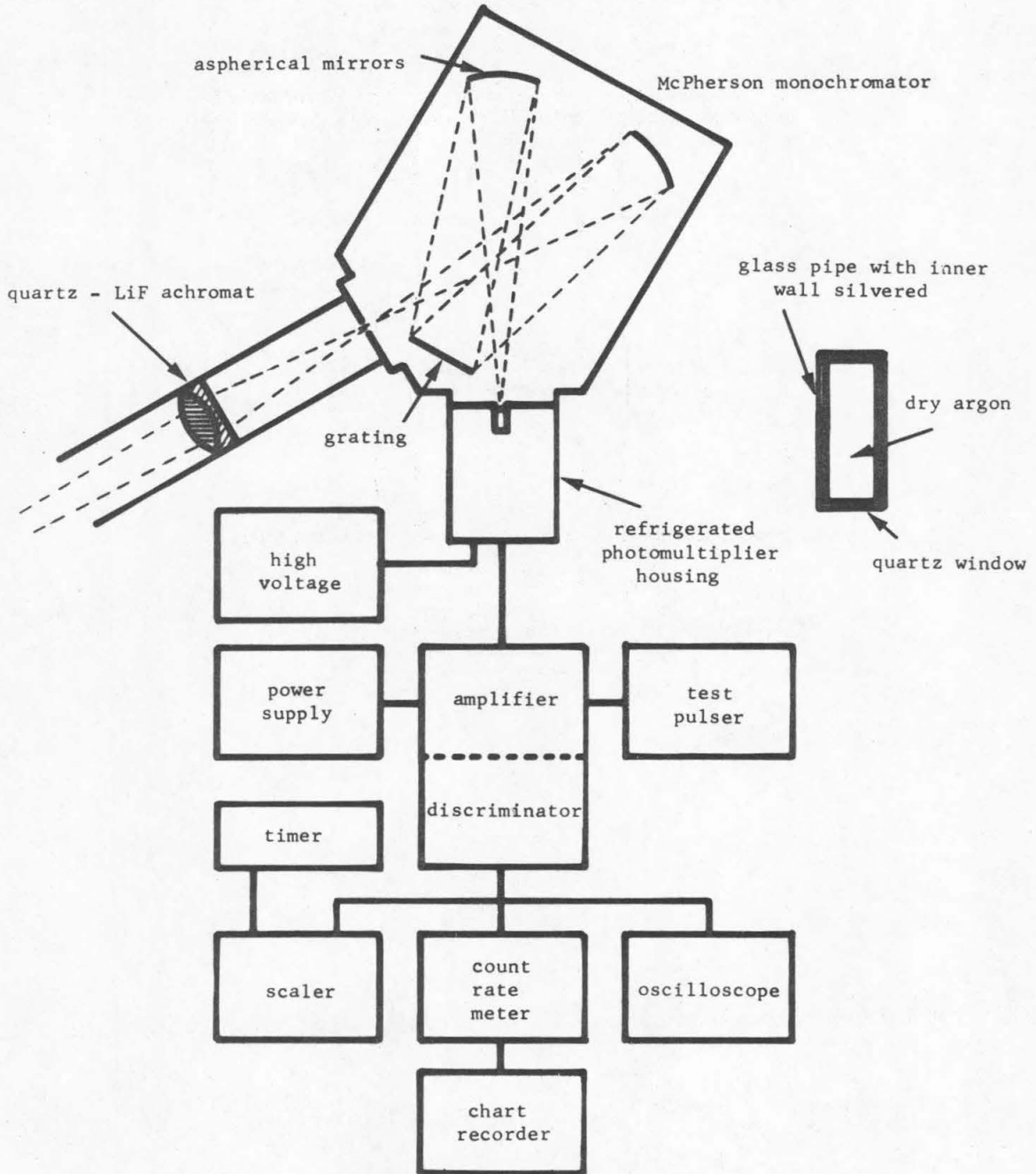


## FIGURE 18

Schematic diagram of the hollow cathode source showing carrier gas supply, pumping system and power supply. The cold traps consisted of coils of copper refrigerator tubing that were immersed in a Dewar of liquid nitrogen or dry ice and alcohol. The hollow cathode source is shown roughly to scale. (refer to page 81)

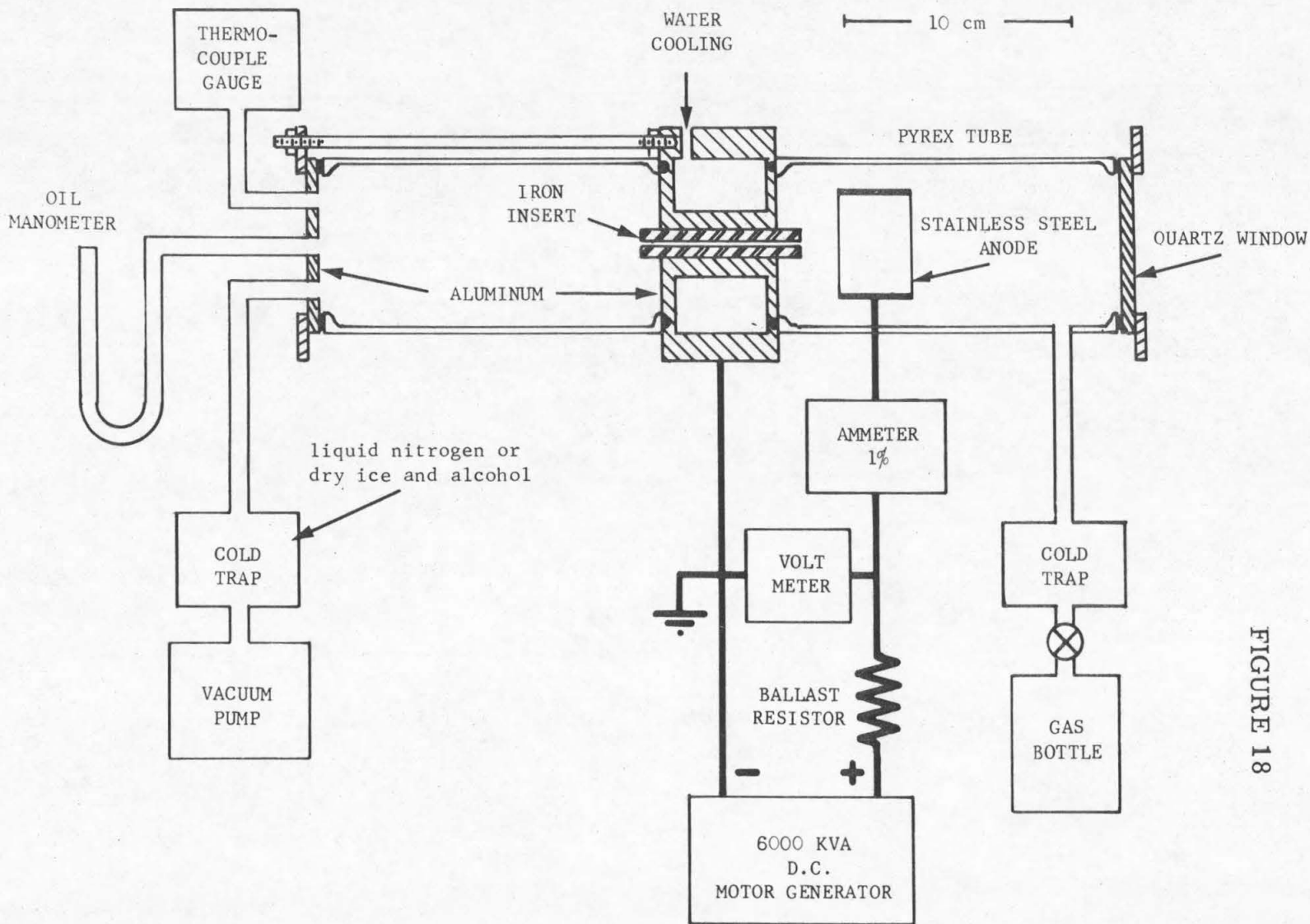


FIGURE 18

## FIGURE 19

Relative detection efficiency of the Rowland spectrometer system in first order as a function of wavelength. The circles were measured as part of this experiment; the diamonds are from Martinez. All data were obtained by observing a standard lamp.

(refer to page 87)

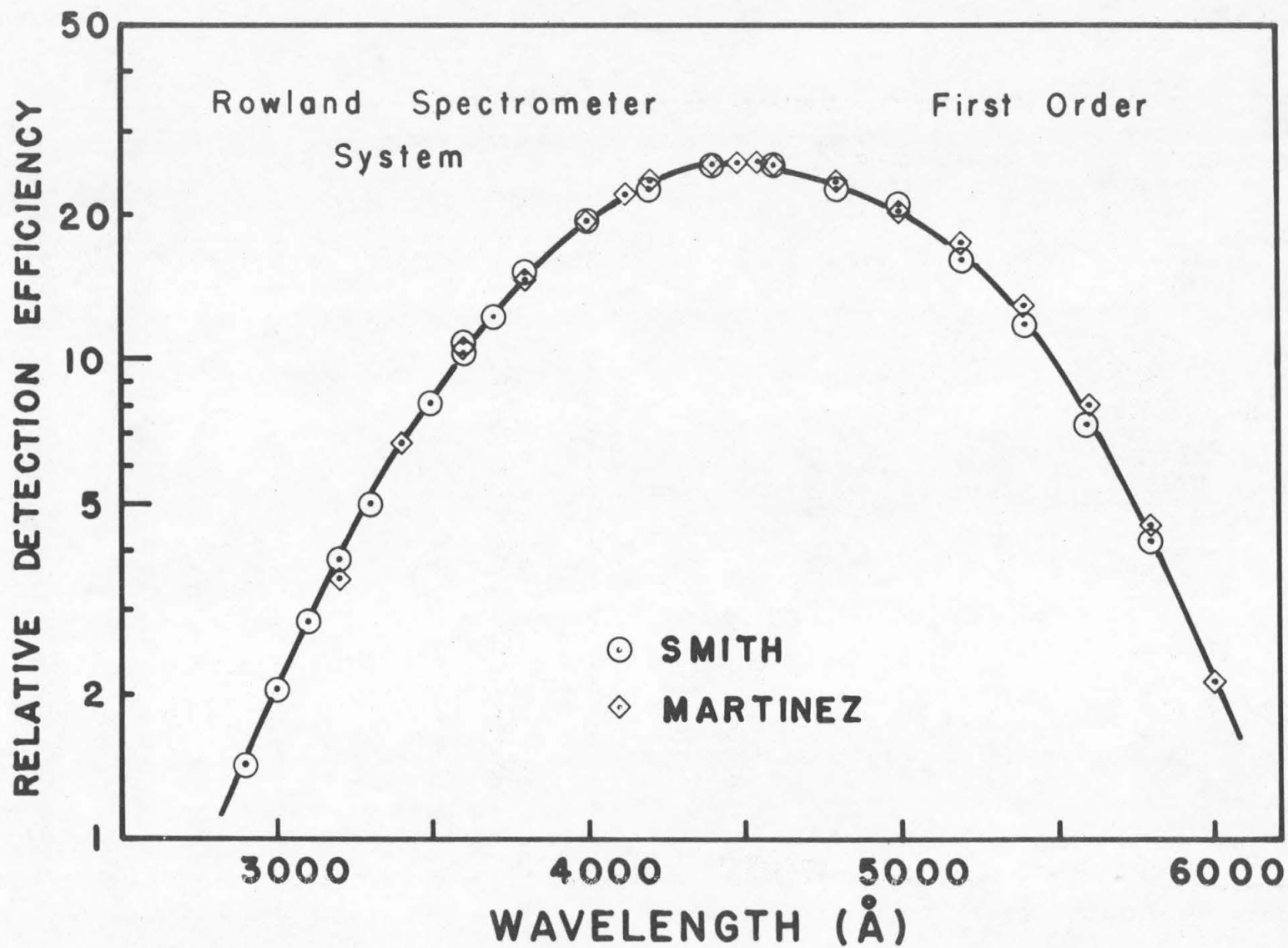


FIGURE 19

## FIGURE 20

Relative detection efficiency of the Rowland spectrometer system in second order. The values represented by open symbols were obtained as part of this experiment. The squares and diamonds refer to two measurements made using the sodium salicylate-photomultiplier detector, while the circles refer to measurements made with the standard lamp. Typical experimental uncertainties are shown. The large uncertainty for the standard lamp datum point at 2500 Å is a consequence of the low output of the lamp at that wavelength. The solid circles are from the measurements of Martinez. (refer to pages 32, 88, 92)

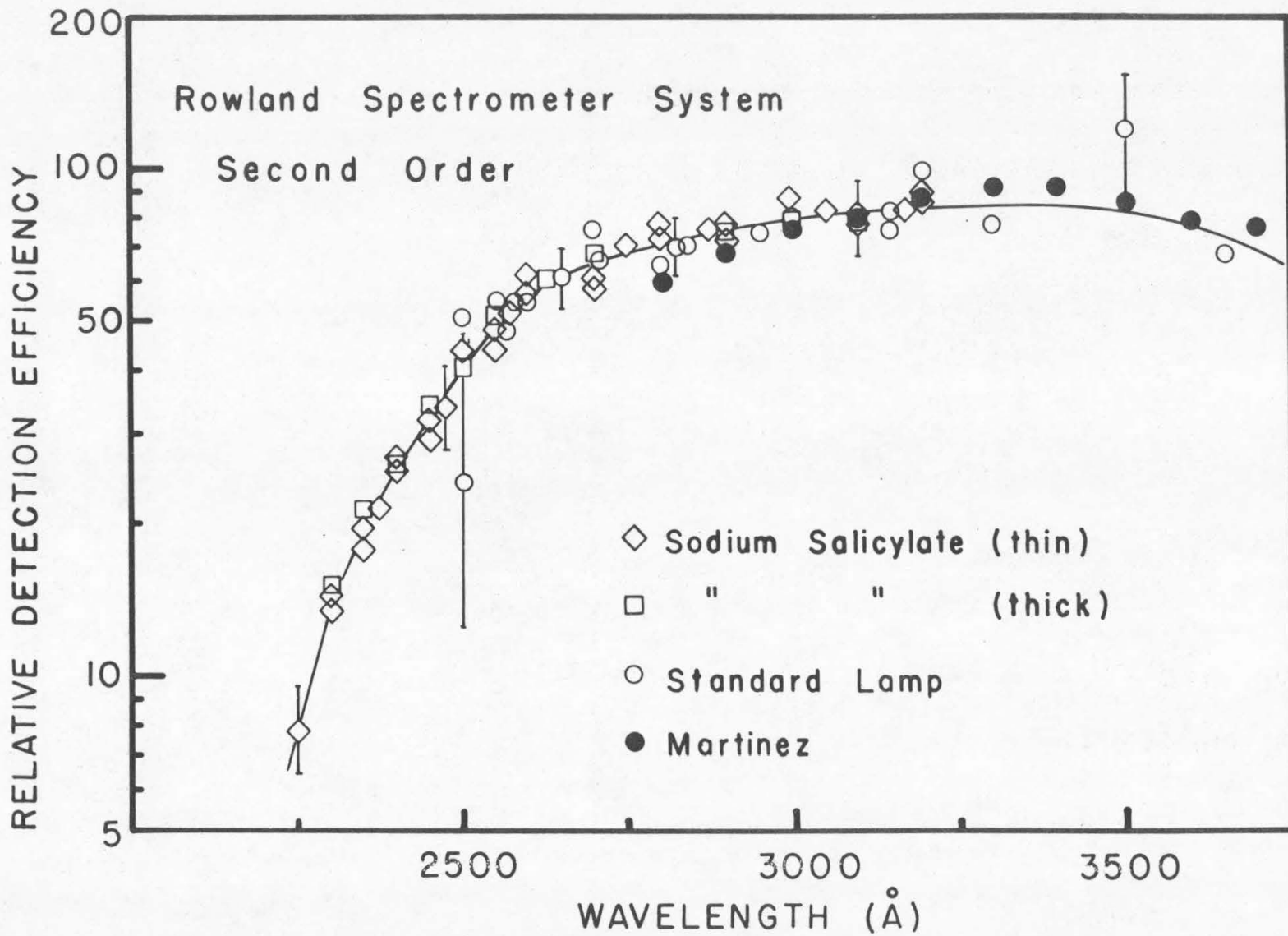
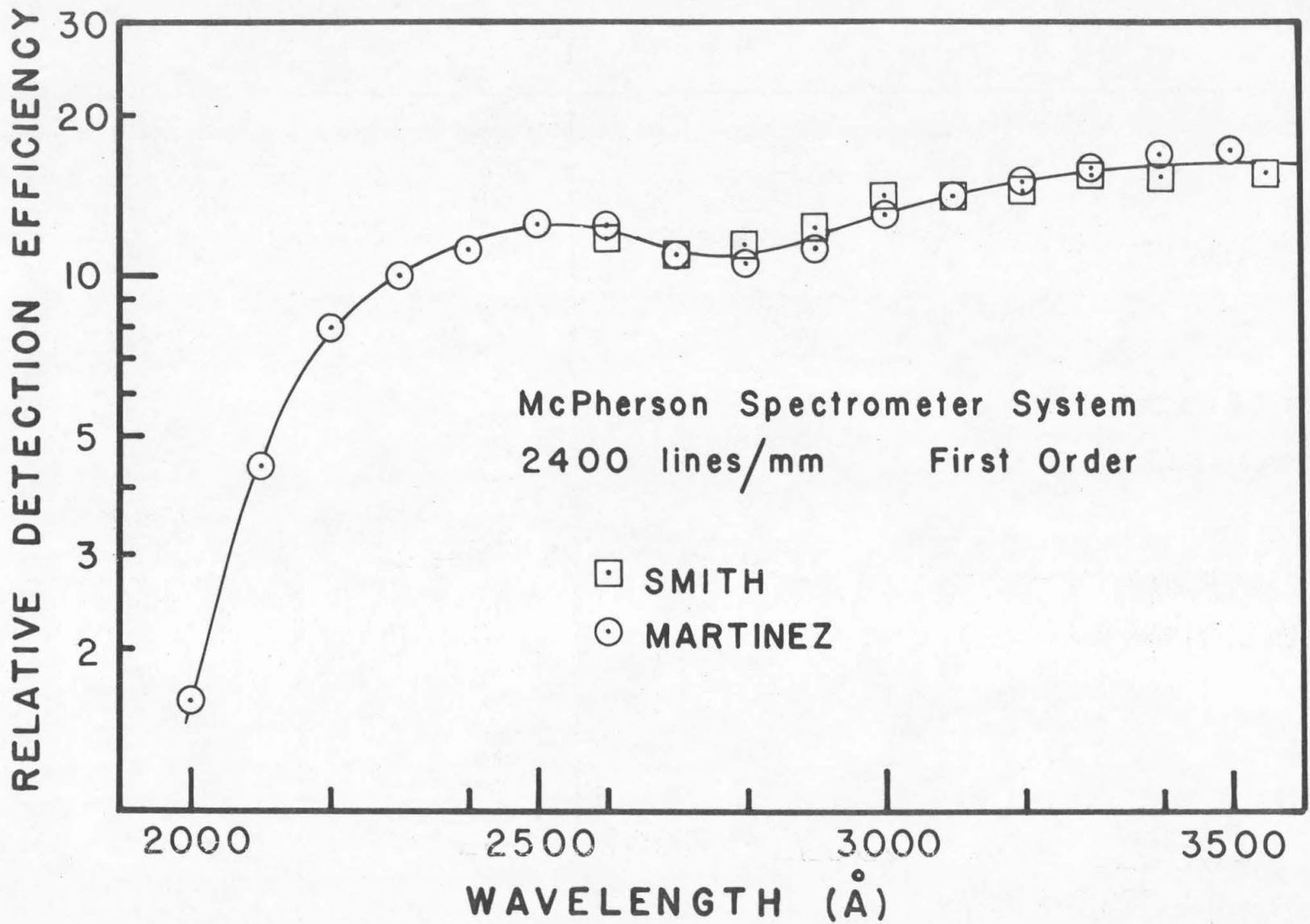


FIGURE 20

## FIGURE 21

Relative detection efficiency of the McPherson spectrometer system as a function of wavelength. The 2400 line/mm grating was used in first order. The squares refer to values obtained as part of this experiment. The circles are from Martinez. Values for  $\lambda \geq 2500 \text{ \AA}$  were obtained by observing a standard lamp. Values for  $\lambda \leq 2800 \text{ \AA}$  were obtained by comparing the detection efficiency to that of a sodium salicylate coated photomultiplier. (refer to page 89)



## FIGURE 22

Schematic diagram of the apparatus used to measure the relative detection efficiency of the Rowland spectrometer for  $\lambda \leq 3000 \text{ \AA}$ . The masks were used to reduce scattered light. Detail of the sodium salicylate-photomultiplier detector is shown. (refer to page 91)

FIGURE 22

